Electrocoagulation for Treatment of Disinfection Byproducts, Organic Matter, and Per-And Polyfluoroalykl Substances.

Donald Rockwood Ryan
Marquette University

ELECTROCOAGULATION FOR TREATMENT OF DISINFECTION BYPRODUCTS, ORGANIC MATTER, AND PER-AND POLYFLUOROALYKL SUBSTANCES

by

Donald Rockwood Ryan

A dissertation submitted to the Faculty of the Graduate School,
Marquette University,
in Partial Fulfillment of the Requirements for
the Doctor of Philosophy

Milwaukee, Wisconsin

May 2023

ABSTRACT

ELECTROCOAGULATION FOR TREATMENT OF DISINFECTION BYPRODUCTS, ORGANIC MATTER, AND PER-AND POLYFLUOROALYKL SUBSTANCES

Donald Rockwood Ryan

Marquette University, 2023

Technologies are needed to treat contaminants such as disinfection byproducts (DBPs), trace organic compounds (TOrCs), and per- and polyfluoroalkyl substances (PFAS) in water to improve consumer safety and mitigate chronic risk. This dissertation focused on evaluating electrocoagulation (EC) and hydrogen peroxide (H_2O_2)-enhanced EC (peroxi-electrocoagulation; EC:H_2O_2) for treatment of these contaminants. The impacts of source water quality (such as natural organic matter [NOM]) on overall performance was assessed, and the non-destructive and destructive pathways involved in treatment were evaluated.

The first objective focused on EC performance for mitigating the formation of regulated DBPs in water to better substantiate EC's performance relative to regulations and conventional treatment technologies. This objective was achieved by conducting a series of EC and conventional coagulation tests for multiple NOM sources and measuring the DBP formation potential following post-treatment chlorination. Overall, EC had similar performance to conventional coagulation in terms of DBP production, indicating that EC may be a competitive DBP mitigation technology.

The second objective focused on enhancing the oxidizing capabilities of iron-EC by adding hydrogen peroxide to boost the oxidant yield via EC:H_2O_2. This process provided oxidative destruction of TOrCs in tandem with non-destructive separation pathways that can treat NOM as well as TOrCs. The energy inputs required for EC:H_2O_2 were favorable compared to other oxidative technologies, substantiating the case for EC:H_2O_2 as a combined destructive and non-destructive process for water treatment.

The third objective assessed EC:H_2O_2 for PFAS mitigation and the influence of six different NOM sources on treatment efficiency. PFAS removal was observed for systems with and without NOM. However, the PFAS treatment pathways were different in NOM-containing systems, wherein more non-destructive removal, such as floatation layer accumulation, occurred. This difference may be due to the interactions between low molecular weight NOM, iron, and PFAS that form complexes that are more susceptible to non-destructive treatment and inhibit destructive treatment. These findings revealed that real-world waters can heavily influence PFAS mitigation processes relative to treatment in synthetic laboratory matrices without background NOM and shift removal pathways. In summary, EC and EC:H_2O_2 may serve as effective water treatment technologies for real-world waters containing NOM.

ACKNOWLEDGEMENTS

This dissertation research is the culmination of my time at Marquette University for my graduate school career. Through this research journey, I've continually been reminded that as researchers we stand on the shoulders of giants. As such, I want to thank the variety of people that have had an important role in enriching my graduate journey. I would like to thank ***all*** my colleagues at the Water Quality Center over my time at Marquette University. Although this is not an exhaustive list, I would like to thank my early research mentors for electrochemistry and emerging contaminants: Emily Maher, Joe Heffron, Yiran Tong, and Saba Seyedi. The McNamara research group over the years: Kassidy O'Malley, Lee Kimbell, Erik Anderson, Kate Harrison, Anthony Kappell, San Marie Thomson, Grace Scarim, Zihao Lu, Veronika Folvarska, Han Meng, Melvin Samuels, and Govindan Karkarei. In addition to my Mayer research colleagues: Sam Juedemann, Synthia Parveen Mallick, Faten Hussein, Will Lynn, and Jonathon Hou. I'd also like to thank my undergraduate research students over the years, without whom this work wouldn't be possible: Jennifer Lavin, Caitlin Graeber, Claire Baldus, Alfonso Acevedo, and Anna Gorrill. Finally, I'd also like to thank my friends who have been a meaningful source of support throughout my graduate studies in Milwaukee: Christen Jarshaw, Emma Albrecht, Isabelle Horvath, Duyen Lam, Greg Dieter, Anne Hunter, Taylor Valencia, Antônio Martins, Kai Bottum, and the collective group of Pseudo Sports Milwaukee.

I also would like to thank the members of my dissertation advisory committee: Drs. Brooke Mayer, Patrick McNamara, Laodong Guo, and Yin Wang. Each day I'm thankful to have mentors that provide me an opportunity to act on my curiosity. I'm grateful for the interdisciplinary nature of this committee that has empowered me to pursue multiple spheres of research questions that help understand the comprehensive nature of these multifaceted problems that environmental engineers are tasked to solve.

I would like to thank Mike Dollhopf as the lab manager of the Water Quality Center research facilities, and Dr. Anna Benko from the Shimadzu Analytical Instrumentation Laboratory and Research Center at the University of Wisconsin – Milwaukee whose expertise on PFAS quantification was a key component of the analyses conducted in this work.

Lastly, I would like to acknowledge the series of funders responsible for aspects of this work including the Marquette College of Engineering SEED Grant, the National Science Foundation: Water, Equipment, and Policy center, and the Jobling Fellowship program at Marquette University

DEDICATION

I would like to dedicate this work to my parents, DeAnna and Chuck West for their continued love and support throughout my academic journey. In addition, I would like to dedicate this dissertation to my friends both new and old, from my friends back home in Oklahoma, to newer friendships that have developed in Wisconsin. To my friends, thank you for always being a source of support since I've made the move up north, and also for staying in touch to see how this new chapter has gone. To my newer friendships in Milwaukee, thank you for making Milwaukee feel like home.

This dissertation is also dedicated to the city of Milwaukee. I'm grateful for the opportunity to pursue my PhD in the "Fresh Coast" city of Milwaukee, Wisconsin as the backdrop of a key chapter in my life to learn about the connectivity of people and their water resources. I've cherished the opportunity to spend many hours at the lake in addition to hours walking along the Milwaukee River on the upper east side. This privilege has additionally been inspirational for informing aspects of my dissertation research by seeing shifts in water quality throughout the different seasons present in Wisconsin. For example, the Milwaukee River was a component of each of my dissertation objectives. Over the years I've walked by the river many times when enjoying time in nature, from seeing it frozen over during the frigid winters, seeing the river overfilled to its floodplain after a large storm, to wading in it in the late summer to sample water for my research.

TABLE OF CONTENTS

LIST OF TABLES

LIST OF FIGURES

CHAPTER 1. INTRODUCTION

Environmental engineers are tasked with working at the interface of society and the natural environment to effectively protect public health and manage environmental resources. Considering the water environment, environmental engineers assess if water is safe to drink and then if water is safe to return to the environment after using it. This cyclical treatment process is achieved using engineered systems like drinking water and wastewater treatment plants. To design these systems, environmental engineers need to understand water quality parameters, such as the levels of bacteria, the presence of chemicals that can interfere with treatment (such as natural organic matter), and the presence of trace organic contaminants. These individual contaminants are often present at very low levels (e.g., parts per billion or parts per trillion), perhaps below health risk thresholds, but the combined "chemical soup" can have major human and ecological health implications. Unfortunately, drinking water cannot be treated using a "one-size-fits-all" treatment technology approach because of the varying environmental chemistry among different water sources. Therefore, a key goal of this dissertation is to understand the performance of emerging water treatment technologies, specifically electrochemical technologies, for a range of trace organic contaminants and understand how the underlying environmental chemistry impacts treatment process efficiency.

1.1 Electrochemical Water Treatment

Water treatment processes generally rely on two overarching classifications of water treatment: destructive treatment and non-destructive treatment. Destructive treatment refers to transformations of target contaminants via chemical reactions such as oxidation that shift contaminants into byproducts, with the ideal treatment goal being mineralization products (e.g., CO_2, H_2O, and F^-). Non-destructive treatment utilizes phase separation processes to remove contaminants from water and subsequently transfer them to another media such as iron flocs or filtration media. Electrochemical treatment may be utilized for both destructive and non-destructive water treatment. Electrochemical water treatment technologies generate chemicals *in-situ* via the electrolysis of electrode materials, which can be beneficial in comparison to conventional treatment in specific applications, e.g., in rural and decentralized treatment. The on-site generation of drinking water chemicals during electrochemical treatment avoids the costs associated with storage and transportation of chemicals. Moreover, small and rural drinking water systems that use surface water are at disproportionately higher risks for disinfection byproduct (DBP) occurrence due to insufficient DBP precursor removal (Allaire et al., 2018; Guilherme and Rodriguez, 2014). Conventional coagulation processes are considered best-available-technologies for DBP precursor removal. However, these processes require additional chemicals, which require transportation, pH adjustment, and chemical storage, that can increase treatment costs. Alternately, electrochemical treatment, such as electrocoagulation (EC) can generate the same coagulant species (i.e., aluminum and iron) as conventional

coagulation, and may be advantageous relative to conventional coagulation for removing DBP precursors, due to the *in-situ* generation of treatment chemicals to improve accessibility and ease of implementation for rural and decentralized systems. Accordingly, EC was the baseline process investigated here in addition to the hybridized peroxi-electrocoagulation (EC:H_2O_2) process for multi-mechanistic removal.

1.2 Organic Contaminants in Water

1.2.1 Disinfection Byproducts and Perfluoroalkyl Substances

The central goal of water treatment focuses on cleaning water for consumer safety. Part of this overall goal is achieved via disinfection to mitigate risks posed by microorganisms. These same disinfectants (e.g., chlorine, chloramine, and ozone) can interact with other components in water (namely natural organic matter [NOM]) to form DBPs. DBPs are regulated under the U.S. Environmental Protection Agency's Disinfectants and Disinfection Byproducts Rule.

Trace organic compounds (TOrCs) are a class of contaminants in environmental waters that includes pharmaceuticals and personal care products, industrial products, and others. These compounds enter receiving waters and drinking water sources via insufficient removal in engineered water and wastewater treatment processes (Kolpin et al., 2002; Westerhoff et al., 2005). TOrCs may result in chronic toxicity and can increase cancer risk, endocrine disruption, antibiotic resistance, and antiviral resistance (Daughton and Ternes, 1999; Huerta et al., 2013; Jones et al., 2003; Kidd et al., 2007).

Advanced treatment technologies, such as advanced oxidation processes (AOPs), are used to remove TOrCs from water.

These AOPs offer an advantage over traditional non-destructive conventional processes (e.g., granular activated carbon, coagulation/flocculation, membrane treatment) because contaminants can be transformed into less harmful compounds (carbon dioxide and water) rather than transferred to a secondary phase that may require additional treatment for contaminant mitigation. UV/H_2O_2 is a commonly employed AOP used in full-scale advanced treatment trains, such as water reclamation facilities. Thus, UV/H_2O_2 can serve as a "benchmark" technology to compare emerging TOrC treatment processes (Miklos et al., 2018). Additionally, iron-based AOPs have been reported for TOrC mitigation (Pignatello et al., 2006; Pratap and Lemley, 1994; Serra-Clusellas et al., 2021). Thus, enhancing the AOP potential of EC-based processes by including an oxidative component via the addition of H_2O_2 may offer improved TOrC removal.

Within the range of TOrCs in water, PFAS have gained recent widespread attention by many regulatory sectors due to PFAS' chronic toxicity paired with its ubiquity and potential for accumulation. PFAS (or "forever chemicals," as dubbed by the media) are used in various applications such as non-stick coatings for cookware, fast food packaging, waterproof raincoats, and firefighting foams. Once in water, perfluorochemicals are highly stable and are notoriously difficult to remove using conventional treatment processes. Prolonged consumption of water contaminated with PFAS may lead to chronic issues such as elevated cancer risk (Kwiatkowski et al., 2020).

PFAS have garnered public attention and have been proposed for regulation at the state and federal level. With PFAS regulations on the horizon, research is critical for advanced treatment processes that are capable of efficiently removing these toxic compounds from water.

1.2.2. Dissolved/Natural Organic Matter and Treatment Implications

A mixture of organic matter can be present in water, leading to classifications such as dissolved organic matter (DOM) and natural organic matter (NOM). NOM is derived from biological materials (plants, bacteria, etc.) in ecosystems surrounding natural waters, whereas DOM can also include synthetic and industrial sources. Organic mixtures complicate water treatment by interfering with processes e.g., clogging water filters, reacting with disinfectants to form harmful DBPs, and outcompeting TOrCs such as PFAS such that water treatment processes do not remove specific targets. Understanding and mitigating NOM is cumbersome for engineers as it varies widely across sources and is unique to each ecosystem. Accordingly, NOM from rivers, groundwaters, lakes, or a mix of all sources will bear unique challenges due to the different compositions and chemodiversity, and this unique composition must be considered in the context of treating and supplying safe drinking water. Without understanding how natural components influence treatment, it is difficult for research to be translated from idealized laboratory waters to the real environmental waters that engineers are tasked to treat. Therefore, research is also needed for emerging

technology (e.g., electrochemical) to understand treatment performance across different source waters and their inherently different challenges.

1.3. Research Chapters

The overarching goal of this research was to assess EC as a treatment technology for a range of contaminants (DBPs, TOrCs, and PFAS) and evaluate the underlying role of environmental chemistry and water quality parameters on process performance. This goal was investigated through three research objectives.

1.3.1. Iron-Electrocoagulation as a Disinfection Byproduct Mitigation Strategy for Drinking Water Treatment.

Prior studies have shown that EC can serve as an effective dissolved organic carbon (DOC) removal strategy, however, no studies have assessed the DBP formation potential attributed to post-chlorination of EC-treated water. Additionally, the majority of existing studies have only assessed removal of one type of DOC source, whereas this chapter focused on comparing different NOM sources and their subsequent DBP formation potential following treatment. Accordingly, the objective of *Chapter 3* was to evaluate EC as a technology for mitigating regulated DBPs compared to conventional DBP mitigation technologies to confirm DBP mitigation and justify the inclusion of EC as a drinking water treatment technology in the context of DBP regulations. To meet this objective, lab-scale EC reactors were used to treat synthetic drinking water sources containing NOM. The DBP, total trihalomethane [TTHM], formation potential following treatment was measured across varying water quality and operational parameters.

1.3.2. Peroxi-Electrocoagulation for Simultaneous Oxidation of Trace Organic Compounds and Removal of Natural Organic Matter at Neutral pH

EC-alone may be effective as a non-destructive technology based on DOC removal via the iron flocs that are generated. Moreover, the presence of iron generated during EC may provide opportunities for destructive treatment of TOrCs following the addition of hydrogen peroxide to encourage oxidative processes. The objective of *Chapter 4* was to evaluate the potential for oxidation of TOrCs during EC:H_2O_2 in the context of water treatment. To meet this objective, lab-scale experiments were conducted to assess the removal of the hydroxyl radical probe compound para-chlorobenzoic acid as a means to elucidate oxidative treatment pathways in this hybridized process. These findings will be useful for evaluating the energy input and H_2O_2 dosing conditions needed for oxidant generation and assessing system performance for different real-world water matrices.

1.3.3. Peroxi-Electrocoagulation for PFAS Mitigation: The Role of Water Quality and Dissolved Organic Matter on Removal Pathways

As PFAS have gained attention due to their potential human health risks, greater understanding is needed to assess their removal in water and wastewater treatment systems. The objective of *Chapter 5* was to provide a proof-of-concept analysis of EC:H_2O_2 for PFAS mitigation. A key aim of this work was to assess the range of PFAS mitigation pathways occurring during EC:H_2O_2. To meet this objective, a series of pathway experiments were conducted to assess how the different system inputs (i.e., EC:H_2O_2, EC-only, H_2O_2 only, Fe^{3+} only, no-electricity) correspond to overall removal, and

to quantify the concentration of PFAS present in the flotation layer following treatment to gauge potential non-destructive pathways. The impact of water quality and DOM was also assessed to investigate treatment in real waters. For DOM analysis, compounds were spiked to reflect the range of organics that can occur in engineered systems in addition to real-world waters. The bulk DOM was characterized to better understand how the chemodiversity of DOM impacts EC:H_2O_2 treatment and how specific DOM constituents can influence PFAS treatment.

Following this introduction, *Chapter 2* includes a literature review on electrochemical treatment and DBPs, removal pathways for TOrCs, and PFAS. After the research chapters 3-5, *Chapter 6* provides a summary of key findings from this dissertation research along with recommendations for future research.

CHAPTER 2. LITERATURE REVIEW

Portions of the following chapter were published as:

Ryan, D.R., Mayer, B.K., Baldus, C.K., McBeath, S.T., Wang, Y., McNamara, P.J., 2021. Electrochemical technologies for per- and polyfluoroalkyl substances mitigation in drinking water and water treatment residuals. AWWA Water Sci 3. https://doi.org/10.1002/aws2.1249

It is included here with modification to satisfy dissertation requirements.

2.1. Electrochemical Water Treatment - Electrocoagulation

Electrochemical drinking water treatment processes such as electrocoagulation (EC) are capable of water treatment through non-destructive and destructive pathways, potentially with lower energy inputs compared to other destructive treatment technologies such as sonolysis, UV advanced oxidation, advanced reduction, and photocatalysis (Chaplin, 2019; Cui et al., 2020; Niu et al., 2016). Electrochemical technologies can be advantageous for drinking water treatment because they generate chemicals on site. Electrochemical treatment may also be applied at various points in the drinking water treatment train, such as after particle separation or for treating the water treatment residuals. These technologies have primarily been studied in the context of wastewater, contaminated groundwater, and fundamental electrolyte matrices (i.e., buffered matrices free of scavengers and interfering parameters). However, they have recently started to be evaluated in the context of drinking water

treatment (Chaplin, 2019; Garcia-Segura et al., 2020; McBeath et al., 2020a; Radjenovic et al., 2020; D.R. Ryan et al., 2021),

2.1.2. Overview of Electrochemistry Relevant to Drinking Water Treatment

Electrochemical treatments utilize electrolytic cells composed of at least one anode, one cathode, and a source of electrons (Figure 2.1). Oxidation reactions occur on the anode and reduction reactions occur on the cathode, with the type of electrode materials determining the specific reactions occurring. Sufficient thermodynamic energy (e.g., working electrode potential, or standard potential [E^0] reported as Volts [V] vs. standard hydrogen electrode [SHE]) must be available for these reactions to occur.

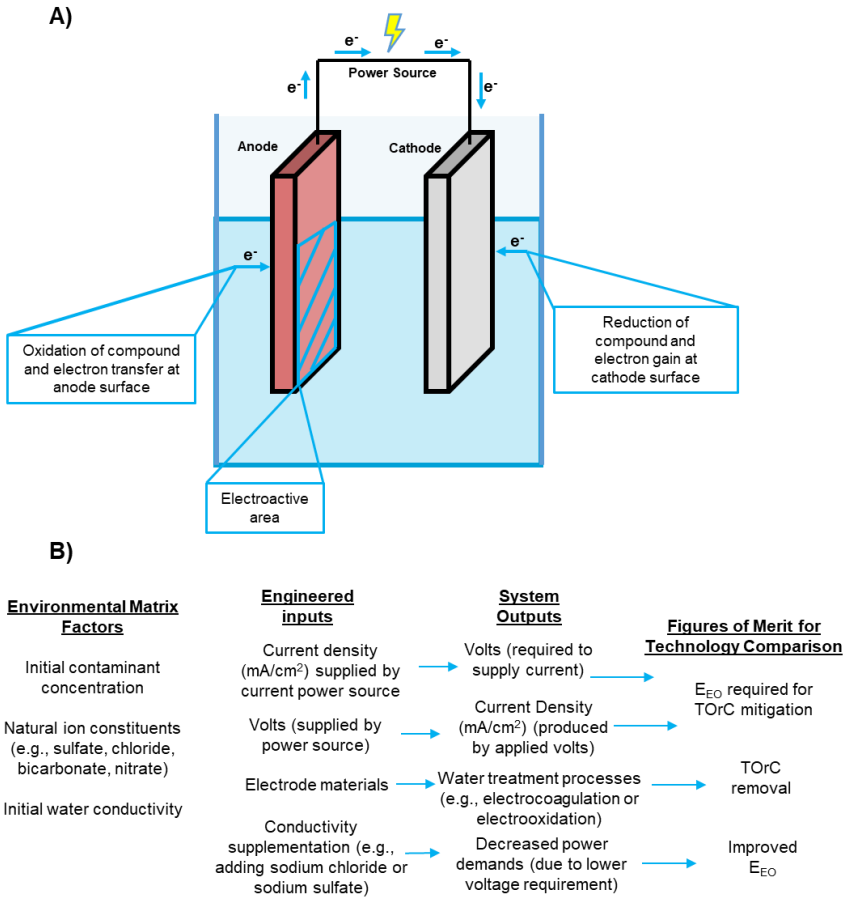

Figure 2.1: A) Electrolytic cell schematic for electrochemical water treatment reactors. In these cells, oxidation reactions occur at the anode and electrons flow to the cathode, where reduction reactions occur. The current density (mA/cm^2) is determined by the amount of current (mA) that passes through the electroactive surface area. B) Additional information is provided for environmental inputs to the electrolytic cell, in addition to engineered inputs and corresponding system outputs and figures of merit for comparing technology. E_{EO} = electrical energy per order.

Electrochemical reactions relevant to water treatment include coagulant generation, oxidant generation, reduction, and direct electron transfer reactions. Coagulants are generated using reactive electrodes such as iron or aluminum ($Fe^0 \rightleftharpoons Fe^{2+} + 2e^-$, $E^0 = 0.441$ V vs. SHE; $Al^0 \rightleftharpoons Al^{3+} + 3e^-$, $E^0 = 1.67$ V vs. SHE) through the process of EC (Bagotsky, 2005). Oxidants are generated using inactive electrode materials such as boron-doped diamond or Ti_4O_7 (e.g., $2Cl^- \rightleftharpoons Cl_2 + 2e^-$, $E^0 = 1.35$ V vs. SHE; $H_2O \rightleftharpoons \bullet OH +$

$H^+ + e^-$, E^0 = 2.73 V vs. SHE) (Bagotsky, 2005). Electrolysis of other ions in water, such as sulfate, carbonate, ferrous iron, and manganese, can also generate additional oxidants and radical species (Barazesh et al., 2016; McBeath et al., 2020b, 2020c; Radjenovic and Petrovic, 2016). Higher levels of ions (e.g., chloride, sulfate, and nitrate) result in higher electrical conductivity that can decrease electrical power demands. For drinking water treatment, low conductivity can be a barrier to implementation due to higher power demands. This issue can be mitigated by supplementing conductivity with salts (e.g., NaCl, Na_2SO_4, etc.) within acceptable ranges of secondary drinking water standards. In summary, the ions in water matrices have a major impact on electrochemistry reaction pathways by affecting which oxidants are generated during treatment and the electrical energy demands attributed to matrix conductivity.

Electrical inputs can be parameterized and compared using the current density (mA/cm^2) applied to the cell and the corresponding voltage. Current density is the current (mA) applied to the electroactive area of the electrodes in an electrochemical cell (Figure 2.1.). Electrochemical treatment is recommended to operate galvanostatically (i.e., constant current) for scaled systems (dos Santos et al., 2014). In galvanostatic systems, a given current density yields an analogous potential (V) based on cell resistance, which is primarily influenced by matrix conductivity which corresponds to the system power demands (Power = Potential*Current). The electrical energy demands can be evaluated based on the electrical energy per order of magnitude removal (E_{EO}, reported as kWh/order-m^3; i.e., kWh hours required to decrease contaminant concentration by 90% in a cubic meter of water treated), which

provides a means to compare contaminant treatability across technologies (Bolton et al., 2001).

The overarching goal of this dissertation research was to evaluate the efficacy of electrocoagulation as a drinking water treatment technology. Within this work, treatment performance was evaluated in waters that reflect drinking water sources that can contain water matrix parameters that may inhibit treatment such as low conductivity and low contaminant concentrations. This work focused on EC treatment of different classes of water contaminants including disinfection byproducts (DBPs), trace organic compounds (TOrCs), and per- and polyfluoroalkyl substances (PFAS) as a specific group of TOrCs.

2.2. Disinfection Byproducts as Drinking Water Contaminants

2.2.1. Disinfection Byproduct Formation and Control Strategies

Disinfection byproducts (DBPs) are potentially carcinogenic, mutagenic, and genotoxic compounds formed during conventional drinking water treatment due to reactions between water constituents, natural organic matter (NOM), and oxidants. Oxidants such as halogenated disinfectants (e.g., sodium hypochlorite, chlorine dioxide, or chloramines) or ozone can react with NOM, naturally occurring inorganic ions (e.g., bromine and iodine), and even TOrCs like pharmaceuticals to form DBPs (Postigo and Richardson, 2014; Richardson et al., 2007). DBPs were first identified in 1974 in the Netherlands (Rook, 1976). Today, more than 500 DBPs have been discovered, and it is estimated that more than half of the total organic halide products are still unknown

(Boorman et al., 1999; Richardson et al., 2007; Richardson and Postigo, 2012). The two primary classes of regulated organic DBPs are trihalomethanes and haloacetic acids. The US EPA's total trihalomethanes maximum contaminant level (MCL) is TTHM = 80 µg/L, representing the sum of chloroform, bromodichloromethane, dibromochloromethane, and bromoform. The EPA's MCL for haloacetic acids is HAA5 = 60 µg/L, representing the sum of five haloacetic acids: monochloroacetic acid, dichloroacetic acid, trichloroacetic acid, monobromoacetic acid, and dibromoacetic acid. These classes of DBPs are typically formed at higher concentrations relative to other DBPs. Thus, TTHM and HAA5 regulations are intended to indirectly manage levels of toxic non-regulated DBPs (although this issue is debated in the literature) (Golea et al., 2017).

National trends from 1982 to 2015 for health-based water quality violations indicate that DBPs are a common violation of the U.S. Environmental Protection Agency's (EPA's) Safe Drinking Water Act (Allaire et al., 2018). In particular, small drinking water systems (which comprise 90% of total drinking water systems) treating surface water in rural areas may be at higher risk of DBPs (Allaire et al., 2018; Charrois et al., 2004). Small drinking water systems may have innate disadvantages in providing clean drinking water compared to larger drinking water systems (>10,000 people) due to smaller utility staff numbers, less consumers and taxpayers leading to lower budgets, less access to technical expertise, and high transportation cost due to more remote locations (Allaire et al., 2018; Charrois et al., 2004).

Accordingly, research is needed to improve access to safe drinking water for these communities by better mitigating DBP formation risk. Electrochemical water

treatment can offer an alternative to conventional water treatment through on-site generation of water treatment chemicals, which negates the costs associated with chemical transportation and storage. These benefits are particularly useful for decentralized operations such as small and rural water treatment facilities (Chaplin, 2019; Ryan et al., 2020). Other advantages of electrochemical reactors include that they are scalable and may be operated as modular processes that can add capacity (Barazesh et al., 2015; Chaplin, 2019).

A proactive approach to preventing DBP occurrence relies on eliminating precursor compounds that may lead to DBP formation rather than removing DBPs after they form. Technologies for removing DBP precursors, as recommended by the EPA, include enhanced coagulation and granular activated carbon (USEPA, 2006). DBP precursors are generally monitored by quantifying the NOM characterization parameters such as dissolved organic carbon (DOC), in addition to the UV absorbance at 254 (UV_{254}) and specific UV absorbance per unit carbon (SUVA) to better gauge the amount of DBP forming compounds present (Ates et al., 2007; Edzwald et al., 1985; Fabris et al., 2008; Golea et al., 2017; Lavonen et al., 2015; Matilainen et al., 2011; Pifer and Fairey, 2012). For small drinking water systems, Guilherme and Rodriguez (2014) reported that a lack of DBP precursor control prior to chlorination led to higher DBP occurrence. Most treatment operations for small drinking water systems include sand filtration followed by chlorination (Jones et al., 2018). However, sand filtration is not generally as effective as coagulation processes in removing DBP precursors from source water. For example, Collins et al. (1992) reported approximately 15% DOC removal by

sand filtration, whereas coagulation may have 15-50% removal (Collins et al., 1992; Crittenden et al., 2012). However, DOC removal may also be variable among different source waters due to different initial concentrations and organic constituents present.

Based on the need for DBP precursor mitigation technologies that may be feasible for small drinking water systems, EC may serve as an option to better mitigate DBP occurrence through precursor removal. EC relies on the electrolysis of metals such as iron and aluminum to add coagulants into water. This method of dosing coagulants may encourage enhanced coagulation processes that are capable of DBP precursor removal. Prior studies have shown that EC can serve as an effective NOM removal strategy for both wastewater and drinking water matrices, and it has also been operated at pilot scale (Chen, 2004; Dubrawski and Mohseni, 2013a; McBeath et al., 2020a). However, the majority of these EC-focused studies have only focused on broad characterization parameters such as DOC and UV absorbance, but did not quantify the amount of DBPs formed following treatment. DOC removal alone is a limited metric for evaluating the DBP formation potential of treated NOM because DOC quantification does not provide information on factors such as chlorine reactivity and DBP precursor properties associated with NOM constituents. Accordingly, research is needed to assess the performance of EC relative to conventional DBP mitigation technologies based on the NOM removal and the quantification of DBPs that are actually formed following treatment. This research gap is assessed in *Chapter 3* of this dissertation.

2.3. Trace Organic Compounds and Advanced Oxidation Processes

In addition to DBPs as contaminants, trace organic compounds (TOrCs) are increasingly being monitored and considered for drinking water regulation. Unfortunately, conventional treatment trains are generally ineffective for TOrC mitigation (Westerhoff et al., 2005). As such, advanced oxidation processes (AOPs) are key water treatment processes used in full-scale advanced-treatment trains for direct and indirect potable reuse to remove TOrCs. In AOPs, reactive radical species (e.g., hydroxyl radicals [HO•] and sulfate radicals [SO_4•]) react with TOrCs to convert them into labile mineralization products (CO_2 and H_2O) from their initial carbon based structures (Von Gunten, 2018). These transformation processes deviate from non-destructive water treatment processes because they aim to destroy TOrCs as opposed to transferring them to another media (i.e., the goal of filtration and membrane processes). Current AOPs used in drinking water treatment trains include ultraviolet irradiation paired with hydrogen peroxide (UV/H_2O_2), ozone-H_2O_2 (O_3/H_2O_2), UV-O_3, and high pH ozonation (Miklos et al., 2018; Von Gunten, 2018).

Different AOPs require varying levels of pretreatment depending on the source water characteristics. For example, humic substances can diminish the feasibility of UV/H_2O_2 by hindering the UV transmissivity or impede ozone-AOPs by selectively quenching ozone. Due to these limitations, AOPs are most often applied at the end of treatment train when the bulk of the oxidant scavengers have been removed. However, these multi-unit treatment trains for TOrC mitigation are less feasible for decentralized and rural water treatment applications due to the additional maintenance and

operational requirements for each individual unit process. Alternately, stand-alone EC may be capable of TOrC mitigation through iron-based treatment processes such as Fenton's oxidation and coagulation/flocculation(Bocos et al., 2016; Garcia-Segura et al., 2017; Maher et al., 2019). Within EC, humic substances may also be removed via sorption to flocs, and subsequently mitigate the negative impacts of natural organic matter on TOrC oxidation(Dubrawski and Mohseni, 2013a; Donald R. Ryan et al., 2021). There is also potential to promote the simultaneous removal of TOrCs by Fenton's oxidation(Garcia-Segura et al., 2017; Pratap and Lemley, 1994). Accordingly, a second aim of this dissertation focused on EC and the hybridized EC process peroxi-EC (EC:H_2O_2) for the mitigation of TOrCs with specific emphasis on PFAS.

2.4. Destructive Processes during Electrocoagulation

In addition to non-destructive removal that is utilized for DBP formation prevention, EC could potentially be used for destructive removal by leveraging the role of Fe^{2+} in this system to generate oxidants. During this, EC may produce oxidation reactions via anode surface oxidation, reactive iron intermediates, or hydroxyl radicals produced by Fenton processes at low pH (Bocos et al., 2016; Heffron et al., 2019a; Kim et al., 2020; Maher et al., 2019). Oxidation mechanisms for EC treatment of TOrCs were suspected to include anode oxidation, reactive oxygen species, and ferryl iron (Maher et al., 2019). To validate these findings, additional electrochemical mechanism experiments are needed to measure the working electrode potentials in EC reactors to substantiate if direct electron transfer reactions of TOrCs occur. For example, the direct

oxidation of organic pollutant species at the anode surface has been observed previously, indicated by an irreversible oxidation peak below the oxygen evolution potential during cyclic voltammetry (Linares-Hernández et al., 2009). Additionally, research is needed using oxidant specific probe compounds such as para-chlorobenzoic acid for hydroxyl radicals to better assess homogenous oxidant formation, these data can subsequently be used to inform the active oxidants during EC:H_2O_2 studies to better assess the removal mechanisms at work within this system and the potential transformation products that could result from these oxidants.

Qian et al. (2019) investigated the oxidizing capacity of iron-EC using a combination of kinetic modeling and quantifying the conversion of benzoate to p-hydroxybenzoic acid (an oxidation byproduct for mechanism analysis). The authors concluded that EC may yield reactive oxidants (such as hydroxyl radicals) via Fenton-like mechanisms (Qian et al., 2019). Accordingly, the oxidant generation during EC as a standalone system is unclear, however the addition of radical promotors such as H_2O_2 may be beneficial for inducing oxidative processes.

2.4.1. Peroxi-Electrocoagulation as a Combined Non-Destructive and Destructive Treatment Process.

Additional research efforts to improve the yield of reactive oxygen species (i.e., hydroxyl radicals, hydrogen peroxide, etc.) in EC could benefit the advancement of destructive PFAS treatment (Garcia-Segura et al., 2017). The addition of H_2O_2 during EC may react with ferrous iron generated during EC to form oxidant species through the hybridized process peroxi-electrocoagulation (EC:H_2O_2)(Garcia-Segura et al., 2017;

Pratap and Lemley (1994). Some of the earliest tests of EC:H_2O_2 for water treatment were conducted by Pratap and Lemley (1998, 1994). These studies established the performance of EC:H_2O_2 for remediation of the herbicides atrazine and metalochlor at neutral pH conditions due to the continuous generation of Fe^{2+}, which allowed effective H_2O_2 utilization, subsequently leading to degradation of the herbicides within the pH range of 4 -7. Since the conception of EC:H_2O_2, the bulk of research has centered on wastewater and industrial treatment by leveraging the combination of coagulation for removing bulk organic pollutants (such as chemical oxygen demand) at high concentrations (mg/L levels)(Behin et al., 2015; Garcia-Segura et al., 2017; Ghanbari and Moradi, 2015a; Kumar et al., 2018; Vasudevan, 2014; Yazdanbakhsh et al., 2015a; Yüksel et al., 2009), with less focus on TOrCs at drinking water-relevant levels (ng/L - µg/L of TOrCS). For TOrCs, Serra-Clusellas et al. (2021) reported the removal of a range of TOrCs, in tertiary wastewater (ranging from 1 ng/L – 890 ng/L) via EC:H_2O_2 treatment of tertiary wastewater at pH 3. Mechanistic analysis further showed the mineralization of erythromycin (Serra-Clusellas et al., 2021). These studies corroborate the feasibility of EC:H_2O_2 for wastewater and industrial treatment, including studies focused on real water matrices. However, these wastewater-based studies simulate different water matrix conditions, treatment challenges, and oxidant doses that do not translate to applications for drinking water treatment of TOrCs. For example, drinking water sources contain lower conductivity, fewer oxidant scavengers, higher levels of dissolved oxygen, and neutral pH conditions, all of which impact the oxidative efficiency of EC:H_2O_2. Accordingly, research is needed to assess how EC:H_2O_2 performs for TOrC mitigation

(PFAS, in particular) in the context of drinking water treatment. This research aim was investigated in *Chapter 4* to verify EC:H_2O_2 as a multi-mechanistic process capable of both TOrC oxidation and non-destructive NOM removal in addition to the role of engineering inputs on system performance. In *Chapter 5*, the applications of EC:H_2O_2 and the removal pathways for per- and polyfluoroalkyl substances (PFAS) were investigated.

2.5. Per- and Polyfluoroalkyl Substances

PFAS are anthropogenic contaminants of major focus in the water industry. PFAS are broadly defined as organic compounds containing perfluoroalkyl moieties (C_nF_{2n+1}−), which are generally linear or branched-chain alkanes with a perfluorinated (CF_2) backbone and a functional group such as carboxylate, sulfonate, phosphonate, or alcohol (Cousins et al., 2020; Kwiatkowski et al., 2020). This broad definition applies to over 4700+ PFAS compounds currently in use (Cousins et al., 2020). Many PFAS, such as perfluoroalkyl acids (PFAAs), are designed to be highly stable, which is the basis of their use in non-stick cookware and aqueous film-forming foam used for firefighting. The stability of the carbon-fluorine bonds and compound hydrophobicity render PFAS highly resistant to environmental degradation, leading to high persistence, bioaccumulation, and occurrence in drinking water sources (Boone et al., 2019; Giesy and Kannan, 2001; Rahman et al., 2014).

A nationwide study measured 17 PFAS from 25 drinking water treatment plants at levels from 1 to 1102 ng/L and reported that the median PFAS concentration was 19.5

ng/L in the final drinking water (Boone et al., 2019). These values exceed maximum contaminant levels in some state-level regulations, e.g., 6 to 18 ng/L perfluorooctanoic acid (PFOA) and perfluorooctane sulfonic acid (PFOS) set by Michigan, New Hampshire, and New Jersey (Michigan Code R. 325.1064g, N.J.A.C.7:10, NH HB1264), and recent federal regulations of 4 ng/L for PFOA and PFOS. The two most commonly studied PFAS compounds are PFOA and PFOS, both of which are 8-carbon chain (C8) compounds. Despite being phased out of production, these compounds persist in the environment and in drinking water at ng/L to µg/L concentrations, with the higher end of the range representing cases of groundwater contamination (Kwiatkowski et al., 2020; Rahman et al., 2014). An estimated 6 million people are served by drinking water supplies containing PFAS concentrations higher than the U.S. Environmental Protection Agency (EPA) advisory level of 70 ng/L (sum of PFOA and PFOS concentrations) at the time of the 2016 study (accordingly, the maximum contaminant level is now 4 ng/L for PFOA and PFOS) (Hu et al., 2016). Many more people in the U.S. face sub-EPA advisory PFAS levels (70 ng/L), with 10-18 million people served by water supplies containing >10 ng/L PFOA and PFOS, and more than 200 million people receive drinking water containing PFOA and PFOS concentrations higher than 1 ng/L (Andrews and Naidenko, 2020).

The drinking water industry could face a major challenge in widely implementing technology to remove PFAS to ng/L levels if PFAS become more widely regulated. In the U.S., six PFAS (PFOA, PFOS, PFNA, PFHxS, PFBS, Genx) were most recently regulated (2023) with maximum contaminant levels of 4 ng/L for PFOA and PFOS, and Hazard Indices below 1 for mixtures containing PFNA, PFHxS, PFBS, and GenX). For comparison,

other regulated organics in drinking water, such as DBPs, are regulated at 60 and 80 µg/L for haloacetic acids and trihalomethanes, respectively, which are orders of magnitude higher than some of the PFAS advisory levels. In February of 2020, the EPA announced a proposed decision to regulate PFOA and PFOS (https://www.epa.gov/newsreleases/epa-announces-proposed-decision-regulate-pfoa-and-pfos-drinking-water). Accordingly, meeting the potential ng/L-level regulatory targets for drinking water will require innovative solutions informed by comprehensive PFAS mitigation research that reflects intended treatment goals. At the same time, research is needed to understand the fate of PFAS in proposed treatment systems, which additionally requires research using higher PFAS (such as µg/L) to operate within feasible concentrations for current analytical instruments. Accordingly, this fundamental µg/L research is necessary for understanding process mechanisms and the behavior of PFAS within systems, such that these processes can later be studied under realistic conditions.

Conventional drinking water treatment plants are generally ineffective for PFAS mitigation (Boone et al., 2019; Rahman et al., 2014; Takagi et al., 2011). Due to these limitations, alternative treatment technologies such as granular activated carbon, ion exchange, nanofiltration, and reverse osmosis may be needed for PFAS mitigation based on their demonstrated PFAS removal capabilities (Belkouteb et al., 2020; Dixit et al., 2021; Gagliano et al., 2020; Glover et al., 2018; Park et al., 2020; Rahman et al., 2014). PFAS treatment technology can be divided into two overarching categories: non-destructive treatment and destructive treatment. Non-destructive treatment

technologies such as granular activated carbon, ion exchange, nanofiltration, and reverse osmosis can remove PFAS. However, non-destructive technology can be limited by the presence of PFAS in concentrated waste streams resulting from treatment (e.g., ion exchange regenerant, membrane concentrate/backwash, and reverse osmosis concentrate), which may require additional treatment before the waste streams are discharged (Radjenovic et al., 2020; Stoiber et al., 2020). For example, Glover et al. (2018) measured 400 ng/L total PFAS in ultrafiltration and nanofiltration membrane backwash water and 600 – 1800 ng/L in reverse osmosis concentrate. Alternately, destructive technologies utilize redox reactions to transform PFAS into smaller organic and inorganic compounds, ideally with complete defluorination (conversion to inorganic fluoride) and mineralization (carbon conversion to CO_2) (Lu et al., 2020).

2.6. Electrocoagulation for PFAS Mitigation

EC may offer both non-destructive and destructive PFAS treatment by electrolysis of sacrificial anode materials such as iron, aluminum, or zinc (Figure 2.2). EC has classically been studied as a phase separation/non-destructive removal technology, although several studies indicated that it may also serve as a destructive removal technology for TOrCs that are recalcitrant to sorption such as estrogenic compounds, acetaminophen, atenolol, and bronopolol (Bocos et al., 2016; Govindan et al., 2020a; Kim et al., 2020; Maher et al., 2019; Qian et al., 2019a). For drinking water treatment, previous EC studies have focused on heavy metals, estrogens, and natural organic matter (NOM); these studies are beneficial for demonstrating performance based on

drinking water metrics (Dubrawski and Mohseni, 2013a; Heffron et al., 2016; Maher et al., 2018; McBeath et al., 2020a; Mohora et al., 2012; Ryan et al., 2020; Vik et al., 1984).

2.6.1. Electrocoagulation as a Non-Destructive Technology for PFAS

The majority of EC studies for PFAS have focused on non-destructive removal mechanisms via sorption to metal hydroxide flocs produced using sacrificial electrodes typically made from iron or aluminum. Additional electrode materials that have been tested in laboratory research include zinc and magnesium (Figure 2.2) (Lin et al., 2015). A comparison among these electrode materials demonstrated that zinc yielded greater PFOA removal (96.7%) relative to iron (10.6%) and aluminum (11.3%) after 10 minutes of treatment (Table 2.1.) (Lin et al., 2015). PFAS sorption to hydroxides was primarily attributed to hydrophobic interactions between PFAS species and the metal hydroxide surface rather than other sorption processes such as ligand exchange, van der Waals forces, π-π interactions, or electrostatic interactions (Lin et al., 2015). The hydrophobic interactions resulted from PFAS' hydrophobic tail sorbing onto the flocs via multilayer sorption (Lin et al., 2015). Accordingly, EC of waters using iron and aluminum with high PFAS concentrations (mg/L levels) can yield high removal efficacy (e.g., 90%), as shown in Table 2.1. Of note, the applied iron and aluminum doses in Yang et al. (2016) and Kim et al. (2020) are much higher than Lin et al. (2015), which may contribute to the higher PFAS removal via iron and aluminum. Other factors that may account for the differences in PFAS removal during iron and aluminum EC summarized in Table 2.1 include the speciation of Fe/Al oxide and hydroxide formation, as different chemical species have

varying functionality as coagulants. Iron and aluminum speciation can be affected by a number of variables including, but not limited to, anode potential, pH, temperature, dissolved oxygen, $[Fe^{2+}]$:$[Fe^{3+}]$, and co-occurring solute concentration and ratios (Dubrawski and Mohseni, 2013b).

Table 2.1: Electrocoagulation treatment performance for PFAS mitigation. All studies conducted electrocoagulation in parallel plate batch reactors or jar tests.

PFAS compound	Electrode material	Initial PFAS conc, mg/L	Water matrix	Current density, mA/cm²	Electrolysis time, min	% Removal	Comments	Ref.
PFOS	Iron	125	2 g/L NaCl, pH=5.2	25	50	99.6		(Yang et al., 2016b)
PFOA	Iron	103	2 g/L NaCl, pH=3.8			78.3		
PFOA	Zinc	207	10 mM NaCl, pH=5	100 mA (electroactive area not provided)	10	96.7	PFAS removal rate was higher for 1.5 mM than 0.5 mM, indicating high concentration leads to higher kinetics	(Lin et al., 2015)
	Iron					10.6		
	Aluminum					11.3		
PFOA	Iron	10	35 mM NaCl, pH=3	40	360	>99	Redox focus, 60% total organic carbon (TOC) removal	(Kim et al., 2020)

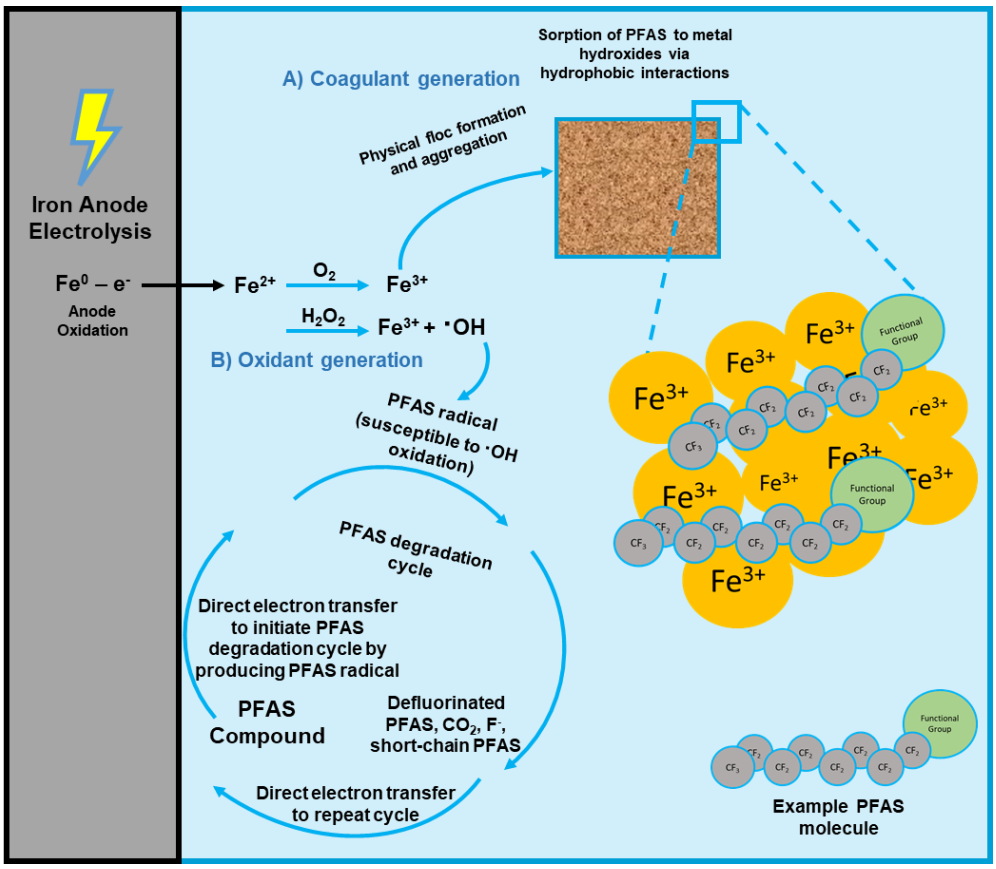

Figure 2.2: PFAS removal mechanisms using electrocoagulation (iron electrodes are shown). The first iron-based reaction occurs due to the dissolution of the anode material to form ferrous iron (Fe^{2+}), which is then oxidized to form ferric iron (Fe^{3+}) and may form hydroxyl radicals (depending on oxidant and pH conditions). **A)** Coagulant generation - the ferric iron can aggregate to form flocs capable of sorbing PFAS due to hydrophobic interactions. **B)** Oxidant generation - The hydroxyl radicals can participate in the PFAS degradation cycle initiated by a direct electron transfer at the electrode surface.

2.6.2. Iron-Electrocoagulation for Destructive PFAS Treatment

In addition to non-destructive PFAS removal, EC could potentially be used for destructive PFAS removal. Accordingly, very little studies have investigated EC as a destructive technology for PFAS. Kim et al. (2020) investigated the oxidative ability of iron-EC for PFOA mitigation and reported removal via direct electron transfer and oxidant generation using high current loading and long electrolysis times. Oxidation

mechanisms were verified by measuring final transformation products including formate (a byproduct of organic oxidation), fluoride (a byproduct of PFAS defluorination), and short-chain PFAS (indicative of long-chain PFAS degradation into shorter chain compounds) (Kim et al., 2020). The transformation product analyses indicated that shorter chain PFAS (perfluoropentanoic acid [PFPeA, C5], perfluorohexanoic acid [PFHxA, C6], and perfluoroheptanoic acid [PFHpA, C7]) were produced via the oxidation of PFOA (Kim et al. 2020). Only 20% defluorination was achieved after 6 hours of electrolysis at a high current density of 40 mA/cm^2 (Kim et al. 2020). The PFOA removal rate was independent of solution pH, which may open up opportunities for EC as an oxidative process during drinking water treatment at neutral conditions (rather than acidic Fenton oxidation conditions of pH 3-4).

For hybridized EC systems such as EC:H_2O_2, destructive and non-destructive treatment has been shown using the combination of high radical promotor doses and long electrolysis times(Li et al., 2021; Singh et al., 2021; Yang et al., 2016a). For PFAS treatment, the addition of H_2O_2 or other radical promotors such as peroxymonosulfate (PMS) improved PFAS removal when treating elevated PFAS concentrations (i.e., 5 - 100 mg/L) using high doses of radical promotors (e.g., 0.66 – 1.7 g/L H_2O_2 (Yang et al., 2016a), 1.7 g/L H_2O_2 (Singh et al., 2021), and 5.6 g/L PMS (Li et al., 2021)). For example, Li et al. (2021) reported 87% PFOS defluorination in 60 min of EC:PMS. In these point-of-concept studies, however, the PFAS concentrations tested were greater than common PFAS concentrations in water and wastewater streams and the amount of radical promotors applied exceeded doses applied for treatment in the real systems (e.g., 5 to

20 mg/L H_2O_2 for UV-advanced oxidation processes in water and wastewater) (Howe et al., 2012; Miklos et al., 2018). Accordingly*, Chapter 5* aims to understand EC:H_2O_2 for PFAS mitigation, by using lower, more realistic H_2O_2 doses for lower PFAS concentrations that may be more representative for water, wastewater, and industrial waters relative to the mg/L levels tested in the aforementioned studies.

2.6.3. Potential Limitations and Research Gaps for Electrocoagulation Implementation

Although EC can be advantageous for PFAS mitigation, potential barriers to implementation need to be considered, including sludge generation and management, long-term electrode quality and electrode passivation, and secondary contamination due to metal release from the electrode alloys (Garcia-Segura et al., 2017). Existing EC studies for PFAS utilized long electrolysis times that may result in sludge generation exceeding typical sludge generation during coagulation processes. Additionally, EC uses sacrificial electrode materials that deteriorate over time, and the efficiency of coagulant generation may be inhibited by electrode passivation. Electrode passivation may be minimized by using polarity reversal, mechanical cleaning, and other techniques summarized by (Ingelsson et al., (2020). Lastly, the electrodes used during EC may potentially be a secondary source of metal contamination depending on the alloys used. For example, manganese is common in steel alloys, causing it to co-dissolve with iron during EC (manganese is regulated at 50 µg/L in the U.S. EPA's National Secondary Drinking Water Regulations) (Zhang and Cheng, 2007). Aqueous zinc may similarly impede zinc-EC. However, Lin et al. (2015) found that the final aqueous zinc

concentration in EC-treated samples was 0.88 mg/L, which falls below the 5.0 mg/L U.S. EPA secondary standard.

More research is needed to assess EC performance in environmental source waters containing NOM, low conductivity, and lower PFAS concentrations (i.e., ng/L - µg/L) to better simulate real drinking water treatment conditions. For example, high contaminant concentrations may add bias in experimental design by causing sorption-based processes to proceed at faster rates, resulting in higher removal than would occur in drinking water scenarios with lower PFAS concentrations (Lin et al., 2015). Micelle/hemi-micelle formation (i.e., the aggregation of surfactants [including PFAS]) may also lead to enhanced sorption. The critical micelle concentration for PFAS has been reported in g/L conditions; however hemi-micelles have been speculated to form at concentrations orders of magnitude less than the critical micelle concentrations (e.g., mg/L PFAS levels, similar to concentrations used in studies discussed in this chapter). The initial PFAS concentration may also govern the contribution of physical removal (non-destructive) versus redox removal (destructive removal) during EC. For example, using a lower initial PFAS concentration than other EC studies (10 mg/L vs. 100 to 200 mg/L; Table 2.1), Kim et al. (2020) observed oxidation-based PFAS removal rather than the sorption-based removal observed in the non-destructive EC studies.

Additionally, research is needed to understand the impact of NOM on EC treatment of contaminants such as PFAS to more fully understand potential challenges associated with different source waters, such as varying levels and characteristics of

NOM, electrolyte compositions, and water matrix pH conditions – all of which can impact treatment performance.

2.7. The Role of Natural Organic Matter on Electrochemical Treatment

For emerging treatment processes to translate to full-scale, research is needed to validate performance in a range of environmental source waters, including variations in NOM. NOM is ubiquitous in environmental waters and serves as the prominent precursor for DBP formation and can serve as an oxidation scavenger to impede drinking water treatment performance. Accordingly, the impact of different NOM sources was evaluated in *Chapter 3* with respect to DBP mitigation. In terms of the fate of TOrCs, such as PFAS, NOM may also co-dissolve PFAS and enhance mass transfer to the electrode, thereby improving removal during EC. For non-destructive treatment, NOM improved PFAS adsorption via granular activated carbon due to the formation of PFAS-NOM complexes that were more amenable to adsorption (Kothawala et al., 2017). Other studies reported that NOM inhibited PFAS removal via sorption due to competition for sorption sites (Gagliano et al., 2020; Yu et al., 2012). Accordingly, the impact of NOM on TOrC and PFAS mitigation remains unclear and more research is needed to understand how NOM characteristics influence PFAS mitigation in electrochemical treatment processes. The NOM-based research gaps were investigated as part of *Chapter 4* and *Chapter 5*.

However, NOM is generally managed using a black-box-approach whereby only overall DOC removal is quantified. This approach disregards unique characteristics of

NOM including physicochemical properties, molecular weight, and reactivity. These characteristics are related to evaluating DBP formation, scavenging trends, and NOM removal trends during treatment (Hua and Reckhow, 2007; Ishii and Boyer, 2012; Matilainen and Sillanpää, 2010). Thus, more research is needed for evaluating how emerging water treatment processes and assess how these treatment approaches can: remove different fractions of NOM. Additional research needs include identifying which NOM components have the largest impact on treatment performance and understanding which NOM components form DBPs and potentially react with TOrCs and PFAS. Accordingly, these findings can guide the selection of water treatment processes for NOM mitigation to improve TOrC mitigation and limit DBP formation. These data can be gathered using NOM characterization techniques (ultraviolet spectroscopy, fluorescence spectroscopy, and molecular size distribution).

2.7.1. NOM Characterization Techniques

The use of NOM characterization techniques such as optical and size fractionation techniques can inform process selection and design. Optical techniques are effective for characterizing chromophoric components of NOM as the measurement is generally rapid and requires minimal sample preparation. UV_{254} is the wavelength of light most heavily absorbed by aromatic compounds. Additionally, specific ultraviolet absorbance (SUVA, the UV_{254} divided by the total dissolved organic carbon content) is effective for analyzing the overall aromaticity per unit carbon. Weishaar et al., (2003) validated SUVA by verifying the aromaticity of NOM isolates from natural waters using

^{13}C nuclear magnetic resonance data, then comparing aromatic content to SUVA which yielded a correlation of $R^2 = 0.97$ (Weishaar et al., 2003).

However, optical techniques bear limitations that need to be considered. Optical techniques can only be used to characterize and understand chromophoric DOM (referred to here as C-DOM), and do not directly provide information for non-chromophoric DOM constituents (NC-DOM). This can be an issue for understanding NOM in a general sense as bulk NOM is comprised of C-DOM and non-chromophoric DOM (NC-DOM). C-DOM has double bonds and aromatics, which absorb light and fluoresce in optical techniques. In contrast, NC-DOM does not contain chromophoric functional groups that can be detected using optical techniques. Therefore, less is known about the chemical composition of NC-DOM and the role of C-DOM is generally overrepresented in the literature (Zhang et al., 2021; Zhou et al., 2016). NC-DOM is generally speculated to contain low molecular weight organics like alkanes and carboxylic acids which contribute to low-SUVA waters (Thurman, 1985). Accordingly, some understanding of NC-DOM can be garnered by quantifying the NOM size distribution and the C-DOM in the fractions. Accordingly, ultrafiltration size fractionation techniques were utilized in this work to better understand how specific size ranges impact treatment performance in *Chapter 5*.

2.8. Conclusions and Research Gaps

The overarching goal of this dissertation research was to assess EC as a treatment technology for a range of contaminants and the role of water matrix

components, namely NOM on process performance. This was investigated through three main research objectives, which are presented in chapters 3 through 5. *Chapter 3* focuses on EC as a DBP mitigation technology. *Chapter 4* describes the evaluation of the hybridized EC:H_2O_2 process for TOrC mitigation. Lastly, *Chapter 5* presents an evaluation of EC:H_2O_2 as a multi-mechanistic removal technology for PFAS.

Generally, EC has been shown to be effective for DOC removal, however no studies have directly compared the performance of EC to conventional coagulation technology with respect to DBP generation after treatment. *Chapter 3* aims to fill this research gap by not only evaluating the TTHM yield following treatment, but also evaluating the treatment efficacy of EC for a range of laboratory and real-world NOM sources and their corresponding DBP yield. These data can be beneficial for the water engineering field as they analyze EC in the context of drinking water treatment of surface waters. Additionally, the comparative analysis between EC and conventional coagulation provides a benchmark for EC in comparison to conventional processes, where EC has an added benefit of *in-situ* coagulant generation that can be advantageous for small treatment systems, remote water treatment processes, and decentralized treatment. Beyond DBP mitigation, EC-based processes may be of interest for mitigating other contaminants, including TOrCs such as PFAS.

EC:H_2O_2 has previously been shown to be effective for wastewater and industrial source, however no studies have assessed EC:H_2O_2 as a drinking water treatment technology. The aim of *Chapter 4* was to fill this gap and assess the potential oxidant generation in EC:H_2O_2 at neutral pH water treatment conditions for synthetic drinking

water sources and real-world water matrices under varying H_2O_2 doses and electrolysis times. Oxidation was assessed via removal of para-chlorobenzoic acid (pCBA) as a common hydroxyl radical probe, and pathway experiments were conducted to gauge the simultaneous non-destructive and destructive removal pathways. Finally, research is needed on the E_{EO} to provide a point of comparison to other AOP processes in the literature. The hypothesis was that EC:H_2O_2 may be practical for water treatment as the Fe^{3+} produced following oxidation via H_2O_2 can participate in coagulation and flocculation processes and remove bulk organics (e.g., NOM) and turbidity. The results inform whether EC:H_2O_2 is a process capable of simultaneous treatment of bulk and trace organics within a single unit process for source water treatment.

Following the TOrC oxidation pathway assessment in *Chapter 4*, the central goal of *Chapter 5* was to evaluate the potential PFAS removal pathways occurring during EC:H_2O_2. EC:H_2O_2 experiments were initially conducted at neutral pH conditions to match system parameters in *Chapter 4* and were then conducted at pH 3 conditions to compare to Fenton studies and other EC:H_2O_2 studies. PFAS mitigation pathways were assessed by a series of control experiments to isolate the potential system contributions that can promote destructive and non-destructive PFAS mitigation. The influence of NOM on PFAS mitigation as a function of different NOM characteristics including optical properties and molecular weight distribution of different sources was also assessed as NOM is sparsely considered in PFAS research to date. This research is one of a limited number of studies to examine the impact of a range of NOM sources and NOM characteristics, and the only study to assess the impact of NOM on PFAS mitigation

during EC:H_2O_2. The results can better inform future implementation of EC:H_2O_2 as a combined destructive and non-destructive technology for PFAS mitigation.

CHAPTER 3. IRON-ELECTROCOAGULATION AS A DISINFECTION BYPRODUCT MITIGATION STRATEGY FOR DRINKING WATER TREATMENT

This chapter was published as:
Ryan, D.R., McNamara, P.J., Mayer, B.K., 2020. Iron-electrocoagulation as a disinfection byproduct control strategy for drinking water treatment. Environ Sci: Water Res Technol 6, 1116–1124. https://doi.org/10.1039/D0EW00106F
It is included here with modification to satisfy dissertation requirements.

3.1. Introduction

Small drinking water systems, i.e., utilities that serve 10,000 people or fewer, comprise approximately 90% of total drinking water systems in the United States (U.S.) (Environmental Protection Agency (EPA), 2011; Goodrich et al., 1992). Small drinking water systems may have innate disadvantages in providing clean drinking water compared to larger drinking water systems due to smaller utility staff numbers, less consumers and taxpayers leading to lower budgets, less access to technical expertise, and high transportation cost due to more remote locations (Allaire et al., 2018; Charrois et al., 2004). These challenges may heighten difficulties in maintaining daily treatment plant operation, which can increase violations of the U.S. Environmental Protection Agency's (EPA's) Disinfectants and Disinfection Byproducts Rule relative to larger municipal treatment operations (Allaire et al., 2018; Charrois et al., 2004). Nationwide trends from 1982 to 2015 for health-based water quality violations indicate that disinfection byproducts (DBPs) are a common violation of the U.S. EPA's Safe Drinking Water Act (Allaire et al., 2018). Accordingly, small drinking water systems treating

surface water in rural areas may be at elevated risk of DBP-related water quality violations (Allaire et al., 2018; Charrois et al., 2004).

DBPs are chronically toxic compounds formed in drinking water treatment plants and water distribution systems due to reactions between oxidizing disinfectants, e.g., free chlorine, and DBP precursors such as natural organic matter (NOM). The potential risks associated with DBPs include increased cancer risk, birth defects, miscarriage, and antibiotic resistance (Lv et al., 2014; Richardson and Ternes, 2018; Wright et al., 2017). Over 600 different DBPs have been identified in drinking water, though a large fraction of the total organic halogens potentially formed remain largely unidentified (Mayer and Ryan, 2017; Richardson and Ternes, 2018; Weinberg et al., 2002). Trihalomethanes (THMs) are the most commonly formed class of DBPs (Richardson et al., 2007). Although THMs are not the most toxic compared to other DBP compound classes, they have been correlated to other nonregulated DBPs that bear greater toxicity potency, such as haloacetonitriles and haloketones (Guilherme and Rodriguez, 2017; Mercier Shanks et al., 2013). Accordingly, THM monitoring is important as an indicator of overall DBP-associated water toxicity.

Three different strategies are used to mitigate DBPs: i) using lower free chlorine doses, ii) using alternative disinfectants, and iii) removing DBP precursors prior to disinfection. Limiting free chlorine may cause utilities to no longer be in compliance with required *Ct* disinfection credits set by the U.S. EPA's Surface Water Treatment Rule. Using alternative disinfectants, such as chloramines, chlorine dioxide, and ozone may impart additional treatment costs, chemical supply and storage requirements, and

require more specialized operation and maintenance expertise. Removal of DBP precursors could be an attractive option for small drinking water systems as this approach decreases the amount of NOM available to react with free chlorine both within the water treatment facility and in the subsequent distribution system.

Guilherme and Rodriguez (2014) reported that a lack of DBP precursor control prior to chlorination was the primary factor leading to higher DBP occurrence in small drinking water systems. Most treatment operations for small drinking water systems include sand filtration followed by chlorination (Jones et al., 2018). However, removal of DBP precursors using sand filtration is generally not as effective as coagulation processes (particularly enhanced coagulation, which targets DBP precursor removal via increased coagulant dose and/or decreased pH, and is considered a best available technology for DBP mitigation) (Environmental Protection Agency (EPA), 1999; Kastl et al., 2004). For example, Collins et al. (1992) reported approximately 15% removal of dissolved organic carbon (DOC) by sand filtration, whereas coagulation may achieve up to 50% removal (Crittenden et al., 2012). Small drinking water systems may not commonly implement coagulation due to operational requirements such as coagulant storage, alkalinity consumption, preliminary and post treatment pH control, and transportation of materials.

Electrocoagulation (EC) may serve as a suitable option for DBP precursor removal for small drinking water systems. In EC, coagulants are generated *in situ* by the electrolysis of anode materials such as aluminum or iron. On-site generation of coagulants using EC may mitigate unique challenges faced by small drinking water

systems by decreasing costs associated with pH control, transportation, and coagulant storage (although there are electrical energy costs associated with electrolysis). Another potential benefit is that EC doses only the metal coagulant without adding additional salts. Through a combination of physical and oxidation-based removal processes, EC has also been shown to treat different classes of drinking water contaminants such as viruses, estrogenic organic compounds, and heavy metals (Heffron et al., 2019a, 2016; Maher et al., 2019).

EC has been evaluated as a DBP precursor (i.e., DOC and NOM) removal strategy (Ben-Sasson et al., 2013; Dubrawski and Mohseni, 2013c, 2013d; Ulu et al., 2014; Vik et al., 1984). For example, early EC research by Vik et al. (1984) showed similar performance relative to conventional coagulation in treating aquatic humus, a form of NOM and DBP precursor material. More recently, McBeath et al. (2020a) used continuous flow pilot-scale EC to treat DOC in a small drinking water system. The study determined that EC can be an effective drinking water treatment technology based on reductions in DBP precursor parameters such as DOC and UV_{254}. However, no studies have assessed the DBP formation potential following EC treatment for drinking water. Monitoring DOC removal alone may not fully demonstrate DBP mitigation because the residual DBP precursors may have varied affinity for DBP production during chlorination across different NOM sources. Additionally, DOC is not explicitly regulated by current U.S. EPA drinking water regulations. Accordingly, work is needed in quantifying the DBP formation potential following EC to more fully understand the extent to which this process can serve as a DBP mitigation strategy to attain regulatory compliance.

The goal of this research was to evaluate the performance of iron-EC to remove DBP precursors in model and actual surface waters and subsequently decrease DBP formation potential. Bench-scale experiments were conducted to assess total trihalomethane (TTHM, the sum of the four trihalomethane species) formation potential resulting from chlorination of DBP precursors remaining after EC. DBP precursor removal resulting from varying EC electrolysis times and water pH was evaluated. The influence of different NOM sources was assessed as different compositions of DBP precursors may be more or less resistant to coagulation treatment and react variably with free chlorine. Iron-based conventional coagulation experiments were conducted in parallel to compare EC against conventional coagulation for reductions in TTHM formation potential.

3.2. Materials and Methods

3.2.1. Water Matrices

A model river water was designed to simulate surface waters based on water quality parameters for the Mississippi River, as described previously (Heffron et al., 2019c). This matrix contained high concentrations of organic matter and low conductivity, as shown in Table 3.1, representing a challenging water matrix for small drinking water systems to treat with respect to DBP production due to high levels of DBP precursors (Environmental Protection Agency (EPA), 2011). In separate NOM spiking experiments, three different laboratory-grade NOM sources were used to prepare three different model river water matrices for NOM comparison experiments:

humic acid sodium salt (humic acid, technical grade, Sigma Aldrich), Suwannee River fulvic acid standard II (SR-fulvic acid, International Humic Substance Society, St. Paul, MN), and Suwannee River natural organic matter (SR-NOM, RO isolate, International Humic Substance Society). All solutions were prepared by dissolving NOM in Milli-Q water and verifying the initial DOC concentration.

Table 3.1. Water quality parameters.

Water Matrix	Alkalinity, mg/L as $CaCO_3$	Chloride, mg/L	DOC, mg-C/L	Bromide, mg/L	Initial pH	Conductivity, µS/cm
Model River Water [a]	120 [b]	12 [c]	5 (9) [d]	0.1 [e]	6 – 8.3	265 – 305 [f]
Buffered Model River Water [a,g]	360 [b]	12 [c]	5 [d]	0.1 [e]	9.1	725
Milwaukee River Water	300	80	9.1	ND [h]	6 - 8.70	730 – 795 [f]

[a] All model waters were prepared in Milli-Q water.
[b] Dosed using sodium bicarbonate (ACS grade, Fisher Scientific, Hampton, NH) or sodium carbonate (>99%, Sigma Aldrich, St. Louis, MO).
[c] Dosed using potassium chloride (ACS grade, Fisher Scientific).
[d] Dosed as humic acid sodium salt, Suwannee River fulvic acid, or Suwannee River natural organic matter. In a subset of tests, an elevated DOC concentration (9 mg-C/L) was used to provide more direct comparison against the Milwaukee River Water.
[e] Dosed using sodium bromide (>99.00%, ACS Grade, Sigma Aldrich).
[f] Conductivity increased following pH adjustment with sulfuric acid (the higher conductivity values are for the water matrix at pH 6. Changes in conductivity and pH did not affect the overall faradaic efficiency (Table A3.1).
[g] A subset of tests were conducted using buffered model river water containing equimolar carbonate and bicarbonate (CO_3^{2-} = HCO_3^- = 2.38 mM) to minimize the influence of pH changes during the treatment processes and to assess process performance at high pH.
[h] ND = Not detected using a Dionex ICS-1100 ion chromatograph (ThermoFisher Scientific, Waltham, MA).

A buffered model river water was tested in a subset of tests in order to minimize the influence of decreased pH following coagulant addition in conventional coagulation tests. Under these buffered conditions, water pH following addition of the conventional coagulant was 9.1; thus, direct comparison EC tests were performed at this buffered water pH.

Real river water samples were also collected from the Milwaukee River (43°04'58.8"N, 87°53'32.4"W) for testing. Milwaukee River water was sampled in 2 L borosilicate glass bottles baked at 550°C and foiled and sealed prior to sampling. Tests of laboratory-grade water showed no measurable DOC from the sampling event.

Specific ultraviolet absorbance (SUVA) was measured to determine the degree of NOM aromaticity (>3 L/mg-m indicates high aromaticity) (Weishaar et al., 2003). The SUVA values were 9.21, 4.15, 3.33, and 3.56 (L/mg-m) for humic acid, Suwannee River (SR)-fulvic acid, SR-NOM, and Milwaukee River NOM, respectively.

3.2.2. Electrocoagulation and Conventional Coagulation Batch Experiments

All experiments were conducted in triplicate in 250 mL Berzelius beakers without a spout. Iron electrodes (1020 steel, Vmetals, Milwaukee, WI) were used as the anode and cathode for EC experiments. Electrodes were sanded prior to each experiment with 320 grit sandpaper to remove rust and provide an even electrode surface during electrolysis. The electrodes were then rinsed with water and pretreated by running electrolysis at 5.55 mA/cm^2, as described previously (Heffron et al., 2019c). Using the pretreated electrodes, EC was performed at a current density of 5.55 mA/cm^2 (current =

75 mA, surface area = 13.5 cm^2 each, and charge loading rate = 22.5 Coulomb/L-min). These electrolysis conditions provided a theoretical iron dosing rate of 6.4 mg-Fe/L-min. The faradaic efficiency of the iron electrodes and experimental parameters used in this work was greater than 83% (Table A3.1), which is similar to the faradaic efficiencies reported in other iron-electrocoagulation studies (Dubrawski et al., 2015; Dubrawski and Mohseni, 2013d). Faradaic efficiency can impact EC performance, e.g., residual iron and potentially DBP formation, due to complex interplays of chemical speciation, local pH, and redox reactions involving dissolved oxygen (Dubrawski et al., 2015). Tests were run with constant mixing (100 rpm or G = 99 s^{-1} using a magnetic stir bar) for varying electrolysis times depending on the target iron dose. After electrolysis, reactors were flocculated by mixing for 10 minutes at 40 rpm (G = 25 s^{-1}) followed by 10 minutes at 20 rpm (G = 9 s^{-1}). The contents were then settled for 20 minutes, as described elsewhere (Volk et al., 2000).

All conventional coagulation experiments were conducted with either ferric sulfate (81%, J.T. Baker, Phillipsburg, NJ) or ferrous sulfate (86-89%, Amresco, Dallas, TX) in the same test water as EC experiments. Conventional coagulation doses were set at approximately 35 mg-Fe/L to match theoretical EC iron doses (as determined through the tests shown in Figure 3.1).

3.2.3. Total Trihalomethane Formation Potential

Following EC and conventional coagulation tests, effluent water was analyzed for TTHM formation potential. The samples were dosed with chlorine (10 – 15% reagent grade sodium hypochlorite, Sigma Aldrich) to form DBPs. A relatively high dose of 3 mg-Cl_2/mg-C of initial DOC was used (similar to other DBP studies (Hand et al., 1995; Kim and Yu, 2007; G Kleiser and Frimmel, 2000)) to maximize TTHM formation potential as opposed to simulating levels of residual disinfectant (Sarathy and Mohseni, 2010). The chlorinated samples were incubated for 48 hours at ambient temperature prior to TTHM analysis (Kim and Yu, 2007; Kleiser and Frimmel, 2000). After incubation, residual chlorine concentrations were measured to verify that free chlorine remained in excess relative to DBP precursors, i.e., that maximum TTHMs formed. Samples were then quenched with ascorbic acid, in accordance with U.S. EPA Method 524.4 (75 mg ascorbic acid per 40 mL of sample) and analyzed for TTHMs.

Specific TTHM formation potential was calculated by normalizing TTHM formation potential to the amount of DOC remaining after treatment to provide a better understanding of the reactivity of each type of NOM (and the fraction remaining after EC) with free chlorine with respect to DBP yield.

3.2.4. Analytical

DOC samples were filtered through a 0.45 µm PTFE syringe filter (Agela Technologies, Wilmington, DE) and acidified with HCl prior to analysis using a Shimadzu TOC V_{CSN} analyzer (Kyoto, Japan), in accordance with U.S. EPA Method 415.3.

Absorbance at 254 nm (UV_{254}) was measured using a Genesys 10UV Spectrophotometer (ThermoFisher Scientific).

TTHMs were sampled and measured in accordance with U.S. EPA Method 524.4 using a gas chromatograph–mass spectrometer (GC-MS 5977A) (Agilent Technologies, Santa Clara, CA) equipped with a GS-GASPRO column (60 m, 0.32 mm) (Agilent Technologies). The purge and trap concentrator was a DL016 Lumin (Teledyne Tekmar, Mason, OH). EPA 501/601 trihalomethanes calibration mix (reference grade, Sigma Aldrich) was used for TTHM quantification and calibration curves. Fluorobenzene (>99.7, Sigma Aldrich) was used as the internal standard for TTHM quantification based on U.S. EPA Method 524.4. Amber sample vials were used for all DOC and TTHM samples. TTHM samples were stored in headspace-free vials. All vials were acid washed in 5% HCl for a minimum of 12 hours, triple-rinsed with deionized water, and baked at 550°C prior to sampling and analysis.

Total iron was measured using Hach (Loveland, CO) FerroVer® Method 8008. Soluble iron samples were measured using a 7700 series inductively coupled plasma-mass spectrometer (ICP-MS) (Agilent Technologies) following filtration through a 0.45 µm PTFE syringe filter and acid digestion in a solution containing 2% HNO_3 and 0.5% HCl. Free chlorine was measured using the DPD method (Hach Method 8021). Chloride was measured using silver nitrate titration (Hach Model 8-P). Alkalinity was measured using titrimetric methods (Hach Model 2443-89). Water pH was measured using an Orion 4 Star pH meter (ThermoFisher Scientific). The water matrix conductivity was measured with a VWR® Pure H_2O Tester (Radnor, PA). Bromide in the Milwaukee River water

sample was measured using an ion chromatograph (ICS-1100, ThermoFisher Scientific) in accordance with U.S. EPA Method 300.00.

3.2.5 Statistical Analysis

Differences in DOC and TTHM formation potential levels were analyzed using one-way and two-way ANOVA performed using GraphPad Prism7 software. Following significant ANOVA results, Tukey's multiple comparison test was conducted to assess differences between each condition. The significance level of all tests was $\alpha = 0.05$.

3.3. Results and Discussion

3.3.1. Total Trihalomethane Formation Potential following Electrocoagulation

EC treatment at lower initial pH reduced TTHM formation potential for the model river water matrix containing humic acid (Figure 3.1). Additionally, at lower initial pH conditions (i.e., pH 6 and 7), lower iron doses were needed to achieve TTHM mitigation (targeting <80 µg/L TTHM, as specified by the U.S. EPA). These findings align with enhanced coagulation studies in which precursor removal and subsequent TTHM mitigation improved under lower pH conditions (Kastl et al., 2004; van Leeuwen et al., 2005). Notably, for an initial pH of 8.3, EC increased solution pH to 9; however, EC did not increase solution pH relative to no-electricity controls for initial pH levels of 6 and 7 (Figure A3.1).

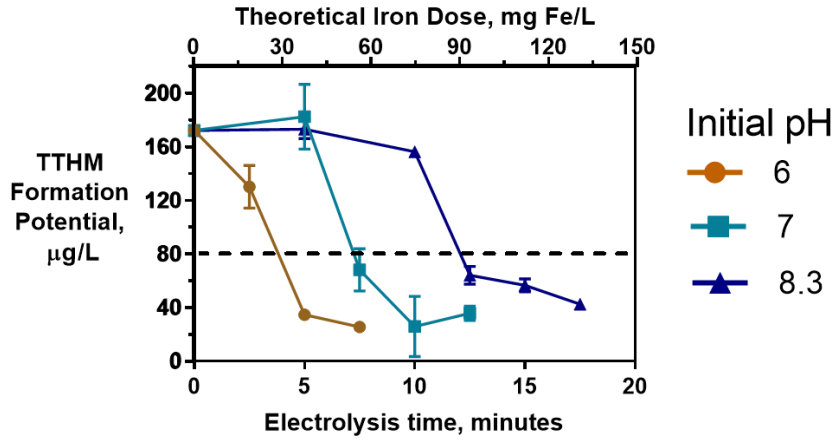

Figure 3.1. 48-hour total trihalomethane (TTHM) formation potential following electrocoagulation of model river water at different initial pH conditions and electrolysis times (corresponding to theoretical iron dose, as shown on the secondary x-axis). The dashed line indicates the U.S. EPA TTHM maximum contaminant level of 80 µg/L. The initial dissolved organic carbon was approximately 5 mg-C/L, dosed as humic acid sodium salt. Error bars show ±1 standard deviation of triplicate experiments.

Treatment of pH 6 water decreased TTHM formation potential more efficiently relative to pH 7 and 8.3. Specifically, higher coagulant doses (>50 mg-Fe/L), i.e., longer electrolysis times, were needed to reduce TTHM formation potential at elevated pH. Higher coagulant doses can yield higher residual iron concentrations and more sludge production, which may reduce treatment process feasibility for small drinking water systems due to residuals management. For example, the total iron residual following EC ranged from 4.6 to 5.8 mg-Fe/L for pH 6 and 8.3 conditions, which exceeds U.S. EPA secondary standards (0.3 mg-Fe/L). However, virtually all of the residual iron was in the particulate form, with very little in the soluble form (0.005 – 0.035 mg-Fe/L, Table A3.2). Residual particulate iron may be more manageable for treatment operations as it is more susceptible to particle separation processes. Accordingly, EC may require

additional optimization with respect to coagulant dosing, particle separation processes, and flocculation steps to minimize residual iron.

Solution pH impacts many factors associated with TTHM formation potential, including iron solubility, floc surface charge, NOM acid-base chemistry, chlorine reactivity with NOM, and charges associated with ionic water constituents. NOM contains carboxylic and hydroxide functional groups that can have complexation reactions with iron hydroxides (Gu et al., 1995). Additionally, adjusting solution pH to lower initial levels drives the pH closer to the pKa range for carboxylic acids (4 to 5), which increases the fraction of non-dissociated carboxylic acid species (Drever, 1982). This protonated form of NOM may be more susceptible to coagulation. This removal trend is reflected in the improved TTHM mitigation observed at lower pH (Figure 3.1). Beyond improved TTHM precursor removal at lower pH, fewer TTHMs form at lower pH levels as TTHMs are formed via a base-catalyzed reaction (Hua and Reckhow, 2007).

Jasper et al. (2017) demonstrated that using mixed metal oxide electrooxidation to treat high-chloride wastewater produced TTHMs as well as other DBPs such as haloacetic acids and perchlorate. Additionally, EC treatment of landfill leachates containing high TOC (7,800 – 14,900 mg-C/L) and chloride (1797 – 6270 mg-Cl/L) can generate both regulated and non-regulated DBPs (Xu et al., 2020). However, in this study, all THM species were consistently below detection following EC treatment without post-chlorination. The chloride content of the model water was low (12 mg/L), so minimal free chlorine was generated following electrolysis (<0.07 mg-Cl_2/L, Table A3.2. Future work is needed to assess DBP production via electrochemical treatment of

drinking water source waters containing higher chloride levels, particularly given that groundwaters (which may contain elevated chloride levels) serve as a prominent supply for small and rural drinking water systems (Environmental Protection Agency (EPA), 2011; Goodrich et al., 1992).

3.3.2. Comparison of Total Trihalomethane Formation Potential after Electrocoagulation versus Conventional Coagulation

For comparison against EC, conventional coagulation was performed using 1) ferric sulfate (commonly used iron-based coagulant) or 2) ferrous sulfate (EC doses ferrous iron as a result of anode oxidation) (Lakshmanan et al., 2009). During EC and ferrous coagulation, ferrous iron is likely oxidized to ferric iron by dissolved oxygen. Since EC gradually doses ferrous iron throughout the electrolysis time, dissolved oxygen may be in excess to ferrous iron. This oxygen-to-ferrous ratio may promote the rate of ferrous oxidation to ferric iron, resulting in more ferric iron formation compared to ferrous-conventional coagulation (wherein coagulant is dosed immediately, resulting in a lower oxygen-to-ferrous ratio in comparison). While dissolved oxygen can influence coagulation processes, it was not directly manipulated or assessed in this study.

Comparison tests of EC and conventional coagulation were conducted using 35 mg-Fe/L as this was the lowest dose needed to achieve removal below the U.S. EPA's TTHM maximum contaminant level using EC (for an initial pH of 6, as shown in Figure 3.1). Two different initial pH scenarios were tested: 6 and 9.1. These two values were selected based on the pH following conventional coagulant addition in the model river

water: for the unbuffered (pH 6) and buffered waters (pH 9.1). These initial pH adjustments facilitated direct comparisons of TTHM mitigation by each process.

EC performed similarly to conventional coagulation with respect to TTHM formation potential, and pH was a strong driver of treatment efficacy in both processes (Figure 3.2). For water at an initial pH of 6, all coagulation treatments decreased TTHM formation potential to below the U.S. EPA TTHM maximum contaminant level. The TTHM formation potential resulting from EC and ferric conventional coagulation treatment was not statistically different when initial pH was 6 (Figure 3.2, $p = 0.96$). However, ferrous conventional coagulation treatment yielded higher overall TTHM formation potential ($p = 0.0011$), demonstrating that ferric-based coagulation is likely to result in better DBP mitigation compared to ferrous-based coagulation.

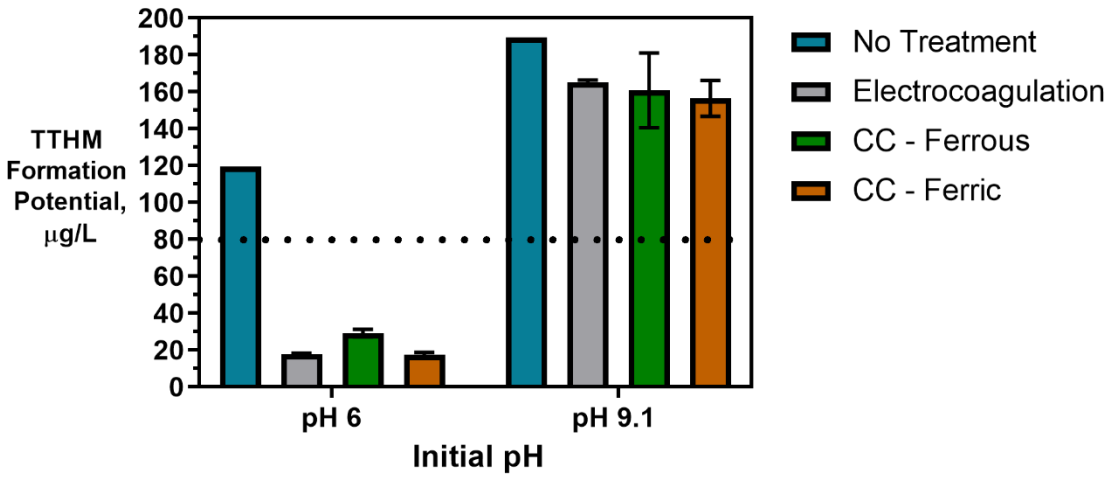

Figure 3.2. 48-hour total trihalomethane (TTHM) formation potential following electrocoagulation and conventional coagulation (CC) treatment of model river water with ferrous sulfate or ferric sulfate. The dashed line indicates the U.S. EPA TTHM maximum contaminant level of 80 µg/L. The pH 9.1 sample was buffered with $[CO_3^{2-}] = [HCO_3^-] = 2.38$ mM. The CC and theoretical electrocoagulation iron doses were approximately 35 mg-Fe/L. Error bars show ±1 standard deviation of triplicate experiments.

When pH was buffered at 9.1 using equimolar CO_3^{2-} and HCO_3^-, TTHM formation potential did not differ statistically among the three iron-based coagulation processes (Figure 3.2, p = 0.27). For initial pH 9.1, the TTHM formation potential was above the U.S. EPA TTHM maximum contaminant level for all processes tested. The increase in TTHM formation potential with increased pH may stem from less effective DOC removal under these conditions (Figure 3.3).

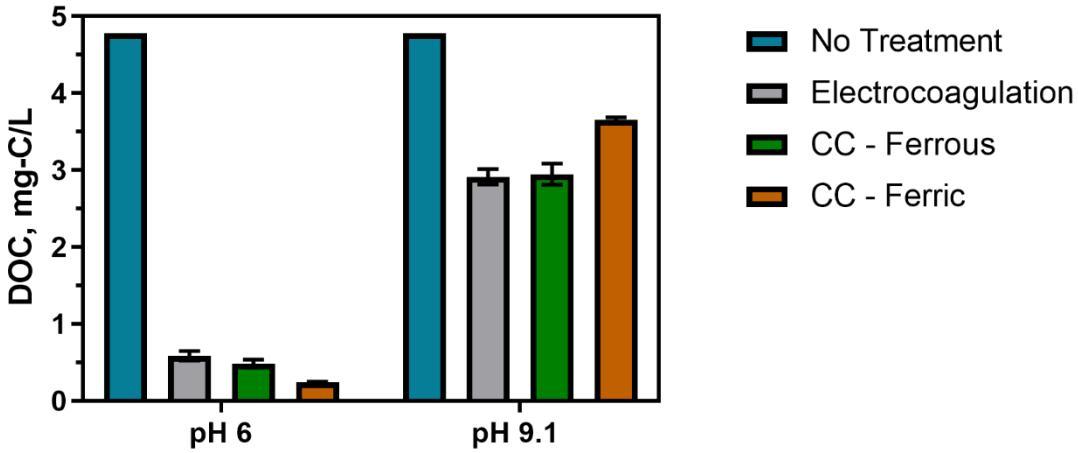

Figure 3.3 Dissolved organic carbon (DOC) remaining in model river water following electrocoagulation and conventional coagulation using ferric sulfate (CC – Ferric) or ferrous sulfate (CC – Ferrous) treatment at an initial solution pH of 6 and 9.1. The pH 9.1 sample was buffered with $[CO_3^{2-}] = [HCO_3^-] = 2.38$ mM. DOC was dosed as humic acid sodium salt. The CC and theoretical electrocoagulation iron doses were approximately 35 mg-Fe/L. Error bars show ±1 standard deviation of triplicate experiments.

3.3.3. The Impact of the Type of Natural Organic Matter on DBP Formation Potential in Electrocoagulation and Conventional Coagulation

3.3.3.1. NOM Source Precursor Removal and Total Trihalomethane Formation Potential Trends Following EC and Conventional Coagulation

EC and ferric conventional coagulation removed DOC for all NOM sources tested (Figure 3.1.a). Humic acid was removed most efficiently (>80%) compared to other NOM sources ($p < 0.05$). This trend agrees with prior studies wherein waters containing high-SUVA NOM (such as humic acid) were more susceptible to coagulation, while waters with lower-SUVA NOM (SR-fulvic acid, SR-NOM) experienced less DOC removal (55 – 70%) (Edzwald, 1993; Lavonen et al., 2015). The lowest DOC removal (approximately 30%) was observed for Milwaukee River NOM when compared to the other NOM sources at equivalent carbon concentrations (Figure 3.1.b). These differences may be attributed to the Milwaukee River NOM containing larger amounts of NOM constituents that are less susceptible to coagulation processes, such as hydrophilic functional groups (Sharp et al., 2006). Ferric-based conventional coagulation (used in lieu of the less common ferrous conventional coagulation (Crittenden et al., 2012)) removed significantly more DBP precursors than EC when treating SR-NOM and Milwaukee River NOM ($p = 0.0133$ and < 0.001, respectively). This improvement may be attributed to ferric-based coagulation adding coagulant instantaneously, leading to larger flocs (Lee and Gagnon, 2016), which may remove more DBP precursors. Alternately, EC steadily doses coagulant throughout the electrolysis period, which may slow floc formation. However, DOC removal was not significantly different for EC and ferric conventional

coagulation when treating humic acid and Suwanee River fulvic acid when the initial DOC was 5 mg-C/L ($p = 0.75$ and 0.33, respectively).

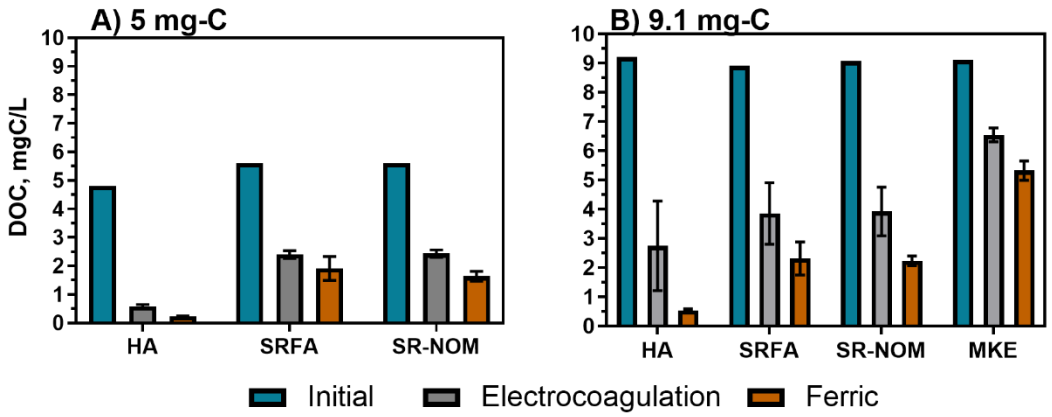

Figure 3.4. Dissolved organic carbon (DOC) following electrocoagulation and conventional coagulation (CC) using ferric sulfate treatment at an initial pH of 6. **A)** model river water containing an initial DOC concentration of approximately 5 mg-C/L for humic acid (HA), Suwannee River Fulvic Acid (SRFA), and Suwannee River NOM (RO isolate, SR-NOM); and **B)** model river water containing an initial DOC concentration of approximately 9.1 mg-C/L compared to the Milwaukee River (MKE). The CC and theoretical electrocoagulation iron doses were approximately 35 mg-Fe/L. Error bars show ±1 standard deviation of triplicate experiments.

The TTHM formation potential of the EC and ferric-conventional coagulation treatments were similar when treating the different NOM sources (Figure 3.5), with the exception of SR-NOM, which was better treated using conventional coagulation ($p = 0.013$ for 5 mg-C/L). EC and conventional coagulation decreased the TTHM formation potential for NOM sources to below the U.S. EPA TTHM maximum contaminant level when the initial DOC concentrations were approximately 5 mg-C/L (Figure 3.5a). For these conditions, coagulation treatments of humic acid yielded the lowest TTHM formation potential ($p < 0.05$). Following EC, TTHM formation potential for the SR-fulvic

acid and SR-NOM waters were not statistically different (p = 0.985 for 5 mg-C/L, p = 0.936 for 9.1 mg-C/L).

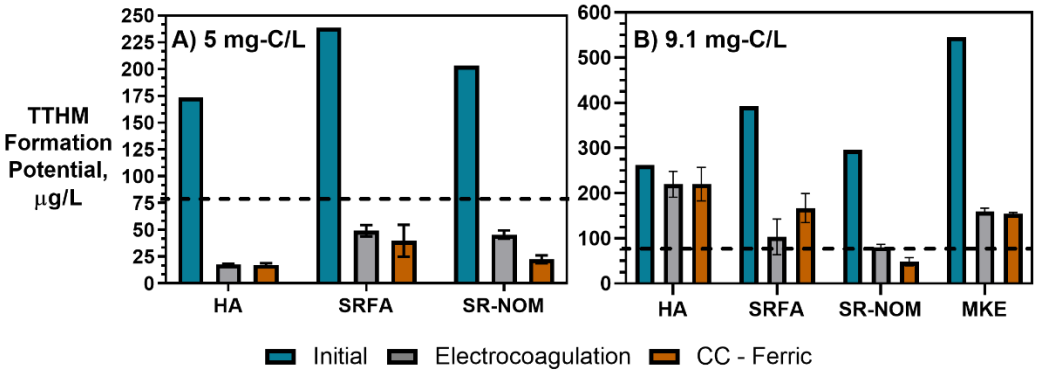

Figure 3.5 48-hour total trihalomethane (TTHM) formation potential following electrocoagulation and conventional coagulation (CC) treatment using ferric sulfate (initial pH 6) for **A)** model river water containing an initial DOC concentration of approximately 5 mg-C/L for humic acid (HA), Suwannee River Fulvic Acid (SRFA), and Suwannee River NOM (RO isolate, SR-NOM); and **B)** model river water containing an initial DOC concentration of approximately 9.1 mg-C/L compared to the Milwaukee River (MKE). The CC and theoretical electrocoagulation iron doses were approximately 35 mg-Fe/L. The dashed line indicates the total trihalomethane U.S. EPA maximum contaminant level of 80 µg/L. Error bars show ±1 standard deviation of triplicate experiments.

The natural water sample, collected from the Milwaukee River, contained 9.1 mg-C/L, and comparative tests were performed using the model waters spiked at the same DOC level using different NOM sources (Figure 3.5b). At these higher initial DOC levels, all NOM sources yielded TTHM formation potential above 70 µg/L after EC (and with the exception of ferric-conventional coagulation of SR-NOM, all were above the U.S. EPA TTHM maximum contaminant level of 80 µg/L). These differences indicate that increased treatment inputs, i.e., coagulant dose, would be needed for elevated NOM levels. Moreover, in the higher NOM tests, humic acid yielded the highest TTHM formation potential (whereas it produced the least for the 5 mg-C/L tests). This

contrasting trend may be attributed to the humic acid not effectively coagulating and flocculating, thus impeding TTHM mitigation. Figure 3.4 indicates that DOC removal was relatively high for the humic acid relative to other NOM sources. However, visual inspection of the sample indicated poor floc formation due to orange colored water with no visual precipitates (indicating the presence of non-settleable iron). This unfiltered humic acid sample was used for TTHM analyses, whereas the sample was filtered for DOC analysis, which seemed to remove the non-settleable iron particles, ostensibly complexed with DOC (adding additional DOC removal). Sharp et al. (2006) found that the humic fraction had a higher charge density (meq/mg-C) than fulvic and hydrophilic fractions, which would require higher coagulant doses for charge neutralization and subsequent removal of humic acid (and related TTHM mitigation) (Sharp et al., 2006). Considering the NOM sources tested here, SR-fulvic acid, SR-NOM, and Milwaukee River NOM may contain lower charge density NOM fractions that were more amenable to coagulation and flocculation using the coagulant dose applied.

3.3.3.2. Specific Total Trihalomethane Formation Potential Resulting from Different NOM Fractions

The mean specific TTHM formation potential decreased after EC for all NOM sources (Figure 3.6). Conventional coagulation generally decreased the specific TTHM formation potential of every NOM source except humic acid. The increase in specific TTHM formation potential after ferric conventional coagulation of humic acid may be attributed to the low amount of residual DOC remaining after treatment (Figure 3.4, 0.24 ± 0.01 mg-C/L for initial pH 6), which would increase the value of a normalized

parameter such as specific TTHM formation potential. Apart from this high value relative to others, the specific TTHM formation potential generally aligned with data from other studies focused on DBP mitigation by ferric coagulation, which ranged from 20 – 105 µg-TTHM/mg-C (Dotson et al., 2010; Gerrity et al., 2009; Kleiser and Frimmel, 2000; Liu et al., 2008; Zhao et al., 2013). The specific TTHM formation potential for the SR-fulvic acid NOM source was not statistically different from SR-NOM and Milwaukee River NOM for all coagulation treatments ($p > 0.1$). These similarities may indicate that the NOM fractions that are resistant to EC and conventional coagulation have similar chemical compositions and reactivity with free chlorine. The NOM fraction that is generally considered to be recalcitrant to coagulation treatment may be low molecular weight and hydrophilic functional groups (Tubi et al., 2013). These remaining fractions can serve as major DBP precursors (Liu et al., 2008; Mayer et al., 2014; Tubi et al., 2013; Wang et al., 2017).

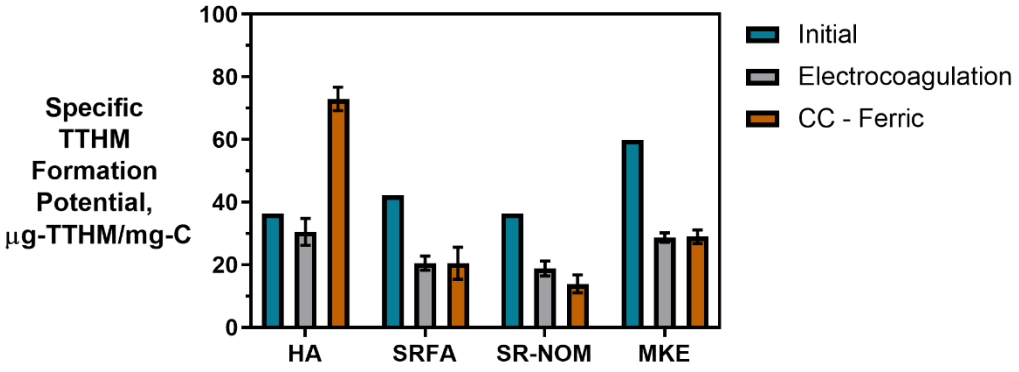

Figure 3.6. 48-hour specific total trihalomethane (TTHM) formation potential using electrocoagulation or chemical coagulation (CC) using ferric sulfate to treat different natural organic matter sources. The CC and theoretical electrocoagulation iron doses were approximately 35 mg-Fe/L. Initial DOC concentrations were approximately 5 mg-C/L for humic acid (HA), Suwannee River fulvic acid (SRFA), and Suwannee River NOM (RO isolate, SR-NOM). The initial concentration was 9.1 mg-C/L for Milwaukee River NOM (MKE). Error bars show ±1 standard deviation of triplicate experiments.

3.4. Conclusions

The goal of this study was to evaluate the performance of EC relative to conventional coagulation for the removal of DBP precursors and the corresponding TTHM formation potential. Overall, EC performed comparably to conventional coagulation with respect to TTHM mitigation. Thus, EC may be applicable as a DBP control strategy, particularly for small drinking water systems, where it offers advantages such as no storage or direct addition of coagulant, no alkalinity consumption, no post treatment pH control requirement, and no concurrent addition of salts. EC was able to treat model waters with a range of NOM sources to TTHM levels specified by the U.S. EPA's Disinfectants and Disinfectant Byproduct Rule when the initial DOC was 5 mg-C/L. However, the coagulant doses tested in this work (for both EC

and conventional coagulation) were not sufficient to treat waters with higher initial NOM levels (9.1 mg-C/L) to U.S. EPA TTHM standards.

Future work is needed to characterize the NOM remaining following coagulation treatment and the potential of other processes, such as electrochemical advanced oxidation, to remove these recalcitrant DBP precursors. The associated characterization data may provide information on the selective pressures electrochemical treatment imparts on NOM and how the residual fractions may influence post-treatment DBP production and speciation. Such aspects are important to consider in future practical implementation of EC technology.

CHAPTER 4. PEROXI-ELECTROCOAGULATION FOR SIMULTANEOUS OXIDATION OF TRACE ORGANIC COMPOUNDS AND REMOVAL OF NATURAL ORGANIC MATTER AT NEUTRAL PH

4.1 INTRODUCTION

Iron has expansive applications for water and wastewater treatment. Different iron-based treatment pathways proceed depending on the valence state of the iron (e.g., ferrous [Fe^{2+}] or ferric [Fe^{3+}]). Iron speciation varies as a function of pH and the presence of dissolved oxygen in water. Ferric iron predominates in the oxygen-rich neutral and basic pH conditions that are typical for water and wastewater treatment. During coagulation, iron is dosed as ferric chloride or ferric sulfate targeting removal of turbidity and natural organic matter (NOM) (Crittenden et al., 2012). Alternately, Fe^{2+} predominantly exists in acidic conditions, and can mediate oxidative treatment via Fenton's reaction, which produces hydroxyl radicals (HO•) that can oxidize trace organic compounds (TOrCs) (Fenton, 1894; Hug and Leupin, 2003; Pignatello et al., 2006). Accordingly, iron-based treatments typically feature *either* non-destructive removal or oxidative destruction due to dominant pathways under different pH conditions (Garcia-Segura et al., 2017). Research is needed to simultaneously promote both non-destructive and oxidative destruction pathways through Fenton's reaction at circumneutral pH for treating multiple classes of contaminants such as bulk organics (i.e., NOM) and TOrCs in a single unit process, which can be beneficial for water and wastewater treatment facilities.

Fenton's reaction relies on non-complexed Fe^{2+} and H_2O_2 as reagents to form HO• (Reaction 1, Table 4.1). Hydroxyl radicals are highly reactive (2.8 V vs. standard

hydrogen electrode) and can react with Fenton's reagents (Reactions 5 and 6) at faster rates (10^8 $M^{-1}s^{-1}$) than the radicals are generated (40 – 80 $M^{-1}s^{-1}$), which terminates Fenton's reaction due to oxidant and reagent depletion and hinders treatment effectiveness. However, in acidic conditions (pH 2 – 4), soluble Fe^{3+} can be recycled into Fe^{2+} (Reaction 2), thereby continuing HO• generation without reagent depletion.

Table 4.1. Fenton's reaction. Iron species are color-coded to reflect the valence state: blue represents ferrous iron (Fe^{2+}) and orange represents ferric iron (Fe^{3+}).

Reaction	Chemical Reaction	Role
1	$\mathbf{Fe^{2+}} + H_2O_2 \rightarrow \mathbf{Fe^{3+}} + HO^{\bullet} + OH^-$	Radical production
2	$\mathbf{Fe^{3+}_{(aq)}} + H_2O_2 \rightarrow \mathbf{Fe^{2+}} + HO_2^{\bullet} + H^+$	Ferrous regeneration via ferric reduction
3	$\mathbf{Fe^{2+}} + \frac{1}{4}O_2 + 2OH^- + \frac{1}{2}H_2O \rightarrow \mathbf{Fe(OH)_{3\,(s)}}$	Oxygenation of ferrous iron, reagent quenching
4	$\mathbf{Fe^{2+}} + HO^{\bullet} \rightarrow \mathbf{Fe^{3+}} + OH^-$	Radical quenching, reagent quenching
5	$H_2O_2 + HO^{\bullet} \rightarrow HO_2^{\bullet} + H_2O$	Radical quenching, reagent quenching

Reactions adapted from (Fenton, 1894; Fischbacher et al., 2017; Haber and Weiss, 1934; Pignatello et al., 2006; Pratap and Lemley, 1998; Stumm and Lee, 1961).

At the neutral pH conditions in water and wastewater treatment, the feasibility of Fenton's reaction is limited for several reasons:

1. Iron speciation shifts toward Fe^{3+}, which is less soluble and more prone to floc formation compared to Fe^{2+}, resulting in termination of the Fenton's reaction cycle by inhibiting regeneration of Fe^{2+} required for oxidant generation.
2. Dissolved oxygen readily oxidizes Fe^{2+} in neutral and basic pH conditions (Reaction 3). Each increase in pH unit increases the oxidation rate of Fe^{2+}

100-fold, leading to less available Fenton's reagents (Heffron et al., 2019b; Stumm and Lee, 1961).

3. Anionic ligands in natural waters (e.g., OH^- and CO_3^{2-}) form complexes with Fe^{2+}, which decreases the amount of non-complexed Fe^{2+} available to react with H_2O_2 to generate oxidants (Fischbacher et al., 2017).

Accordingly, pH limitations restrict Fenton applications to a narrow pH range (pH 2 – 4), which impedes implementation in water and wastewater treatment due to the intensive pH adjustments. Additionally, acidic waters can enhance corrosion of infrastructure and shift the pH of natural waters following discharge (Fischbacher et al., 2017).

To facilitate Fenton oxidation at neutral pH, the key premise relies on generating or stabilizing the Fe^{2+} needed to react with H_2O_2 to form HO•. Accordingly, electrochemical water treatment processes, such as electrocoagulation (EC), may be used for Fenton oxidation at neutral pH by generating non-complexed Fe^{2+} via anodic dissolution of iron electrodes (Lakshmanan et al., 2009). Continuous generation of Fe^{2+} can be advantageous for Fenton oxidation at neutral pH by minimizing the need for Fe^{3+} reduction to Fe^{2+} via H_2O_2 (Reaction 2). Prior research has also shown that EC alone can generate HO• to treat TOrCs through the *in-situ* generation of Fe^{2+} at the anode and H_2O_2 production at the cathode (Govindan et al., 2020b; Maher et al., 2019; Qian et al., 2019b). During electrolysis, the microenvironment near the anode surface is acidic (Chaplin, 2014). Accordingly, Fenton reactions may occur at the vicinity of the anode surface even if the bulk solution pH is circumneutral, potentially leading to oxidative

conditions at neutral pH between H_2O_2 and the iron anode surface. Supplemental addition of H_2O_2 as a radical promotor, known as peroxi-electrocoagulation (EC:H_2O_2), can further enhance EC's oxidizing capacity and serve as a multi-mechanistic process. During EC:H_2O_2, Fe^{2+} is continually generated at low concentrations (nM/s based on Faraday's law) over the course of electrolysis, such that non-complexed Fe^{2+} is available for oxidation by H_2O_2. As a result, less Fe^{2+} is "wasted" as a Fenton's reagent by non-radical generating side reactions such as ligand complexation or oxygenation (Lakshmanan et al., 2009). This combination of Fe^{2+} reagent generation and minimal reliance on Fe^{3+} reduction to Fe^{2+} can make EC:H_2O_2 an advantageous dosing method compared to *ex-situ* reagent dosing in Fenton applications.

Pratap and Lemley (1998, 1994) demonstrated point-of-concept use of EC:H_2O_2 for remediation of the herbicides atrazine and metalochlor at neutral pH conditions. Since the inception of EC:H_2O_2, research has primarily focused on coagulation/flocculation during industrial wastewater treatment for removing bulk organic pollutants (such as chemical oxygen demand) at high concentrations (mg/L levels) (Behin et al., 2015; Garcia-Segura et al., 2017; Ghanbari and Moradi, 2015a; Kumar et al., 2018; Vasudevan, 2014; Yazdanbakhsh et al., 2015a; Yüksel et al., 2009). However, these high-strength wastewater studies do not translate well to applications for municipal wastewater and drinking water treatment. For example, environmental waters have lower conductivity, fewer oxidant scavengers, higher dissolved oxygen, and neutral pH conditions, all of which impact the oxidative efficiency of EC:H_2O_2 and speciation of iron in water. Considering iron's treatment capabilities, EC:H_2O_2 may also

offer an opportunity for simultaneous treatment of TOrCs and bulk organics (e.g., NOM and chemical oxygen demand) in a single unit process as the Fe^{3+} produced following Fenton's reaction can subsequently contribute to physical removal (i.e., non-destructive removal) of contaminants through coagulation, flocculation, and sedimentation processes.

The goal of this research was to evaluate EC:H_2O_2 for simultaneous treatment of both TOrCs and NOM at neutral pH conditions. Para-chlorobenzoic acid (pCBA) was selected as the representative TOrC, and also served as a HO• probe for advanced oxidation process (AOP) effectiveness (Gerrity et al., 2012). The relative impacts of current density (i.e., iron dosing rate), H_2O_2 dose, and the corresponding $[H_2O_2]_{initial}/[Fe^{2+}]_{generated}$ ratio were tested in synthetic matrices. Experiments were conducted to differentiate non-destructive removal via EC-only from oxidative destructive removal and to assess the contribution of potential oxidants generated in EC:H_2O_2 such as HO• and H_2O_2. Experiments were also conducted using surface water, groundwater, and wastewater sources to evaluate the influence of water quality parameters (i.e., dissolved organic carbon [DOC], pH, conductivity, and ions) and the feasibility of EC:H_2O_2 for different treatment applications. Finally, electrical energy per order of magnitude reduction (E_{EO}) was calculated for all matrices to provide a means of comparing EC:H_2O_2 energy requirements relative to other advanced oxidation processes.

4.2 MATERIALS AND METHODS

4.2.1. Experimental Protocols for EC:H_2O_2 Tests of pCBA Removal

The EC:H_2O_2 batch experiments were conducted for 15 minutes of electrolysis with 150 rpm mixing (G = 180 s^{-1}) in 4 mM HCO_3^- buffer solutions containing 400 µg/L pCBA. Electrolysis was performed in 200 mL polypropylene beakers using 1020 steel iron electrodes (VMetals, Milwaukee, WI), which were sanded and wet polished with 320 grit silicon carbide sandpaper prior to experiments. An XPH 75-2D Dual DC power supply (Sorenson Electronics, Cedar City, UT) was used to carry out electrolysis at currents ranging from 40 mA to 200 mA through a submerged electroactive surface area of 13.5 cm^2, as described in Ryan et al. (2020). The power supply was equipped with a polarity reversal device to alternate the anode and cathode every 30 seconds based on prior works (Maher et al., 2018). For evaluating oxidative treatment, pCBA (99%, Sigma Aldrich, St. Louis, MO) was selected as the HO• probe due to the resistance to sorption on iron flocs and frequent use as a radical probe to demonstrate the treatability of TOrCs by HO• exposure (Gerrity et al., 2012; Pi et al., 2005; Rosenfeldt et al., 2006; Vanderford et al., 2007). Compared to other TOrCs, pCBA is classified as having "moderate reactivity" with HO•, as reported by Gerrity et al. (2012), which is similar to TOrCs of concern such as atrazine and 1,4-dioxane.

Three reactor inputs – current density, H_2O_2 dose, and the corresponding $[H_2O_2]_{initial}/[Fe^{2+}]_{generated}$ ratio – were evaluated to gauge their relative influence on treatment. For EC experiments, the current density was synonymous with the iron

loading rate. The iron applied in each test was varied by adjusting the current density (and consequently the iron loading rate). For these experiments, the current density ranged from 3 to 15 mA/cm^2 (charge loading rate = 12 - 60 Coulomb/L-min, iron loading rate = 3.5 – 17.3 mg-Fe^{2+}/L-min). The H_2O_2 stock (ACS reagent grade, Sigma Aldrich, St. Louis, MO) was added at the beginning of EC:H_2O_2 experiments at levels ranging from 10 to 200 mg H_2O_2/L to assess pCBA treatment resulting from a fixed amount of H_2O_2 available for Fe^{2+} to generate radicals. The corresponding $[H_2O_2]_{initial}/[Fe^{2+}]_{generated}$ was 0.3 – 1.6 based on current density and H_2O_2 inputs. Notably, the $[H_2O_2]_{initial}/[Fe^{2+}]_{generated}$ ratio reflects the total H_2O_2 added at the beginning of the reaction, divided by the amount of Fe^{2+} generated by EC (estimated by Faraday's Law) by the end timepoint when pCBA removal ceased due to H_2O_2 depletion. The end timepoint of the pCBA degradation reaction was determined as the time point at which less than 10% difference in pCBA removal compared to the preceding time point was observed, likely indicating depletion of H_2O_2. Samples were collected every 2.5 minutes for 10 minutes, with a final sample at 15 minutes for kinetic analyses. Kinetic curves were fit to at least four data points ($R^2 > 0.95$ for all) to calculate first order rate constants for pCBA degradation for samples collected prior to H_2O_2 depletion, assessed as noted above.

4.2.2. Removal Pathway Control Experiments

Experiments were conducted under the same electrolysis and current density conditions described in *Section 4.2.1* to isolate the impact of different system inputs and delineate the potential treatment pathways in EC:H_2O_2, including oxidation by HO• and

H_2O_2 as well as physical removal by sorption to iron flocs. For HO• oxidation controls, methanol was spiked in stoichiometric excess (12 mM MeOH) of pCBA and H_2O_2 to quench HO• that would otherwise react with pCBA. In this case, H_2O_2 is reactive with electron-dense compounds and unlikely to react with unsaturated alcohols such as MeOH. For H_2O_2 controls, 30 mg-H_2O_2/L was spiked into the reactors containing the iron electrodes and stirred for 15 minutes to assess the potential pCBA removal due to H_2O_2 under treatment conditions without electricity.

Kinetic analyses were conducted to estimate the competition between H_2O_2 and O_2 as a function of H_2O_2 inputs and water chemistry conditions (H_2O_2 dose, O_2, and pH). These tests assessed the feasibility of HO• generation under neutral pH conditions and informed mechanistic analyses (oxidation by O_2 will limit HO• production by generating Fe^{3+}). The relative rates of oxidation and associated rate constants are provided in Appendix A4.5.

4.2.3. Water Quality Conditions

All EC:H_2O_2 experiments were conducted in 4 mM bicarbonate solution (with the exception of the environmental waters) to simulate buffered conditions for neutral pH environmental waters containing alkalinity, and to supply an electrolyte for electrochemical reactions (Table 4.2). Environmental waters were sampled to assess the impact of water quality and treatment performance in real waters relative to synthetic waters containing different NOM sources (Table 4.2). These analyses are important for informing the role of other environmentally relevant water quality parameters such as

NOM characteristics and concentration, conductivity, and divalent cations, all of which can impact treatment efficacy. A sample from the Milwaukee River (Milwaukee, WI) was used to test the impact of NOM and mid-range conductivity water. Groundwater from a drinking water well in West Bend, WI, was tested to reflect low dissolved organic carbon (DOC) and high conductivity conditions. Finally, primary effluent from an urban water reclamation facility in Milwaukee, WI, was tested for the impact of high DOC due to anthropogenic NOM and other oxidant scavengers (such as bulk chemical oxygen demand). The wastewater also served as a point of comparison to previous EC:H_2O_2 wastewater studies. For DOC quantification experiments, a sedimentation phase was required after EC:H_2O_2 to allow the flocs to settle prior to DOC analysis. Batch tests were performed as described in *Section 4.2.1* followed by an additional tapered flocculation phase (10 minutes at 40 rpm [G = 25 s^{-1}] and 10 minutes at 20 rpm [G = 9 s^{-1}]) and a 20-minute sedimentation period to remove flocs (method adapted from Ryan et al. (2020)).

Table 4.2. Water quality parameters.

Water Matrix	Initial pH	H_2O_2 demand, mg/L[a] (% H_2O_2 removal)	DOC, mg-C/L	Alkalinity, mg/L as $CaCO_3$	Conductivity, µS/cm	Ca^{2+}, mg/L	Mg^{2+}, mg/L
Bicarbonate Buffer[b]	8.3[c]	0 (0%)	0, 7.5[d]	210	370[e]	0	0
Groundwater	7.30	10 (33%)	3.3	400	1430	70	40
River Water	8.4	5 (15%)	7.0	240	755	30	20
Primary Wastewater Effluent	7.1	23 (75%)	55	280	1400	40	15

[a] H_2O_2 demand is reported as the decrease in H_2O_2 concentration after 15 minutes (the length of batch experiments), where the initial concentration was 30 mg/L H_2O_2.

[b] All model waters were prepared in Milli-Q water with 4 mM HCO_3^-.

[c] pH varied from 3 to 10.3 depending on experiments. The unadjusted pH was 8.3.

[d] For NOM tests, NOM was added as International Humic Substance Society Suwannee River NOM.

[e] Conductivity varied for pH tests due to addition of acid (HCl) or base (NaOH) for pH adjustment. At pH 3, conductivity = 920 µS/cm. At pH 6.3, conductivity = 450 µS/cm. At pH 10.3, conductivity = 750 µS/cm.

4.2.4. Analytical Measurements

Liquid chromatography-mass spectrometry was utilized to quantify pCBA (method adapted from Vanderford et al. (2007)). All pCBA samples were filtered through 0.22 µm PTFE syringe filters (Agela Technologies, Wilmington, DE) prior to analyses. Additional information on chromatography and mass spectrometry conditions is provided in Appendix A4.1. The H_2O_2 concentrations before and after each experiment were measured using Hach Model Hyp-1 test kits. The DOC was measured

via a Shimadzu TOC – V_{CSN} based on U.S. EPA Method 415.3. All DOC samples were filtered through 0.45 µm PTFE filters (Agela Technologies) prior to analyses. ICP-MS (7700 series, Agilent Technologies, Santa Clara, CA) was used to measure cations in real-world water samples. Alkalinity was measured via titration using Hach Model 2443-89 test kits.

4.2.5. Electrical Energy per Order

Electrical energy per order of magnitude reduction (E_{EO}), as shown in Eqn. 4.1, was estimated to provide a figure of merit for comparing energy requirements (kWh/m^3-order) for EC:H_2O_2 to other oxidative treatment technologies (Bolton et al., 2001). The voltage reading was recorded for each current density during each test to calculate power (power = voltage * current). First order rate constants were used to normalize treatment times across experiments as different reactor inputs and water quality conditions required different treatment times for 90% removal.

$$E_{EO} = \frac{P}{V \times 0.4343k \times 3600 \times 1000} \quad \text{(EQN. 4.1)}$$

Where P is power in W, V is volume in m^3, and k is the first order rate constant in s^{-1}. The coefficient of 0.4343 = log (C_0/C_i) for one order of magnitude reduction. The conversion factor 3600 is used to convert seconds to hours, and 1000 is used to convert W to kW.

4.2.6. Data Analysis and Interpretation

GraphPad Prism (version 9.5.1.) software was used to conduct one-way and two-way ANOVA followed with post-hoc Tukey's multiple comparison test, Pearson correlations, and multivariable linear regressions. Multivariable linear regressions were used as explanatory models to evaluate the contributions of system inputs (H_2O_2, Fe^{2+}, and $[H_2O_2]_{initial}/[Fe^{2+}]_{generated}$) and the impact of water quality parameters. Independent variables for the EC:H_2O_2 process were selected based on Pearson correlations and normalized using the min-max method. This min-max normalization method was conducted to minimize the artificial impacts of independent variables on the dependent variable due to different scales and ranges of inputs (e.g., rate constants were on the order of 10^{-4} s^{-1}, whereas H_2O_2 ranged from 10 to 100 mg/L) (Borkin et al., 2019). The independent variables for reactor inputs (pH, $[H_2O_2]_{initial}/[Fe^{2+}]_{generated}$, and current density) were selected for the multivariable linear regression model based on their correlation to the dependent variables: pCBA removal, pseudo-first order rate constant, and E_{EO}. For environmental waters, $DOC_{initial}$, alkalinity, pH, and conductivity were selected as the independent water quality variables. All independent variables selected for multivariable linear regression were not multicollinear with other variables based on variance inflation factors < 5 for all regressions (Akinwande et al., 2015).

4.3. RESULTS AND DISCUSSION

4.3.1. Para-chlorobenzoic Acid Removal for Hydroxyl Radical Validation

Removal of pCBA during EC:H_2O_2 primarily proceeded via oxidation at neutral pH conditions due to the system's combination of iron and H_2O_2 (Figure 4.1). EC-only controls yielded an average pCBA removal of approximately 15%, presumably due to the low levels of HO• that can be generated during EC alone (Qian et al., 2019, Maher et al., 2019). For EC:H_2O_2 + MeOH experiments, the high MeOH concentration (12 mM) scavenged the oxidants and resulted in negligible pCBA degradation. This scavenging indirectly underscores the role of homogeneous oxidants (such as HO•). Negligible pCBA removal in the EC:H_2O_2 + MeOH test further indicates that pCBA does not sorb to iron flocs. The 'No Electricity Control' experiments demonstrated that potential reactions between H_2O_2 and the iron electrode surface had minimal removal relative to the EC:H_2O_2 conditions with electricity ($p<0.0001$, one-way ANOVA) at circumneutral pH conditions. Overall, these data demonstrate that the addition of H_2O_2 can enhance oxidant production in EC:H_2O_2 relative to EC alone and induce an oxidative process at neutral pH conditions.

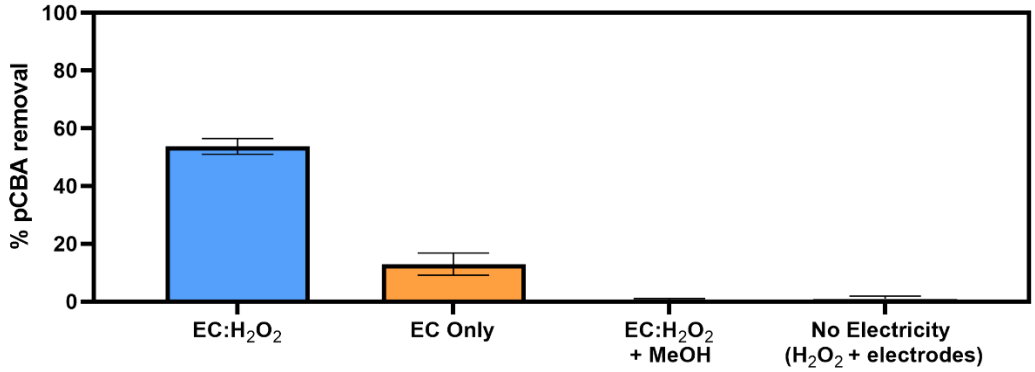

Figure 4.1. Mechanisms for pCBA removal during EC:H_2O_2 at 7.40 mA/cm^2. A series of controlled batch experiments were run in 4 mM bicarbonate buffer at pH 8.3 for 15 minutes. In "EC only," electrolysis was conducted using iron electrodes with no peroxide addition. For "EC:H_2O_2 + MeOH", methanol was spiked in stoichiometric excess of pCBA (12 mM MeOH:2.5 µM pCBA) to quench oxidants that would otherwise degrade pCBA. In "No Electricity (H_2O_2 + electrodes), 30 mg/L H_2O_2 was spiked into the solution with the iron electrodes and mixed for 15 minutes. All experiments were conducted in duplicate and error bars indicate ± 1 standard deviation. EC-only results are the average of all duplicate experiments for each EC-only control, including current densities of 3.5 mA/cm^2, 5.5 mA/cm^2, 11.1 mA/cm^2, and 15 mA/cm^2, where n = 8.

The occurrence of oxidation at neutral pH conditions during EC:H_2O_2 is important in the context of Fenton literature since traditional Fenton oxidation proceeds at pH 3. These conventional Fenton conditions limit the feasibility of EC:H_2O_2 applications as the high acidity can damage infrastructure, enhance corrosion, and incur chemical costs for acidifying and neutralizing water during treatment.

4.3.2. The Impact of Reactor Inputs on pCBA Degradation During EC:H_2O_2: Removal and Kinetics

Following oxidant verification, the impact of EC:H_2O_2 reactor inputs and water quality were assessed. The discussion centers on the role of $[H_2O_2]_{initial}/[Fe^{2+}]_{generated}$ ratios, current density, and pH. Multivariable linear regressions were used to parameterize the contribution of all inputs.

4.3.2.1. The Impact of H_2O_2 Dose, Current Density, and Iron Dose on pCBA Removal at Neutral pH Conditions

The efficacy of H_2O_2 dose for pCBA removal varied as a function of the $[H_2O_2]_{initial}/[Fe^{2+}]_{generated}$ ratio (Figure 4.2A). The presence of H_2O_2 only improved treatment when Fe^{2+} was present in the system ($R^2_{H2O2\text{-}all:removal}$ = 0.003, p=0.99 Pearson correlation, Table A4.8.1). With 10 – 40 mg/L H_2O_2, there was a positive correlation between pCBA removal and H_2O_2 dose during EC:H_2O_2 when iron was also present in the system ($R^2_{H2O2:removal}$ = 0.84, p <0.05 Pearson correlation, Table A4.8.2). Once H_2O_2 exceeded 30 mg/L in the presence of Fe^{2+}, pCBA removal began to plateau around 50 – 60% pCBA removal for $[H_2O_2]_{initial}/[Fe^{2+}]_{generated}$ ratios ranging from 0.3 to 0.7. In contrast, the higher $[H_2O_2]_{initial}/[Fe^{2+}]_{generated}$ ratio of 1.6 resulted in less pCBA removal compared to the same H_2O_2 dose applied at lower ratios. Alternately, for H_2O_2 concentrations greater than 40 mg/L, the H_2O_2 dose did not significantly correlate ($R^2_{H2O2 > 40 : removal}$= -0.377, p = 0.136, Pearson correlation, Table A4.8.3) and resulted in less pCBA removal. For example, 50 mg/L H_2O_2 had approximately 60% pCBA removal when applied at $[H_2O_2]_{initial}/[Fe^{2+}]_{generated}$ = 0.35; when the ratio increased to $[H_2O_2]_{initial}/[Fe^{2+}]_{generated}$ = 1.6, pCBA removal decreased to 40% for all H_2O_2 doses. The inhibition of pCBA removal at higher H_2O_2 levels aligns with the scavenging impact of H_2O_2 and competition between matrix constituents. Although more H_2O_2 can be beneficial for HO• generation via Fenton's reaction, higher H_2O_2 levels lead to a higher degree of oxidant scavenging and decreased radical availability for pCBA removal (Appendix 4.3).

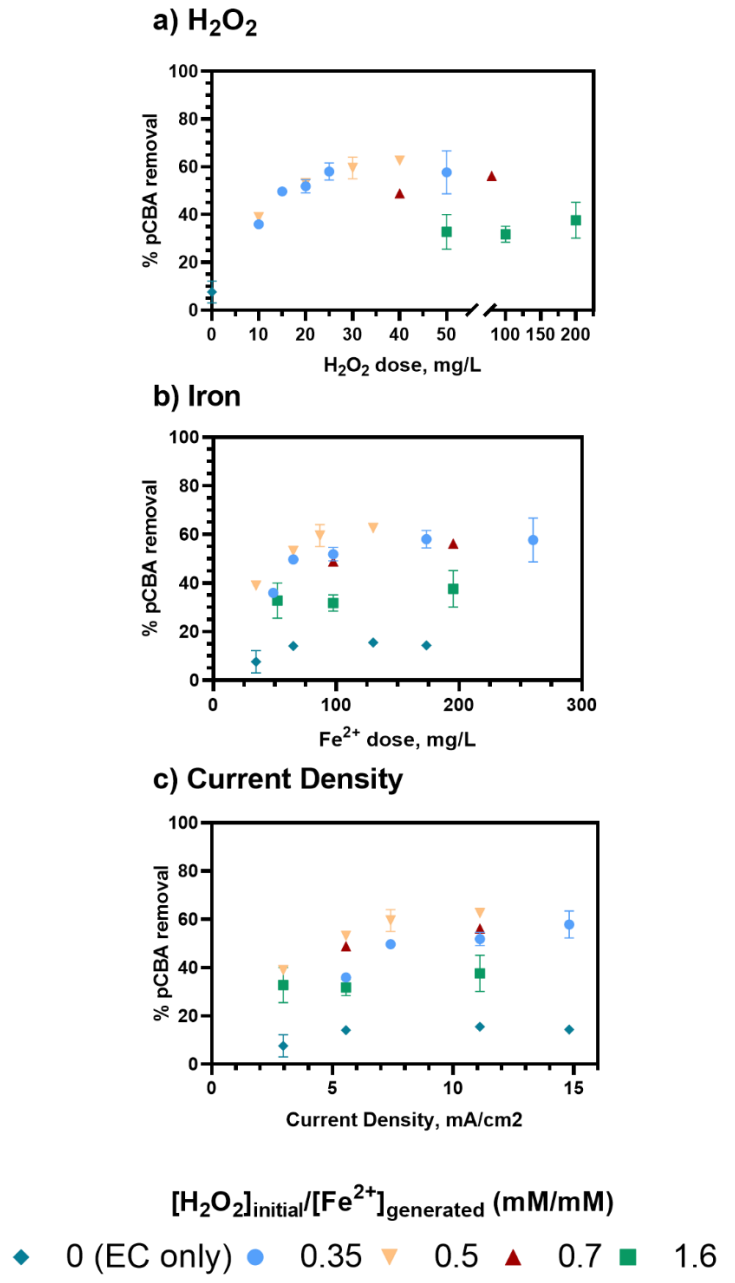

Figure 4.2. pCBA removal after 15-minute EC:H_2O_2 batch experiments as a function of **A)** H_2O_2 dosed into the system at time 0, **B)** Total ferrous iron generated (estimated by Faraday's law) over the course of the EC:H_2O_2 experiment, and **C)** Current density, with is proportional to the iron loading rate (mg-Fe/L). Iron loading rates were estimated using Faraday's law, where 3 mA/cm^2 = 3.5 mg-Fe/L-min, 5.5 mA/cm^2 = 6.5 mg-Fe/L-min, 7.4 mA/cm^2 = 8.6 mg-Fe/L-min, 11.1 mA/cm^2 = 13 mg-Fe/L-min, and 15 mA/cm^2 = 17.4 mg-Fe/L-min. All experiments were conducted in duplicate and error bars indicate ± 1 standard deviation.

The key role of current density in this study was to adjust the iron loading rate to add Fe^{2+} as Fenton's reagent (Figure 4.2B). When no H_2O_2 was present (i.e., EC-only), pCBA removal was consistently less than 20% regardless of current density (Figure 4.2C). Hence, EC had effective pCBA removal only when H_2O_2 was present, as the $[H_2O_2]_{initial}/[Fe^{2+}]_{generated}$ ratio was the key driver of treatment efficacy. During EC:H_2O_2, pCBA removal improved with increases in current density up to 7.4 mA/cm^2 ($R^2_{current\ density\ =\ 3\ to\ 7.4\ mA/cm2}$ = 0.63, p = 0.008, Pearson correlation, Table A4.8.4) and plateaued after 7.4 mA/cm^2 ($R^2_{current\ density\ >\ 7.4\ mA/cm2}$ = 0.141, p = 0.6, Pearson correlation, Table A4.8.5). As treatment inputs increased, the higher ratio of $[H_2O_2]_{initial}/[Fe^{2+}]_{generated}$ = 1.6 had the least pCBA removal for EC:H_2O_2 regardless of current density. The plateau in pCBA removal for higher current density may suggest that a minimum level of iron is needed for this system, and beyond that level, additional iron no longer improves treatment. Here, the lowest Fe^{2+} loading rate was 3.5 mg Fe/L-min (resulting from 3 mA/cm^2 current density).

In summary, $[H_2O_2]_{initial}/[Fe^{2+}]_{generated}$ ratios were the key driver for pCBA removal where lower ratios (0.33 – 0.7) had higher removal ($\beta_{H2O2/Fe=0\text{-}0.7}$ = 0.77, p<0.0001, Table A4.8.6, multivariable linear regression: "%R, low ratio, neutral pH") from minimal HO• scavenging, and higher ratios (1.6) decreased removal ($\beta_{H2O2/Fe=0.3\text{-}1.6}$ = -0.42, p=0.0008, Table A4.8.6, multivariable linear regression: "% R EC: H_2O_2 neutral pH"). This finding is important when considering materials requirements including the *ex-situ* H_2O_2 additions and the power demands associated with iron generation. For this system, H_2O_2 levels determined the treatment capacity because pCBA removal ceased after depletion of the

one-time dose of H_2O_2 at the start of the test, whereas the Fe^{2+} was continually generated via electrolysis.

It is important to note that $[H_2O_2]_{initial}/[Fe^{2+}]_{generated}$ ratios do *not* translate to the actual ratio of H_2O_2 relative to Fe^{2+} at any timepoint during the test. During EC:H_2O_2, H_2O_2 is initially in large excess to Fe^{2+} as Fe^{2+} is formed during EC, which may drive the rate of oxidant formation resulting from interactions between Fe^{2+} and H_2O_2. This excess is a result of Fe^{2+} being generated at nM levels (e.g., 2500 nM/s for 7.4 mA/cm^2 based on Faradays law) during electrolysis, which highlights the benefits of using iron electrolysis for Fe^{2+} dosing to avoid side reactions and encourage efficient Fe^{2+} utilization by H_2O_2.

4.3.2.2. The Impact of $[H_2O_2]_{initial}/[Fe^{2+}]_{generated}$ and Current Density on pCBA Oxidation Rate During EC:H_2O_2

Pseudo-first order kinetic modeling offered good data fits, enabled comparison to other AOP processes in the literature, and is used in E_{EO} calculations. For a fixed current density of 5.5 mA/cm^2, $[H_2O_2]_{initial}/[Fe^{2+}]_{generated}$ = 0.35, 0.5, and 0.7 had similar pseudo-first order rate constants (1.1 x 10^{-3} to 1.3 x 10^{-3} s^{-1}) before H_2O_2 depletion (Figure 4.3A, Appendix Table A4.6.1). As the ratio increased, the rate of pCBA removal declined, which corroborates the removal findings in Sect. 4.3.2.1. Notably, for $[H_2O_2]_{initial}/[Fe^{2+}]_{generated}$ = 0.35 and 0.5, pCBA removal stagnated after 7.5 minutes and 10 minutes, respectively. Accordingly, H_2O_2 should be continually dosed at lower concentrations in EC:H_2O_2 operations in order to continue oxidative reactions without adding excess H_2O_2 that can lead to quenching.

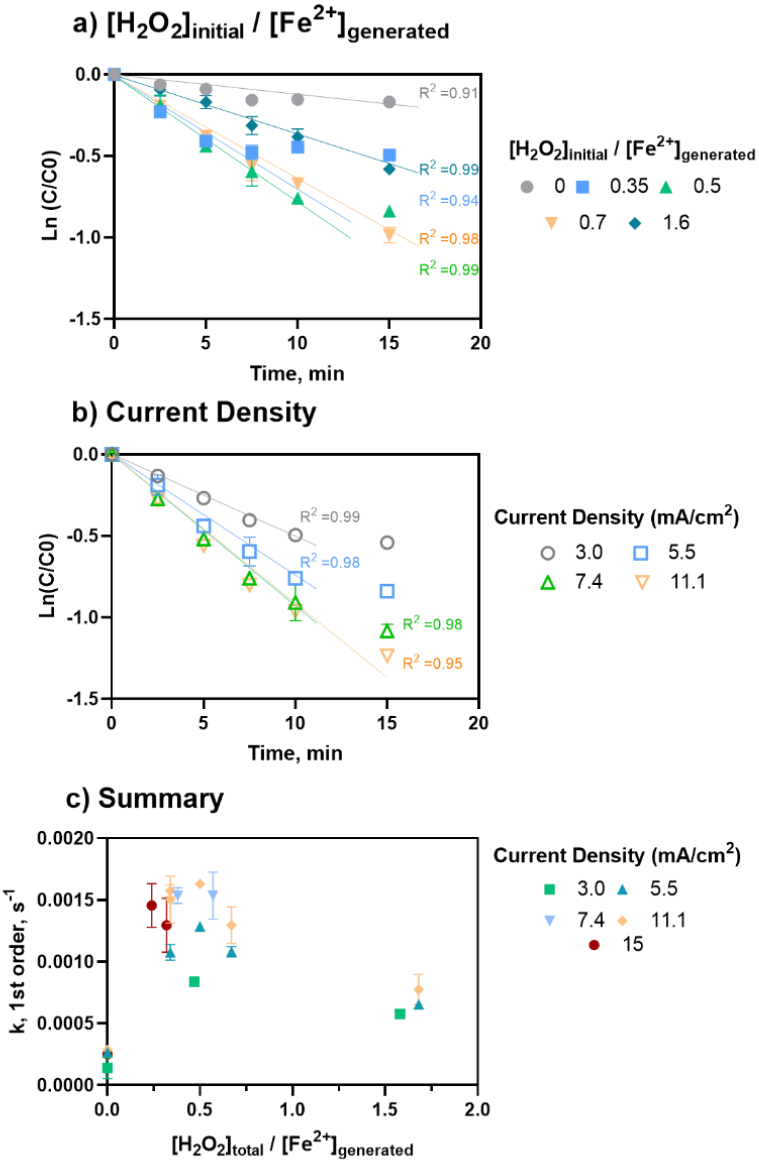

Figure 4.3. Summary of pseudo-first order rate constants for degradation of para-chlorobenzoic acid (pCBA) following 15-minute EC:H_2O_2 batch experiments. All experiments were conducted in 4 mM HCO_3^- buffer at pH = 8.3. Samples were taken every 2.5 minutes for a total of 15 minutes. **A)** Pseudo-first order kinetic curves showing the impact of $[H_2O_2]_{initial}/[Fe^{2+}]_{generated}$ ratios for a fixed current density of 5.5 mA/cm^2. **B)** Pseudo-first order kinetic curves showing the impact of current density for a fixed $[H_2O_2]_{initial}/[Fe^{2+}]_{generated}$ of 0.5. **C)** Summary of pseudo-first order rate constants for all EC:H_2O_2 batch experiments for all current density and $[H_2O_2]_{initial}/[Fe^{2+}]_{generated}$ ratios. Pseudo-first order constants were determined and verified based on $R^2 \geq 0.95$ over the course of treatment to capture the linear range prior to H_2O_2 depletion. The end timepoint of the pCBA degradation reaction used in kinetic modeling was determined as the time point at which pCBA removal was less than 10% different than the preceding time point. Error bars show ± 1 standard deviation of duplicate experiments.

As shown in Figure 4.3, for a fixed $[H_2O_2]_{initial}/[Fe^{2+}]_{generated}$ ratio of 0.5, the rate constants were comparable for current densities of 5.5, 7.4, and 11.1 mA/cm^2 (1.3 to 1.6 x 10^{-3} s^{-1}, Appendix Table A4.6.1). However, 3 mA/cm^2 had the lowest rate of removal (8.4 x 10^{-4} s^{-1}, Appendix Table A4.6.1). This trend aligns with the removal data, in which the removal plateaued as current (i.e., iron loading rate) increased, indicating that additional iron after a threshold level no longer improved treatment.

Overall, the ratio had the highest influence on rate of removal based on multivariable linear regressions ($\beta_{[H2O2]/[Fe2+]=0-0.77}$ = 0.76±0.11, p<0.0001, multivariable linear regression: "k, EC:H_2O_2 low ratio, neutral pH") (Figure 4.3C, Table A4.8.6.). Considering both major inputs in terms of $[H_2O_2]_{initial}/[Fe^{2+}]_{generated}$ ratios, pseudo-first order rate constants were grouped into three clusters for a range of current densities at neutral pH conditions (Figure 4.3C) to understand the general impact of different ratio levels. The clusters were EC-only conditions (i.e., no H_2O_2), $[H_2O_2]_{initial}/[Fe^{2+}]_{generated}$ ratios = 0.3 – 0.7, and $[H_2O_2]_{initial}/[Fe^{2+}]_{generated}$ ratios greater than 0.7. The lower $[H_2O_2]_{initial}/[Fe^{2+}]_{generated}$ ratios of 0.3 – 0.7 had the highest rate constants, ranging from 1.1 x 10^{-3} to 1.6 x 10^{-3} s^{-1}. The higher ratios of >0.7 to 1.6 resulted in lower rate constants, ranging from 5.8 x 10^{-4} to 7.7 x 10^{-4} s^{-1} ($\beta_{[H2O2]/[Fe2+]=0.3\ to\ 1.6}$ = -0.59±0.11, p<0.0001, multivariable linear regression: "k, EC:H_2O_2 only, neutral pH"). For all cases, experiments containing H_2O_2 had faster rates of pCBA removal compared EC-only controls (1.4 x 10^{-4} to 2.7 x 10^{-4} s^{-1}). However, higher levels of H_2O_2 (greater than 40 mg/L) did not increase the rate of pCBA removal, likely due to radical quenching by H_2O_2. This is notable given that the effective H_2O_2 doses found in this study is less than

reagent demands in other EC:H_2O_2 studies for industrial treatment applications (Behin et al., 2015; Garcia-Segura et al., 2017; Ghanbari and Moradi, 2015a; Kumar et al., 2018; Vasudevan, 2014; Yazdanbakhsh et al., 2015a; Yüksel et al., 2009). Overall, these findings indicate that less H_2O_2 may be required than previously thought for effective oxidation.

4.3.2.3. The Impact of pH on Oxidation Rate

The impact of pH on pCBA oxidation was assessed to evaluate the interplay of Fe^{2+}, H_2O_2, and pCBA over a range of acid/base conditions. As pH decreased, pCBA removal increased and the rate of oxidation accelerated (Figure 4.4). At basic pH = 10.3, minimal removal was observed. At pH = 6.3, the maximum rate of pCBA degradation was observed (amongst the circumneutral pH levels tested), $k = 4.6 \times 10^{-3}\ s^{-1}$ (1.6 times faster than the rate at pH = 8.3). Removal of pCBA ceased after 5 minutes (as indicated by the stagnation of the kinetic curve), likely due to depletion of H_2O_2 at these conditions. Measurements of the H_2O_2 remaining after 5 minutes demonstrated roughly 70% loss of the initial 30 mg/L H_2O_2 at pH 6.3 and 95% loss at pH 3 (Appendix A4.9). Depletion of the H_2O_2 helps explain the stagnated pCBA removal, likely due to decreased formation of oxidants. Accordingly, H_2O_2 should be continually dosed at lower concentrations in EC:H_2O_2 to encourage continuous oxidative reactions and improve TOrC treatment.

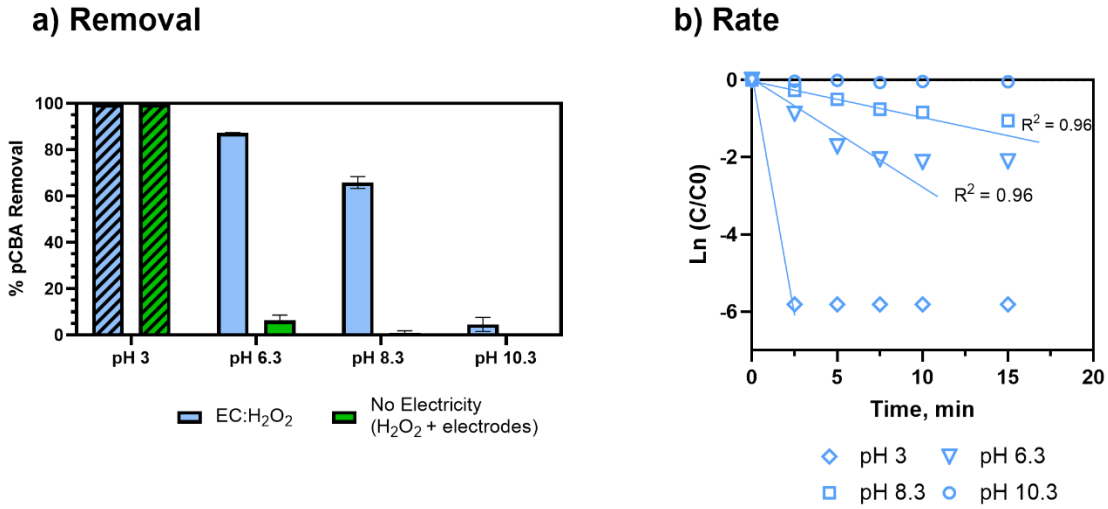

Figure 4.4. Degradation of pCBA at different pH conditions prepared in 4 mM bicarbonate buffer. During EC:H_2O_2, current density = 7.4 mA/cm^2, H_2O_2 = 30 mg/L, 15 minutes of treatment time. **A)** Removal of pCBA as a function of pH. The no electricity control experiment shows removal due only to iron electrodes and the addition of 30 mg/L H_2O_2. Striped bars indicate concentrations below the limit of detection (4 µg/L). **B)** pCBA removal rate as a function of pH. R^2 correlations are not shown for pH 3 due to insufficient points above the limit of detection after treatment (removal at all pH 3 treatments was calculated using the limit of detection as the final concentration). R^2 is not shown for pH 10.3 due to no removal. The end timepoint of the pCBA degradation reaction used in kinetic modeling was determined as the time point at which pCBA removal was less than 10% different than the preceding time point. Error bars show ± 1 standard deviation of triplicate experiments. Of note, the error bars for B are not visible due to low standard deviation.

The acidic conditions (pH 3, encouraging Fenton's reactions) resulted in the greatest and fastest pCBA removal (>99% removal, to below the detectable limit). However, at pH 3, enhanced corrosivity led to >99% pCBA removal even without electricity, wherein increased iron dissolution was visually observed. For no electricity controls, pCBA removal was likely due to non-faradaic iron dissolving from the electrodes (30 mg Fe/L) and reacting with *ex-situ* H_2O_2 (98% H_2O_2 removal; Appendix A4.9) to generate HO•. The no-electricity control resulted in a $[H_2O_2]_{initial}/[Fe^{2+}]_{generated}$ ratio of 1.5. Although this ratio was toward the upper end of ratios tested, the pH 3

conditions were expected to enhance the rate of reaction. For circumneutral conditions, the no-electricity controls had minimal pCBA removal, indicating no oxidant generation in the absence of electricity at the conditions tested.

Overall, the pCBA removal trends agree with the kinetic modeling performed to estimate the competition between H_2O_2 and O_2 for oxidizing Fe^{2+} (Appendix S4.5). The modeling scenarios included 0 to 200 mg/L H_2O_2 concentrations. At pH 6.3, the rate of Fe^{2+} oxidation by H_2O_2 was up to 10 orders of magnitude higher than Fe^{2+} oxidation by O_2, suggesting that there was minimal competition for ferrous oxidation between H_2O_2 and O_2. Accordingly, these kinetic analyses support that HO• generation was driven by Fe^{2+} oxidation via H_2O_2 (not O_2). Removal was minimal at pH 10.3, likely due to enhanced O_2 activity (Figure 4.4). As pH increases, the inhibition of HO• generation due to O_2 becomes more apparent given that the oxidation of Fe^{2+} by O_2 is second order with respect to [OH^-] (based on Stumm and Lee, 1961) and increases 100-fold for each pH unit increase (Appendix A4.5).

The pseudo-first order rate constants were used to estimate the HO• concentration (Appendix A4.2). For pH 8.3, [HO•] ranged from 2 – 4.1 x 10^{-13} M for the $[H_2O_2]_{initial}/[Fe^{2+}]_{generated}$ ratios of 0.33 to 0.7. At pH 6.3, when pCBA treatment was more effective, [HO•] was approximately 9 x 10^{-13} M. These estimates of radical concentrations can be applied to future studies to compare the [HO•] yield for a range of TOrC oxidation technologies such as UV/H_2O_2.

4.3.2.4. Multivariable Linear Regression Analysis of EC:H_2O_2 Process Inputs

To evaluate the roles of independent variables, multivariable linear regressions were conducted to consider the influence of all reactor input experiments at neutral pH and for variable pH experiments. The key parameters incorporated into the regression were $[H_2O_2]_{initial}/[Fe^{2+}]_{generated}$ ratios, pH, and current density. These independent variables were selected based on preliminary Pearson correlations and were not multicollinear (Appendix A4.8).

Overall, $[H_2O_2]_{initial}/[Fe^{2+}]_{generated}$ ratios, pH, and current density were significantly correlated to pCBA removal (p=0.028, 0.008, and <0.0001, respectively, multivariable regression "%R all"). The most influential parameter for pCBA removal was pH (β_{pH}=-0.91±0.15, multivariable linear regression: "%R, all"), where lower pH led to higher pCBA removal. The ratio of $[H_2O_2]_{initial}/[Fe^{2+}]_{generated}$ and current density had smaller impacts relative to pH, but similar magnitude contributions to one another ($\beta_{[H2O2]/[Fe2+]}$ = 0.22 ± 0.09, $\beta_{current\ density}$ = 0.36 ± 0.09, multivariable linear regression: "%R, all").

A separate regression was performed for experiments with $[H_2O_2]_{initial}/[Fe^{2+}]_{generated}$ ratios = 0 – 0.77 to rank the inputs that yielded higher rate constants and higher pCBA removal. For these tests, pH still had the greatest influence (β_{pH}=-0.79±0.08, p<0.0001, multivariable linear regression: "k, all") followed by $[H_2O_2]_{initial}/[Fe^{2+}]_{generated}$ ratios ($\beta_{[H2O2]/[Fe2+]}$ = 0.38±0.05, p<0.0001, multivariable linear regression: "k, all"). However, variations in current density alone had an insignificant influence on rate of pCBA removal ($\beta_{current\ density}$ = 0.09±0.05, p=0.073, multivariable

linear regression: “k, all”), implying that pH and $[H_2O_2]_{initial}/[Fe^{2+}]_{generated}$ ratios are the key parameters influencing oxidant production.

4.3.3. Co-treatment of pCBA and NOM Using EC:H_2O_2 to Treat Environmental Waters and Synthetic Matrices.

4.3.3.1. pCBA Removal in NOM-Containing Waters

In environmental source waters (i.e., river water and groundwater), EC:H_2O_2 oxidized pCBA, indicating that EC:H_2O_2 can treat real waters containing relatively low DOC levels typical of natural source waters in addition to synthetic matrices (Figure 4.5A). The matrices with the lowest levels of DOC (groundwater and bicarbonate [no DOC]) had similarly high pCBA removal ($p=0.8$, ANOVA: post hoc Tukey multiple comparison*)*, whereas the matrices containing moderate DOC levels (river water and SR-NOM) had less pCBA removal and performed similarly to one another ($p>0.99$, ANOVA: post hoc Tukey multiple comparison). Notably, the synthetic matrices had similar removal efficacy to the real waters in spite of increased complexity in real water sources.

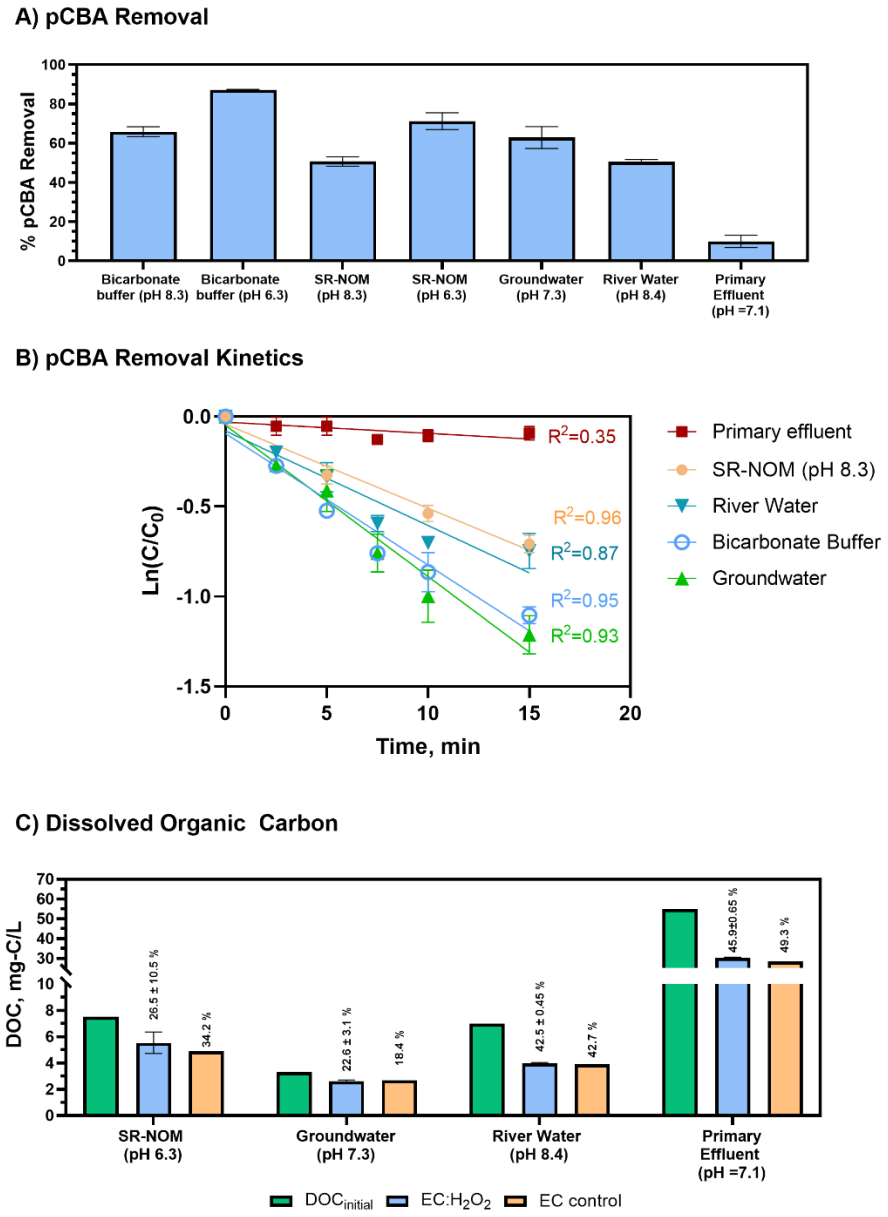

Figure 4.5. Removal of pCBA and dissolved organic carbon (DOC) in synthetic and real-world waters following 15 minutes of EC:H_2O_2 (7.40 mA/cm^2, H_2O_2 = 30 mg/L). **A)** pCBA removal following EC:H_2O_2 (C_i = 400 µg/L for all matrices). **B)** Pseudo-first order degradation of pCBA in EC:H_2O_2 at $[H_2O_2]_{initial}/[Fe^{2+}]_{generated}$ ratio = 0.55 (7.4 mA/cm^2, 30 mg H_2O_2/L) in synthetic and real-world waters. **C)** DOC in the waters initially and remaining following EC:H_2O_2 or EC-only treatment. A pH 6.3 test was conducted for SR-NOM to reflect enhanced coagulation conditions. Bicarbonate Buffer is not included in panel C) as there was no DOC in the synthetic matrix. The % DOC removal by EC:H_2O_2 is shown in vertical text above each bar. All DOC and pCBA data are from the same batch experiments for the respective water matrix. Error bars show ± 1 standard deviation of triplicate experiments, with the exception of the "EC control" values in panel C, which are single replicates.

The initial concentration of DOC had a small impact on pCBA removal (β_{DOC}=-0.07, p=0.34, not including primary effluent) for matrices containing low- to mid-range DOC levels (<10 mg-C/L) that reflect drinking water source matrices. This trend implies that the presence of NOM may not heavily impede pCBA oxidation when treating typical environmental source waters.

Compared to real-world waters and synthetic matrices, the primary effluent had the least pCBA removal. Decreased removal was likely due to high H_2O_2 demand (Table 4.2) and high DOC levels. In this case, the high H_2O_2 demand rapidly depleted the H_2O_2 that was initially dosed into the reactor, which hindered HO• production. Thus, for EC:H_2O_2 applications, the water's H_2O_2 demand should be accounted for to gauge potential negative impacts on process performance. For example, Serra-Clusellas et al. (2021) demonstrated TOrC mitigation via EC:H_2O_2 at pH = 3 in municipal tertiary treated wastewater containing ng/L TOrCs by using elevated 220 – 440 H_2O_2 mg/L doses (resulting in $[H_2O_2]_{initial}/[Fe^{2+}]_{generated}$ ratios of 1.7 to 2 during treatment), which offset oxidant scavenging by wastewater constituents.

A multivariable regression of all test matrices showed that $DOC_{initial}$ and pH were the key water quality parameters that impacted pCBA removal (β_{DOC} = -0.72±0.18, p=0.008 and β_{pH} -0.81±0.08, p=<0.0001, respectively). Pearson correlations showed that $DOC_{initial}$ and H_2O_2 demand were multicollinear ($R^2_{DOC\ vs\ H2O2\ demand}$= 0.893, p<0.05, Pearson correlations). As anticipated, higher DOC levels typical of wastewater impeded treatment efficacy, whereas lower DOC conditions improved radical yield and offered less competition for oxidants. However, it is important to note that other water matrix

constituents beyond DOC (including chemical oxygen demand, reduced metals, and sulfides, which were not assessed in this study) also likely contributed to H_2O_2 depletion and impeded DOC removal.

4.3.3.2. DOC Removal in Environmental Waters

In terms of bulk organics, EC:H_2O_2 appears to offer similar levels of DOC removal compared to EC-only, with the added benefit of TOrC mitigation based on pCBA removal (Figure 4.5C). The favorable reproducibility of DOC removal via EC:H_2O_2 replicates relative to single EC-only as a point of reference suggests that DOC removal primarily proceeds through non-destructive pathways as EC-only was previously shown to have minimal pCBA removal via oxidants at the conditions tested.

The river water and SR-NOM matrices are of particular interest for DOC removal given that they are representative of surface waters that could be treated for drinking water. Using EC:H_2O_2, DOC removal for the river water complied with recommendations in the US EPA's Enhanced Coagulation Guidance manual (>30% DOC removal for matrices containing >120 mg/L as $CaCO_3$ alkalinity) (Environmental Protection Agency (EPA), 1999). The synthetic SR-NOM matrix only had effective DOC removal when pH was 6.3. At pH 8.3, EC:H_2O_2 formed no flocs or precipitates in SR-NOM, indicating unsuccessful coagulation and precipitation and subsequent sedimentation of flocs (Appendix A4.11). This difference between real and synthetic waters suggests that other constituents in environmental waters (such as divalent cations, i.e., calcium and magnesium) may improve coagulation processes in real waters by promoting ionic

interactions between NOM and ions that promote co-sorption to flocs, as shown for a calcium-fulvic acid-goethite iron mineral system (Weng et al., 2005).

Overall, the addition of H_2O_2 during EC:H_2O_2 can enhance treatment applications by simultaneously treating TOrCs such as pCBA as well as bulk organics such as DOC in a single unit process in lieu of a multi-stage treatment train such as coagulation/flocculation/sedimentation followed by filtration and oxidation to achieve both non-destructive removal and oxidative destruction of contaminants.

4.3.4. Engineering Implications: Rate Constants and Electrical Energy per Order

4.3.4.1. Pseudo-First Order Rate Constants for Treating Environmental Waters

Pseudo-first order rate constants are key figures of merit for evaluating operational parameters by accounting for matrix-specific scavengers. The pseudo-first order rates for pCBA removal were 1.3 x 10^{-3} s^{-1} and 1.6 x 10^{-3} s^{-1} for river water and groundwater, respectively (Figure 4.5B, Table 4.3). These values satisfy the proposed breakeven point k = 2.1 x 10^{-5} s^{-1} for TOrC treatment technologies to be competitive based on technoeconomic analyses (Stirling et al., 2020).

Table 4.3. Electrical energy per order of magnitude removal (kWh/m^3) values for EC:H_2O_2 operated in bicarbonate buffer. Values are the averages of duplicate experiments ± one standard deviation.

$[H_2O_2]_{initial}$/ $[Fe^{2+}]_{generated}$	Current Density, mA/cm^2				
	3	5.5	7.4	11.1	15
0.35		0.74 ± 0.04	3.13 ± 0.13	6.10 ± 0.21	12.54 ± 2.12
0.5	0.76 ± 0.03	0.62 ± 0.02	3.15± 0.39	5.89 ± 0.06	
0.7		0.74 ± 0.03		7.45 ± 0.84	
1.6	1.11 ± 0.08	1.22 ± 0.05		12.56 ± 2.01	

4.3.4.2. Electrical Energy Per Order: Impact of Reactor Inputs for Bicarbonate Buffer

In terms of energy requirements, higher current densities resulted in higher E_{EO} values ($\beta_{current\ density}$=-0.36±0.09, p<0.0001, multivariable regression: "$E_{EO,}$ all"), whereas $[H_2O_2]_{initial}/[Fe^{2+}]_{generated}$ ratios had less impact ($\beta_{[H2O2]/[Fe2+]}$=-0.36±0.09, p=0.16). For the lower current densities, 3 and 5 mA/cm^2, the E_{EO} was 0.62 ± 0.02 and 1.22 ± 0.05 kWh/m^3, respectively, when operated at pH 8.3 conditions. The higher current densities of 7.4 to 15 mA/cm^2 had E_{EO} values ranging from 3.13 ± 0.13 to 12.54 ± 2.12 kWh/m^3 due to the additional electrical loading (Table 4.3.). When pH decreased to 6.3, the E_{EO} decreased from 2.86 ±0.2 kWh/m^3 to 0.68±0.004 kWh/m^3 for the same current density of 7.4 mA/cm^2. This improvement in energy efficiency was likely due to a combination of the faster rate of removal at pH 6.3 and the solution's increased conductivity due to chloride addition (HCl was used for pH adjustment).

With the exception of low current density experiments, these E_{EO} values exceed the recommended 1 kWh/m^3 threshold to be competitive with conventional HO•-mediated advanced oxidation processes (AOPs) such as UV/H_2O_2 and ozone-based AOPs (Miklos et al., 2018). However, the benchmark E_{EO} values for conventional AOPs rely on preliminary treatment technologies such as coagulation and membrane filtration to remove oxidant scavengers, primarily DOC. Additional DOC removal technologies will add materials and energy demands to overall treatment of TOrCs that are not accounted for in standalone E_{EO} values for conventional AOPs. Alternately, EC:H_2O_2 offers the benefit of simultaneous TOrC and DOC treatment, which can minimize

preliminary treatment needs and decrease overall energy inputs compared to conventional AOP treatment trains.

4.3.4.3. Electrical Energy Per Order: Impact of Water Quality

The E_{EO} values for the real water experiments ranged from 0.7 to 7.5 kWh/m^3 (Table 4.4) as a function of water quality, pCBA removal, and the voltage input to achieve the fixed current of 7.4 mA/cm^2. Of the environmental waters, groundwater had the lowest E_{EO} at 1.0±0.13 kWh/m^3, while the river water E_{EO} was 1.91±0.21 kWh/m^3. The matrix with the highest E_{EO} was SR-NOM (7.57±0.20 kWh/m^3) due to low pCBA removal and low matrix conductivity. Primary effluent had the second highest E_{EO} of 6.49±1.34 kWh/m^3. Notably, primary effluent had the least pCBA removal of all waters tested (<20%); however, the water's high conductivity led to low voltage input, leading to a relatively low E_{EO} in spite of the poor pCBA treatment performance.

Table 4.4. Figures of merit for pCBA treatment in varying water matrices, including pseudo-first order rate constants (k) and electrical energy per order (E_{EO}) of magnitude removal values for EC:H_2O_2. For all experiments, current density = 7.4 mA/cm^2 and H_2O_2 = 30 mg/L. pH = 3 is not included due to insufficient data points to model a pseudo-first order rate constant prior to H_2O_2 depletion. pH 10.3 is not shown due to poor removal that did not provide viable data for pseudo-first order rate constants to estimate E_{EO} values.

Water Matrix	k, s^{-1}	E_{EO}, kWh/m^3
Bicarbonate Buffer (pH 8.3)	1.2 x 10^{-3}	2.86±0.20
Bicarbonate Buffer (pH 6.3)	4.7 x 10^{-3}	0.68±0.005
Bicarbonate Buffer + NOM	6.3 x 10^{-3}	7.57±0.20
Bicarbonate Buffer + NOM (pH 6.3)	2.9 x 10^{-3}	1.13±0.08
Groundwater	1.6 x 10^{-3}	1.00±0.13
River Water	1.3 x 10^{-3}	1.91±0.21
Primary Effluent	2.5 x 10^{-4}	6.49±1.34

Multivariable regressions were used to assess how water quality in environmental and synthetic water matrices influenced E_{EO}. The E_{EO} trends followed the removal trends, where DOC concentration and alkalinity increased E_{EO} by decreasing pCBA removal and increasing treatment inputs (β_{DOC}=1.2±0.15, p<0.0001; $\beta_{alkalinity}$=0.45±0.11, p=0.0013, multivariable regression: "$E_{EO,}$ Water Quality"). In terms of water quality parameters, $DOC_{initial}$ had the largest negative influence on E_{EO}. For parameters that improved E_{EO}, higher water matrix conductivity improved E_{EO} by reducing the electrochemical cell's power demands ($\beta_{conductivity}$=-0.29±0.1, p<0.0001, multivariable regression: "$E_{EO,}$ Water Quality" Appendix 4.12). Accordingly, groundwater

required the lowest E_{EO} of the environmental waters due to the low DOC concentration and high conductivity. The energy demands of the EC:H_2O_2 system are in the range of competitive performance, making EC:H_2O_2 a promising option for scaled applications for treating TOrCs in environmental waters such as groundwater and river water, with the added benefit of DOC removal in the same reactor.

4.4. Conclusions

The goal of this research was to evaluate EC:H_2O_2 as a combined destructive and non-destructive treatment technology at neutral pH. This performance was assessed as a function of reactor inputs and solution pH. The treatment efficacy of environmental source waters containing varying levels of NOM, scavengers, and ionic constituents was also evaluated. Neither current density nor H_2O_2 alone promoted pCBA oxidation, although the combination of these parameters heavily influence performance. At neutral pH conditions, $[H_2O_2]_{initial}/[Fe^{2+}]_{generated}$ ratio was the key driver of oxidative performance, where ratios <0.7 had higher pCBA removal and higher ratios (0.7 – 1.6) decreased pCBA removal, likely due to H_2O_2 scavenging.

For water quality, pH was the key driver of improved removal, where lower pH conditions minimized the competition between H_2O_2 and O_2 for oxidation of Fe^{2+} to better encourage radical generation. When treating groundwater and river water, EC:H_2O_2 had both oxidative treatment of TOrCs *and* non-destructive treatment of DOC. The pseudo-first order rate constants and E_{EO} values demonstrated that EC:H_2O_2 is competitive with other AOPs for TOrC treatment based on energy requirements and

treatment performance, with an added benefit of DOC removal due to coagulation and flocculation in the same reactor.

Future work is needed to evaluate EC:H_2O_2 from a systems engineering perspective wherein the additional benefits such as DOC removal and *in-situ* chemical generation are parameterized to compare against the treatment costs associated with conventional treatment trains. Additionally, the byproducts generated during EC:H_2O_2 should be evaluated. For example, the co-dissolution of regulated metals from iron electrodes (e.g., manganese) could add secondary contamination. Finally, research is needed to inform reactor setups for EC:H_2O_2 and to explore H_2O_2 dosing technologies such as air-diffusion cathodes that can promote *in-situ* H_2O_2 generation, thereby decreasing *ex-situ* chemical additions and enhancing the process' potential as a small footprint decentralized treatment technology.

CHAPTER 5. PEROXI-ELECTROCOAGULATION FOR PFAS MITIGATION: THE IMPACT OF WATER QUALITY AND DISSOLVED ORGANIC MATTER ON REMOVAL PATHWAYS

5.1. INTRODUCTION

Per- and poly-fluoroalkyl substances (PFAS) are of great concern in waters across all sectors due to their environmental persistence, widespread occurrence, and chronic toxicity (Kwiatkowski et al., 2020). These issues are reflected in the surge of PFAS studies and the implementation of regulations in the United States (U.S) for multiple environmental-related agencies, including recent drinking water maximum contaminant levels (2023 at time of writing) and lifetime health advisories set by the US Environmental Protection Agency (EPA). Additional efforts and incentives to "treat PFAS at their source" to better limit downstream contamination include hazardous waste classification under the EPA's Resource Conservation and Recovery Act (RCRA), hazardous substance classification under the Comprehensive Environmental Response, Compensation, and Liability Act (CERCLA) for superfund sites, and inclusion in the National Pollutant Discharge Elimination System (NPDES) for industrial sources. Accordingly, PFAS treatment technologies are needed across these arenas for PFAS mitigation in drinking water, the PFAS-laden residuals from drinking water treatment, municipal wastewater, industrial wastewater, and other PFAS sources such as landfill leachates. Due to the interconnectivity of these different water sources, research on the impact of water quality characteristics is needed to better guide the design and implementation of emerging PFAS treatment technologies.

Electrochemical water treatment processes are progressively being researched as treatment technologies for PFAS mitigation in drinking water, wastewater, industrial wastewater, and other high-strength matrices such as landfill leachate. Electrochemical processes have garnered interest due to their *in-situ* generation of chemicals, which can be beneficial for water and wastewater applications for rural, decentralized, and small footprint systems, which may translate to potential PFAS mitigation applications (Chaplin, 2019; Radjenovic et al., 2020). Electrocoagulation (EC) can serve as a non-destructive technology for PFAS mitigation for higher-strength industrial matrices by sorbing PFAS compounds to metal (e.g., iron, zinc, or aluminum) hydroxide flocs (Kim et al., 2020; Lin et al., 2015; Yang et al., 2016b). The continuous production of Fe^{2+} during iron-EC can be leveraged by the *ex-situ* addition of H_2O_2 to induce peroxi-electrocoagulation (EC:H_2O_2), which enhances EC's oxidant generation capacity by producing hydroxyl radicals and other reactive oxygen species that may improve PFAS removal and degradation (Pratap and Lemley, 1994). The EC:H_2O_2 process has previously been used to treat trace organic compounds such as pesticides and pharmaceuticals and personal care products in wastewater (Pratap and Lemley, 1994; Serra-Clusellas et al., 2021). For PFAS treatment, the addition of H_2O_2 or other radical promotors such as peroxymonosulfate (PMS) improved PFAS removal when treating elevated PFAS concentrations (i.e., 5 - 100 mg/L) using high doses of radical promotors (e.g., 0.66 – 1.7 g/L H_2O_2 (Yang et al., 2016a), 1.7 g/L H_2O_2 (Singh et al., 2021), and 5.6 g/L PMS (Li et al., 2021)). For example, Li et al. (2021) reported 87% PFOS defluorination in 60 min of EC:PMS. In these proof-of-concept studies, however, the PFAS concentrations tested

were greater than common PFAS concentrations in water and wastewater streams and the dose of radical promotors applied exceeded doses applied for treatment in the real systems (e.g., 5 to 20 mg/L H_2O_2 for UV-advanced oxidation processes in water and wastewater) (Howe et al., 2012; Miklos et al., 2018). In terms of environmental sources, a survey of 171 PFAS sites including contaminated sites, landfills, industrial sites, and wastewater treatment plants found that 80% of the total sites tested contained under 2 µg/L PFAS, whereas the remaining 20% of highly contaminated sites ranged between 2 to 10 µg/L (Helmer et al., 2022).

The EC:H_2O_2 process may be effective for PFAS treatment by utilizing destructive and non-destructive processes for PFAS mitigation. Destructive processes can transform the initial PFAS compound (potentially via oxidation during EC:H_2O_2) into fluorinated byproducts and eventually achieve complete defluorination via a series of oxidation pathways to produce CO_2 and F^-. Non-destructive pathways during EC:H_2O_2 can include (1) sorption to iron hydroxides and (2) separation and accumulation into the flotation layer foam formed by cathodic bubble generation during electrolysis. Recently, the EC-generated flotation layer has been considered as a PFAS removal pathway via foam fractionation, due to the surfactant nature of PFAS (Shi et al., 2021). Previous aeration and dissolved air flotation studies have used foam fractionation as a non-destructive technique for treating highly concentrated PFAS matrices (µg/L to mg/L levels) such as landfill leachates and aqueous film forming foam (AFFF) formulations (Buckley et al., 2022; Burns et al., 2021; Lee et al., 2017; McCleaf et al., 2021; Meng et al., 2018; Robey

et al., 2020). Accordingly, these studies can inform better understanding of the role of the flotation layer during EC and EC:H_2O_2.

Research is limited in terms of EC and EC:H_2O_2 studies that have considered the relative contributions of the range of destructive and non-destructive removal pathways for PFAS treatment during EC:H_2O_2. For example, foam fractionation results in non-destructive PFAS removal that may be misreported as sorption to iron hydroxides if a study does not consider the foam layer, which can over-estimate the role of sorption to iron-oxides. In addition to the uncertainties in pathway contribution, the presence of realistic water quality parameters such as dissolved organic matter (DOM), pH, and ionic strength can impact PFAS mitigation and are not well reflected in point-of-concept electrochemical studies conducted in idealized electrolyte matrices. For example, higher salt concentrations can increase ionic strength and subsequently decrease PFAS' critical micelle concentration, thereby decreasing its water solubility and improving non-destructive treatment (Buckley et al., 2022; McCleaf et al., 2021; Meng et al., 2018).

The impacts of water quality, particularly the presence of DOM, are important considerations in water and wastewater treatment processes as DOM is ubiquitous in process streams. Accordingly, "DOM" is used in reference to organic matter in this chapter to include the broad range of organics that can occur in water, wastewater, and industrial matrices as opposed to "natural organic matter (NOM)" used to describe organics in environmental source waters. Interactions between DOM and PFAS can impact destructive and non-destructive removal trends in treatment applications. For example, DOM can scavenge oxidants during oxidative treatment processes, inhibiting

removal of target compounds (Von Gunten, 2018; Westerhoff et al., 1999). For non-destructive removal, DOM may decrease PFAS removal by outcompeting PFAS for sorption sites in granular activated carbon (GAC) and ion exchange (IX) technologies or DOM may enhance PFAS removal by complexing with PFAS and improving mass transfer to sorptive media (Dixit et al., 2020; Gagliano et al., 2020; Kothawala et al., 2017). Additionally, DOM has previously been correlated to PFAS occurrence in the foams generated in PFAS-contaminated natural waters due to the surfactant nature of PFAS and the formation of hydrophobic PFAS-DOM complexes at the air-water interface (Schaefer et al., 2022; Schwichtenberg et al., 2020).

However, the influence of DOM on PFAS removal pathways during EC:H_2O_2 is complicated by DOM's chemodiversity and the range of constituent parts. As such, more research is needed to understand and identify how DOM parameters influence PFAS treatment. Accordingly, operational parameters such as molecular weight distribution and optical geochemistry techniques (e.g., UV and fluorescence spectroscopy) are needed to understand the nuances of DOM constituents and functionalities. This information can inform understanding of how different DOM fractions and functionalities that comprise DOM most heavily impact overall PFAS treatment (Ishii and Boyer, 2012; Li et al., 2020; Matilainen et al., 2011; Yang et al., 2015).

The overarching goal of this research was to evaluate the removal pathways of PFAS treatment during EC:H_2O_2 and to better understand the impact of water quality characteristics on treatment performance. Four different PFAS were assessed: perfluorooctanoic acid (PFOA), perfluorooctanesulfonic acid (PFOS), 6:2 fluorotelomer

sulfonate (6:2 FtS), and 5:3 fluorotelomer carboxylic acid (5:3 FTCA). The first objective was to assess the impact of water quality (pH and DOM) on PFAS removal via EC:H_2O_2. The second objective was to elucidate the contribution of each PFAS removal pathway (i.e., destruction (via oxidation) and non-destructive pathways (sorption, flotation)) to better understand what PFAS-related residuals are generated from EC:H_2O_2 treatment. The third objective was to determine the impact of DOM source characteristics (molecular weight distribution, UV spectroscopy, and fluorescence spectroscopy) on PFAS treatment and fate trends to better understand how specific DOM parameters that are present in water, wastewater, and industrial waters can shift and impact PFAS treatment trends as technologies are increasingly applied for PFAS mitigation in the water and wastewater sector. These findings will help to advance understanding of the applicability of EC:H_2O_2 for treating different water and wastewater matrices.

5.2. MATERIALS AND METHODS

5.2.1. Electrochemical Experiments

5.2.1.1. Target PFAS

Four PFAS compounds were selected for this study (Table 5.1). The compounds were PFOA (95%, Sigma Aldrich, St. Louis, MO), PFOS (spiked as PFOS-potassium salt, ≥98%, Sigma Aldrich, St. Louis, MO), 6:2 FtS (97%, Synquest laboratories, Alachua, FL), and 5:3 FTCA (97%, Synquest laboratories, Alachua, FL). Fluorotelomers (e.g., 6:2 FtS and 5:3 FTCA) are replacements for PFOA and PFOS in some products and have been detected in the environment at elevated concentrations following the ban of PFOA and

PFOS in the US (Cousins et al., 2020; Maldonado et al., 2022). The 5:3 FTCA and 6:2 FtS compounds are also commonly referred to as “PFAS precursors”, but are also PFAS themselves under the EPA’s Contaminant Candidate List 5 (CCL5) definition of PFAS. Accordingly, all four compounds are collectively referred to as PFAS in this work.

Table 5.1 PFAS chemical characteristics. Chemical structures were adapted from reported Pubchem structures.

PFAS compound	Structure	Functional group	Molecular Weight, g/mol	Chemical Formula
5:3 FTCA	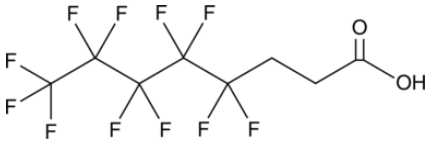	Carboxylate	342	$C_8H_5F_{11}O_2$
PFOA	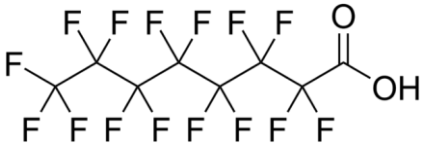	Carboxylate	414	$C_8H_8F_{15}O_2$
6:2 FtS	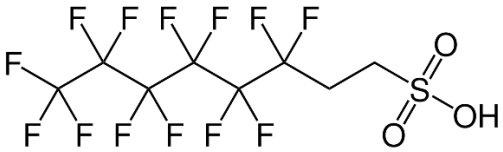	Sulfonate	428	$C_8H_5F_{13}O_3S$
PFOS	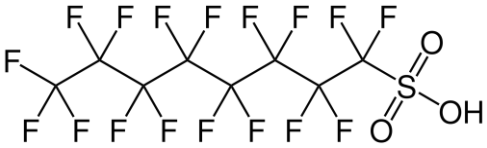	Sulfonate	500	$C_8HF_{17}O_3S$

The four PFAS (PFOA, PFOS, 5:3 FTCA, and 6:2 FtS) were spiked at equimolar levels of 0.5 µM, (PFOA = 207 µg/L, PFOS = 250 µg/L, 5:3 FTCA = 171 µg/L, 6:2 FtS = 214 µg/L) into EC:H_2O_2 test waters. These concentrations are greater than levels typically

occurring in natural waters (i.e., less than 200 ng/L, as reported by Franke et al. (2019)) that are of concern for drinking water treatment. However, they are closer to the ranges of PFAS concentrations typically present in landfill leachates, concentrated waste streams from nanofiltration and reverse osmosis (Franke et al., 2019), ion exchange regenerant brines (up to 1 mg/L per Wang et al. (2021)), and wastewater (15 to >1500 ng/L as reported by Lenka et al. (2021)). Accordingly, the higher concentrations used in this study reflect highly contaminated sources, and also enable accurate quantification of >99% PFAS removal using the LC-MS 2020.

5.2.1.2. Batch Experiments

The EC:H_2O_2 experiments were conducted for 20 minutes at a current density of 7.4 mA/cm^2 with a stir rate of 100 rpm (G = 99 s^{-1}) using glass stir bars in parallel plate batch reactors using 1020 steel iron for the anode and cathode. The electrodes were connected to an XPH 75-2D dual DC power supply (Sorenson Electronics, Cedar City, UT) equipped with a polarity reversal device to alternate the anode and cathode every 30 seconds. Controls conducted with no electricity had negligible PFAS losses in the reactor (Section 5.3.2.). During EC:H_2O_2, 60 mg/L H_2O_2 was added to the reactor every 5 minutes to stimulate oxidative reactions throughout the EC:H_2O_2 experiment. Prior EC:H_2O_2 and Fenton studies have applied relatively large H_2O_2 doses ranging from 100 mg/L to 1000 mg/L (Ghanbari and Moradi, 2015b; Pratap and Lemley, 1998; Serra-Clusellas et al., 2021; Singh et al., 2021; Yang et al., 2016a; Yazdanbakhsh et al., 2015b). However, depending on the water matrix, elevated H_2O_2 doses can limit oxidant treatment

efficacy due to radical quenching by H_2O_2. Accordingly, to minimize radical quenching, 60 mg/L H_2O_2 was selected as a mid-range dose compared to doses applied for water (e.g., 5 – 20 mg/L H_2O_2 for UV/H_2O_2 applications in full advanced treatment during water reuse), wastewater, and industrial wastewater treatment (Howe et al., 2012; Miklos et al., 2018). The 5-min interval additions of *ex-situ* H_2O_2 were based on preliminary experiments that showed that roughly 85±5% of the H_2O_2 was utilized after 5 minutes of EC:H_2O_2 at pH 3 (Appendix 5.2). Intermittent H_2O_2 has been shown to improve EC:H_2O_2 performance compared to a single initial large dose (Pratap and Lemley, 1998; Yang et al., 2016a). Additionally, incremental H_2O_2 addition helped maintain the pH in the pH 3 – 4 range (for pH 3 experiments) needed for oxidative conditions (Appendix 5.2). Following EC:H_2O_2 experiments, the residual H_2O_2 was measured using Hach Model Hyp-1 test kits.

5.2.1.3. Experimental Approach to Test the Impact of Water Quality on PFAS Removal

All experiments were conducted in 4 mM HCO_3^- solution as the baseline matrix to buffer the system and reflect the alkalinity found in water and wastewater at pH 6.3. Two different pH levels were studied: 6.3 and 3. The pH 6.3 system was selected to reflect circumneutral pH conditions in water and wastewater treatment. The pH 3 system (adjusted via 3 N HCl) was selected to provide favorable conditions for oxidant generation via Fenton's reaction (Pignatello et al., 2006; Waite, 2006). Previous EC studies focused on PFAS mitigation also used pH 3 conditions (Kim et al., 2020; Li et al., 2021; Yang et al., 2016).

5.2.1.4. Experimental Approach to Assess Removal Pathways during EC:H_2O_2

Removal pathway experiments were conducted to assess the contribution of each system input that can lead to destructive and non-destructive PFAS pathways during EC:H_2O_2, including oxidant generation, sorption to iron, and flotation layer accumulation. Experiments were conducted based on the system inputs (i.e., electricity, iron electrodes, and H_2O_2) during EC:H_2O_2 and their resulting pathway. In this work, destructive treatment refers to the transformation of the parent PFAS compound. However, defluorination (based on fluoride detection) was not included in this work due to the low initial PFAS concentration (0.5 μM) that would result in fluoride generation below detection. Non-destructive treatment refers to the separation of PFAS from the aqueous phase to a separate media such as iron flocs and foam. All removal pathway experiments were conducted at pH 3. In addition to the EC:H_2O_2 experiments, EC-only controls were performed to examine PFAS removal via sorption to iron and flotation layer accumulation (due to cathodic bubble generation from the electrolytic cell). To further isolate the role of iron in the absence of a flotation layer, no electricity controls including "Fe^{3+} coagulation" and "electrodes only" were conducted. Additionally, a "No-Electricity (H_2O_2 + Electrodes)" control was conducted to assess potential oxidants generated at pH 3 due to reactions between H_2O_2 and the electrode surface. The H_2O_2-only experiments were conducted by adding 60 mg/L H_2O_2 every 5 minutes (240 mg H_2O_2/L total addition, the same as EC:H_2O_2 tests) to assess PFAS removal due to H_2O_2 alone. Finally, an EC:H_2O_2 experiment using only PFOA (not the four-PFAS mixture) was conducted to gauge short-chain PFCA formation due to PFOA degradation.

Following EC:H_2O_2 experiments, 20 mL of the flotation layer (approximately 10% of the reactor volume) containing a mixture of iron flocs and foam, were pipetted from the perimeter and upper layer of the reactor. The extracted flotation layer was poorly soluble in water and was mixed with 20 mL of methanol to dissolve the foam mixture prior to filtration and liquid chromatography mass spectrometry (LC-MS) quantification. To quantify the potential flotation layer accumulation pathway, a PFAS enrichment factor was defined as $C_{flotation\ layer}/C_{bulk}$ to reflect the ratio of PFAS in the flotation layer (i.e., removed via flotation layer accumulation) relative to the concentration in the bulk solution, similar to foam fractionation studies (Meng et al. 2016).

5.2.2. PFAS Analysis

Following experiments, PFAS were quantified by LC-MS. Prior to analysis, PFAS samples were filtered through 0.22 µm polyethersulfone (PES) syringe filters (Millipore Sigma, Burlington, MA). There was ≤5.1% difference between filtered vs. non-filtered controls for all PFAS (with the greatest difference for 6:2 FtS, Appendix 5.1), indicating that losses due to filtration were minimal. For µg/L experiments, a Shimadzu LCMS 2020 (Kyoto, Japan) was used to quantify degradation of spiked PFOA, PFOS, 6:2 FtS, and 5:3 FTCA. Using a method adapted from Min and Wang (2023), a Shimadzu LCMS/MS 8060 was used to quantify ng/L-levels of short-chain perfluorocarboxylic acid (PFCA) transformation products including perfluorobutanoic acid (PFBA), perfluoropentanoic acid (PFPeA), perfluorohexanoic acid (PFHxA), and perfluoroheptannoic acid (PFHpA) (standards were 98%, 97%, ≥98%, ≥97% purity, respectively, purchased from Sigma

Aldrich, St. Louis, MO). These short-chain compounds were selected for measurement based on previous studies that showed the production of short-chain PFCAs as PFAS degraded (Kim et al., 2020; Radjenovic et al., 2020). An internal standard containing ^{13}C-labeled PFAS compounds (Product No. MPFAC-C-ES; Wellington Laboratories containing ^{13}C-labeled versions of PFBA, PFPeA, PFHxA, PFHpA, PFOA, and PFOS) was added to each sample. PFOA and 5:3 FTCA were quantified relative to the internal standard M8PFOA (m/z = 421), and PFOS and 6:2 FtS were quantified relative to the internal standard M8PFOS (m/z = 507). Additional information on the PFAS quantification method is provided in Appendix 5.1.

5.2.3. Dissolved Organic Matter Characterization

Four laboratory DOM sources and a natural river water, reflecting a range of characteristics, were analyzed to assess how DOM characteristics influence PFAS removal during EC:H_2O_2 treatment (through, e.g., oxidant scavenging, hydrophobic and ionic co-sorption reactions depending on functional groups present, and foam stabilizing reactions). Oxalic acid (98%, Sigma Alrich; St. Louis, MO) and salicylic acid (sodium salicylate, 99%, Alfa Aesar; Haverhill, MA) are low molecular weight acids that can also serve as bi-dentate ligands. Oxalic acid has lower reactivity with oxidants, whereas salicylic acid has higher reactivity. Suwannee River natural organic matter (SR-NOM) (RO Isolate, International Humic Substance Society, Denver, Colorado) was selected as a laboratory-grade reference for environmental DOM containing a mixture of organic constituents. Humic acid (Humic acid sodium salt, Sigma Aldrich, Milwaukee, WI) was

used as a representative of high molecular weight, highly aromatic DOM moieties. In addition to the laboratory DOM sources, the Milwaukee River (MKE River, Milwaukee, WI) was sampled to study a real water containing a diverse mixture of organic constituents.

DOM was quantified as dissolved organic carbon (DOC) using a TOC V_{CSN} (Shimadzu, Kyoto, Japan) based on EPA method 415.3. Optical techniques including the UV_{254}, and specific ultraviolet absorbance (SUVA) were performed using a Genesys50 spectrophotometer (ThermoScientific, Waltham, MA) for wavelengths 200 to 400 nm. Finally, ultrafiltration using regenerated cellulose membrane discs (Millipore, Burlington, MA) was used to fractionate DOM as a function of molecular weight, (<1 kDa, 1-3 kDa, 3-10 kDa, and >10 kDa). All DOM filtration separations were operated using a concentration factor of 10 (volume/volume) (Xu and Guo, 2017). Following molecular weight fractionation, the DOM fractions were quantified using a Shimadzu TOC-L (Kyoto, Japan). The DOC-based size fractionation method was selected for this investigation to include non-chromophoric DOM moieties that are generally excluded from chromophoric DOM analytical size characterization techniques such as UV-based size exclusion chromatography. Fluorescence was analyzed to measure the electron excitation emission matrices (EEMs) and calculate the fluorescence index (FIX), biological index (BIX), and humic index (HIX) of the bulk DOM and low molecular weight DOM (<1 kDa) using a Shimadzu RF 6000 spectrofluorometer (Kyoto, Japan). Characteristics of the DOM sources (molecular weight distributions, optical parameters, reactivity, and fluorescence indices) are shown in Table 5.2, Table 5.3, and Figure

5.1**Error! Reference source not found.**. EEMs for the SR-NOM, humic acid, and MKE River are provided in Appendix 5.6.

Table 5.2. Dissolved organic matter characteristics.

DOM source	Molecular weight (g/mol)	pKa	SUVA, (L/mg C-m)	Description
		Single Organic Compounds		
Oxalic Acid	90.0	1.28, 4.28	0.21	Low molecular weight, slow HO• reactivity ($k_{HO•}$= 1.4 x 10^6 $M^{-1}s^{-1}$) [a]
Salicylic Acid	138	2.97	0.51	Low molecular weight, Fast HO• reactivity ($k_{HO•}$= 2.2 x 10^{10} $M^{-1}s^{-1}$) [a]
		Bulk Organic Matter		
SR-NOM	Mixture (Figure 5.1)	Mixture of acid and base constituents	3.1	Laboratory grade river surrogate, mild reactivity ($k_{HO•}$= 3.3 x 10^8 $M^{-1}s^{-1}$) [b]
Humic Acid			7.6	High molecular weight, aromatic, humic surrogate
MKE River			3.2	Environmental river sample

[a] Rate constants from Buxton et al. (1988)
[b] Rate constants from Ahn et al. (2017)

Table 5.3. Fluorescence indices for the bulk DOM studied: SR-NOM, humic acid, and MKE River. The DOM was analyzed at pH 3 to reflect the treatment conditions utilized for comparison in 5.3.1.2. and 5.3.5. in which the impact of DOM is discussed.

DOM Source	Freshness Index (FIX)	Biological index (BIX)	Humic Index (HIX)	HIX/BIX
SR-NOM	1.15	0.52	11.92	23.11
Humic acid	1.03	0.43	32.89	76.12
MKE River	1.48	0.75	7.25	9.63

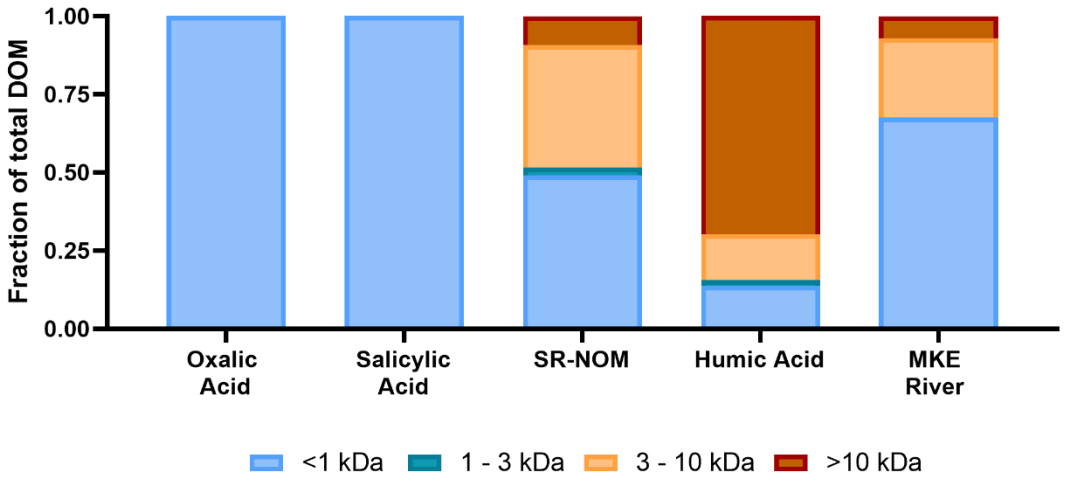

Figure 5.1. The molecular weight size distribution of the DOM tested here, based on ultrafiltration size fractionation. Molecular weight was fractionated into the size ranges <1 kDa, 1- 3 kDa, 3 - 10 kDa, and >10 kDa. Ultrafiltration was performed on water adjusted to pH 3 for SR-NOM, humic acid, and the MKE River using a concentration factor of 10. The DOM was analyzed at pH 3 to reflect the treatment conditions utilized for comparison in 5.3.1.2. and 5.3.5. in which the impact of DOM is discussed.

5.2.4. Statistical Analyses

Statistical analyses including one-way ANOVA, two-way ANOVA, and Tukey's multiple comparison post-hoc analysis were conducted using GraphPad Prism 9 software using $\alpha<0.05$ as an indicator of significance. Pearson correlations were also conducted to assess the strength of correlation between DOM characteristics and PFAS mitigation via EC:H_2O_2.

5.3. RESULTS AND DISCUSSION

5.3.1. Peroxi-Electrocoagulation for PFAS Removal

5.3.1.1. The Impact of pH

After 20 min of EC:H_2O_2 treatment at circumneutral pH, PFAS removal trends were PFOS > 6:2 FtS ≥ 5:3 FTCA > PFOA (Figure 5.2). Where PFOS had the highest removal at 53 ± 6.5% ($p < 0.0001$, one-way ANOVA). The PFOS removal may have been highest due to the high electronegativity of the sulfonate functional group, which can promote sorption to metal hydroxide flocs via charge neutralization. Previous research showed that PFOS had the highest sorption relative to other PFAS (Xiao et al., 2013; Yang et al., 2016b). Additionally, PFOS has been shown to have the highest accumulation at the air-water interface (e.g., the flotation layer) relative to other PFAS such as PFOA and 6:2 FtS (Schaefer et al., 2022). Removals of 6:2 FtS and 5:3 FTCA were not statistically different ($p = 0.49$, Tukey's post-hoc analysis), at 26 ± 5.1% removal and 19 ± 5.1% removal, respectively. These fluorotelomers may be susceptible to multiple

removal pathways, including hydrogen abstraction carried out by hydroxyl radicals at the C-H alkyl groups (the fluorotelomers are not fully fluorinated whereas PFOA and PFOS are). Additionally, 6:2 FtS also contains a sulfonate group that can promote removal through non-destructive pathways in a similar manner to PFOS. Alternately, 5:3 FTCA is lower molecular weight and more hydrophilic than the other PFAS tested, so removal through oxidation is most likely due to the poor affinity of shorter chain PFAS to be removed via non-destructive pathways (Ateia et al., 2019).

Of the PFAS tested, PFOA had the least removal (less than 5%). This poor removal aligns with previous studies where PFOA is generally more recalcitrant than PFOS in terms of non-destructive pathways due to the carboxylic acid group that improves water solubility (Xiao et al., 2013). Additionally, PFOA is fully fluorinated, thereby minimizing the likelihood of hydroxyl radical oxidation via hydrogen abstraction. Given the negligible removal of PFOA at circumneutral pH, and that PFOS was the only compound with more than 50% removal, PFAS mitigation using EC:H_2O_2 appears to perform poorly compared to other non-destructive processes such as granular activated carbon, ion exchange, reverse osmosis, and nanofiltration at neutral pH conditions.

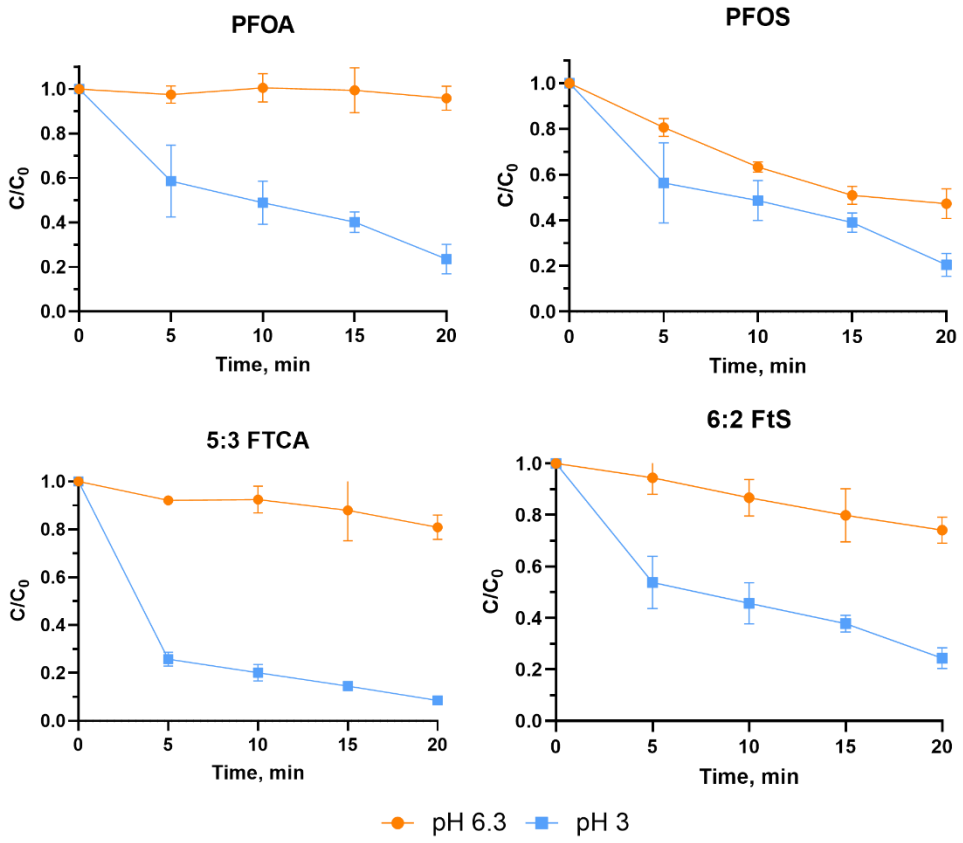

Figure 5.2. The impact of pH on removal of PFAS during EC:H_2O_2. All four PFAS (PFOA, PFOS, 5:3 FTCA, and 6:2 FtS) were spiked at 0.5 µM. All experiments were conducted in 4 mM HCO_3^-, where pH 3 experiments were adjusted using 3 N HCl (final Cl^- = 170 mg Cl^-/L). The EC:H_2O_2 experiments were run at 7.4 mA/cm^2 for 20 minutes with additions of 60 mg/L of H_2O_2 every 5 minutes. Samples were collected every 5 minutes (during treatment, reactor volume changed less than 1% from sampling and H_2O_2 addition). Error bars indicate ±1 standard deviation of triplicate experiments.

For all cases, PFAS removal was greater at pH 3 relative to pH 6.3 (Figure 5.2). At pH 3, removal trends shifted where 5:3 FTCA had the highest removal, 91.5 ± 0.9%, after 20 min (p=0.01, one-way ANOVA; 5:3 FTCA as control column), compared to PFOA, 6:2 FtS, and PFOS, which had statistically similar removals ranging from 75.6% to 79.5% (p=0.65, one-way ANOVA). The high level of removal of 5:3 FTCA relative to other PFAS

indicates that the compound is more susceptible to oxidants that are generated through Fenton reactions at pH 3.

Improved PFAS treatment at pH 3 compared to pH 6.3 can be attributed to improvements in both destructive and non-destructive pathways. First, at pH 3, oxidant generation deriving from Fe^{2+} and H_2O_2 interactions greatly improves and leads to removal via hydroxyl radicals and oxidant species. In terms of non-destructive pathways, the iron oxides carry a positive surface charge and higher zeta potential at acidic conditions, which can lead to greater sorption of PFAS anions (all PFAS in this work are expected to be in their anionic forms at pH 3) (Johnson et al., 2007; Uwayezu et al., 2019). Additionally, the HCl addition required to adjust the pH to 3 increased the ionic strength (920 µS/cm at pH 3 vs. 450 µS/cm at pH 6.3). Higher ionic strength solutions decrease the critical micelle concentration of PFAS, which decreases PFAS solubility and encourages the formation of micelles and hemi-micelles (Radjenovic et al., 2020). These micelles are more readily removed via non-destructive pathways such as sorption and foam fractionation due to their higher molecular size that promotes mass transfer, and potential accumulation in the foam layer due to enhanced buoyancy of the aggregated compounds (Buckley et al., 2022; Lee et al., 2017; McCleaf et al., 2021; Radjenovic et al., 2020). Due to the higher PFAS treatment efficacy, the remainder of tests in this study were conducted at pH 3.

5.3.1.2. The Impact of Dissolved Organic Matter on PFAS Removal

The presence of DOM had mixed impacts on PFAS removal during EC:H_2O_2 depending on the DOM source and the PFAS species being treated (Figure 5.3). For PFOA, the presence of oxalic acid inhibited treatment relative to the bicarbonate-only system ($p < 0.0001$, Tukey's post-hoc comparison). However, oxalic acid did not decrease the removal of 5:3 FTCA, PFOS, and 6:2 FtS. The presence of organic anions (e.g., carboxyl and phenolic groups in the oxalic acid) can form iron-organic complexes that impede reactions between H_2O_2 and iron, as well as interfere with non-destructive processes between iron and target compounds (Daugherty et al., 2017; Fischbacher et al., 2017). This potential impedance is supported by the higher H_2O_2 residuals observed following treatment of the oxalic acid compared to other matrices (21 ± 3.2 mg H_2O_2/L as compared to less than 5 mg H_2O_2/L for other DOM-containing experiments with higher removal (Appendix 5.2)).

.

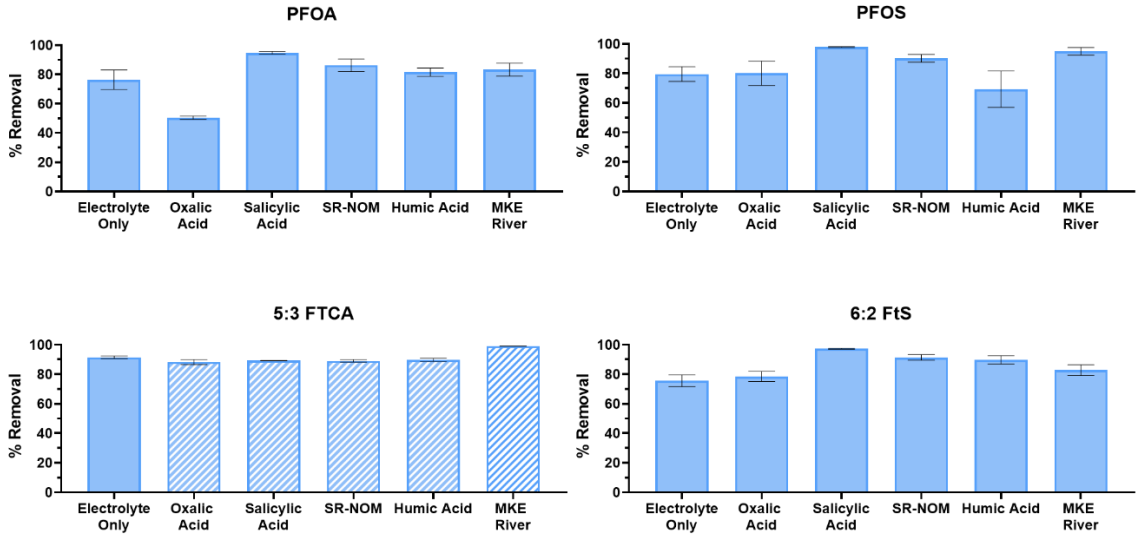

Figure 5.3. The impact of DOM on PFAS removal via EC:H_2O_2 at pH 3, where the pH was adjusted using 3 N HCl. All four PFAS (PFOA, 5:3 FTCA, PFOS, and 6:2 FtS) were spiked at 0.5 µM each in 4 mM HCO_3^- as the electrolyte source (Final Cl^- = 170 mg Cl^-/L). The EC:H_2O_2 experiments were run at 7.4 mA/cm^2 for 20 minutes. During EC:H_2O_2, 60 mg/L of H_2O_2 was spiked every 5 minutes. All DOM sources were added at 10 mg-C/L except for Electrolyte-only (no DOM added). For environmental water, the DOC concentration was 7.0 mg-C/L in the MKE River. Error bars indicate ±1 standard deviation of triplicate experiments. Striped bars indicate removal below the detection limit of 18 µg/L for 5:3 FTCA; the concentration in these treated samples was set at the detection limit for % removal calculation

Alternately, other DOM sources (salicylic acid, SR-NOM, and MKE River) improved the mean removal of PFOA, PFOS, and 6:2 FtS (Figure 5.3). This improved removal may derive from complexation between PFAS, iron, and DOM, which can increase mass transfer between oxidants and PFAS and/or promote sorption to iron flocs and flotation layer accumulation (Lee et al., 2017; McCleaf et al., 2021; Shutova et al., 2016). With the exception of PFOA, PFAS removal was greater than 70% regardless of the DOM source matrix, with 5:3 FTCA having the highest removal (consistently below detection). The role of DOM on the potential removal and fate pathways of PFAS within this system is discussed in greater detail in *Section 5.3.5*.

5.3.2. PFAS Mitigation Pathways

Additional control experiments were conducted to contextualize the potential removal pathways during EC:H_2O_2 based on the system inputs (i.e., electricity, iron electrodes, H_2O_2) (Figure 5.4). The relative contribution from the various PFAS mitigation pathways depended heavily on the type of functional groups in the PFAS compounds (carboxylic acid for PFOA and 5:3 FTCA or sulfonic acid for PFOS and 6:2 FtS). The carboxylic acid-based PFAS (PFCAs) had minimal removal via EC-only compared to the sulfonic acid-based PFAS (PFSAs). Higher relative PFSA removal was potentially due to their electronegative nature, which improves removal by non-destructive processes.

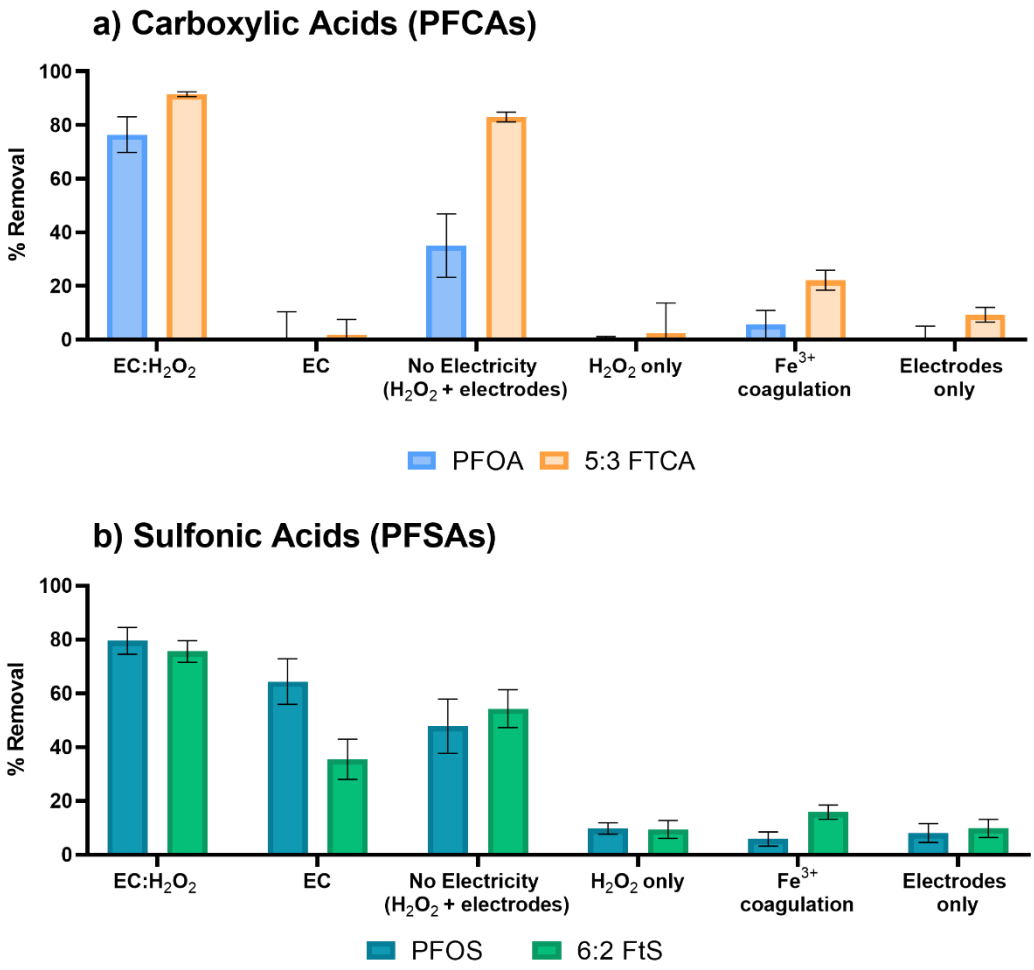

Figure 5.4. Control experiments to evaluate EC:H_2O_2 pathways for treatment of A) carboxylic acid-containing PFAS and B) sulfonic acid-containing PFAS. All four PFAS (PFOA, 5:3 FTCA, PFOS, and 6:2 FtS) were spiked at 0.5 µM each in 4 mM HCO_3^- at pH 3, where pH was adjusted using 3 N HCl (Final Cl^- = 170 mg Cl^-/L). The EC:H_2O_2 experiments were run at 7.4 mA/cm^2 for 20 minutes. During electrolysis, 60 mg/L of H_2O_2 was spiked every 5 minutes. During EC-only, electrolysis was run at 7.4 mA/cm^2 for 20 minutes. In "No Electricity (H_2O_2 + electrodes)", 60 mg/L H_2O_2 was spiked every 5 minutes in the presence of the iron electrodes. In H_2O_2 only, 60 mg/L of H_2O_2 was spiked every 5 minutes. For Fe^{3+} coagulation, 190 mg Fe^{3+}/L was spiked as $FeCl_3$•$6H_2O$ to match the estimated iron concentration generated during EC and EC:H_2O_2. For Electrodes only, reactors were stirred for 20 minutes with the electrodes in the solution. Error bars indicate ±1 standard deviation of triplicate experiments.

5.3.2.1. Perfluorocarboxylic Acid Mitigation Pathways

For PFCAs, the oxidative treatments that yielded removal, EC:H_2O_2 and "No Electricity (H_2O_2 + electrodes)", resulted in the highest PFOA and 5:3 FTCA mean removal, whereas the non-destructive controls, EC only, Fe^{3+} coagulation, and Electrodes only, had low PFCA removal. The flotation layer enrichment factor was less than 1 for all no-electricity control experiments, indicating that flotation layer accumulation was not a prominent non-destructive removal pathway in these tests (Appendix A5.3).

The removal of 5:3 FTCA may largely be due to the destructive component of EC:H_2O_2 because the EC:H_2O_2 and "No Electricity (H_2O_2 + electrodes)" were not statistically different ($p = 0.45$, 5:3 FTCA). The "No Electricity (H_2O_2 + electrodes)" resulted in low PFOA removal, yet was still higher than all other non-destructive pathways. The similar removal between EC:H_2O_2 and "No Electricity (H_2O_2 + electrodes)" may imply that PFCAs are susceptible to oxidation via the reactive oxygen species generated by H_2O_2 and the iron anode surface at low pH. In the "No Electricity (H_2O_2 + electrodes)" tests, 88.5 ± 2.3% of H_2O_2 was removed, in the presence of the iron electrodes at pH 3, demonstrating that H_2O_2 was reactive at these conditions and likely contributed to PFOA removal. In addition to the H_2O_2 depletion following "No Electricity (H_2O_2 + electrodes)", the residual dissolved iron following treatment was approximately 20 mg/L, indicating non-faradaic iron generation at the conditions tested which leads to oxidant generation at the conditions tested based on the combination of H_2O_2 being depleted, iron being generated, and 5:3 FTCA being removed (Appendix A5.7). Oxidant

formation was additionally confirmed for the "No Electricity (H_2O_2 + electrodes)" at pH 3 in *Chapter 4: Section 4.3.2.3.* based on pCBA removal at similar conditions tested. However, when H_2O_2 only was spiked into the system without iron electrodes, PFAS removal was less than 10% for all cases, indicating that destructive removal via oxidation only occurred when iron and H_2O_2 were both present (i.e., via Fenton's reactions).

Previous EC-only studies have shown that PFAS oxidation occurs at pH 3 (Kim et al., 2020; Yang et al., 2016a). However, 5:3 FTCA (the target PFAS most susceptible to oxidation) demonstrated negligible removal in the EC-only system, indicating that hydroxyl radicals may not have been generated under the electrochemical conditions used in this work. This difference may be due to the low current density (7.4 mA/cm^2) and shorter treatment times (20 minutes) applied in this work as compared to the higher current densities (20 – 80 mA/cm^2 for PFOA removal) and longer treatment times used in other studies that demonstrated hydroxyl radical activity in EC-only systems (Kim et al., 2020). Kim et al. (2020) reported that EC-only resulted in complete removal of PFOA following 6 hours of electrolysis at pH 3, accompanied by up to 20% defluorination and the production of shorter chain PFAS. In this study, EC-only likely had poor destructive treatment under the tested conditions; accordingly, EC-only is hereafter described in terms of non-destructive pathways such as sorption to flocs and flotation layer accumulation.

5.3.2.2. Perfluorosulfonic Acid Mitigation Pathways

For PFSAs (including PFOS and 6:2 FtS), both EC:H_2O_2 and EC-only treatments yielded significant removal relative to controls (*p = 0.083, one-way ANOVA*), potentially indicating that non-destructive removal contributed to PFSA mitigation (i.e., removal due to sorption to iron and flotation layer accumulation). To assess the role of iron, additional Fe^{3+} conventional coagulation experiments were conducted to vet iron-based removal in the absence of bubble and foam generation due to electrochemical reactions at the cathode. Both PFSAs had greater removal in EC-only treatments relative to Fe^{3+} coagulation, indicating that flotation layer accumulation was likely the dominant non-destructive pathway. During EC-only, the enrichment factor was 3.5 ± 0.15 and 2.3 ± 0.201 for PFOS and 6:2 FtS, respectively, indicating PFAS partitioned from the bulk solution into the flotation layer. For all other pathway controls (i.e., all tests other than EC and EC:H_2O_2), the flotation enrichment factors were less than 1.3 (Appendix 5.3). The "No Electricity (H_2O_2 + electrodes)" control removed more than 50% of both PFSAs, likely due to enhanced oxidant activity at pH 3. Compared to PFOS, 6:2 FtS is more susceptible to oxidative reactions due to its C-H bonds. Considering all pathway control tests, PFSAs were removed by both destructive and non-destructive pathways during EC:H_2O_2.

Overall, the PFAS removal pathways in EC:H_2O_2 can be difficult to isolate due to the combined role of multiple removal pathways involving iron and H_2O_2, all of which can occur simultaneously and have confounding impacts. For example, at pH 3, iron is more positively charged, which can improve sorption of anionic PFAS to iron, in turn

improving sorption to flocs and accumulation in the flotation layer. At the same time, the oxidant yield via Fenton's reactions also improves at pH 3, which leads to higher levels of oxidative removal. Accordingly, future studies that assess defluorination are needed to better delineate the role of the potential pathways of oxidation, non-destructive removal via sorption to flocs, and flotation layer accumulation.

5.3.3. Oxidation Byproducts Following EC:H_2O_2

Short-chain PFCAs were quantified following pathway experiments to verify oxidation during EC:H_2O_2. Shorter chain PFCAs (PFBA, PFPeA, PFHxA, and PFHpA) were generated following destructive treatment relative to initial conditions (Figure 5.5). Alternately, EC-only experiments did not yield short-chain PFAS, indicating that oxidation did not occur in the EC-only system under the conditions tested. These data align with the removal data (Figure 5.5), wherein EC:H_2O_2 had the highest removal of parent compounds (ostensibly transformed to shorter-chain PFAS). Of the transformation products assessed here, PFPeA and PFHxA were present at the highest concentrations. This trend aligns with previous studies that reported production of PFPeA and PFHxA following oxidation of 5:3 FTCA and 6:2 FtS (Abada et al., 2018; Carrillo-Abad et al., 2018; Yang et al., 2014; Zhang et al., 2020).

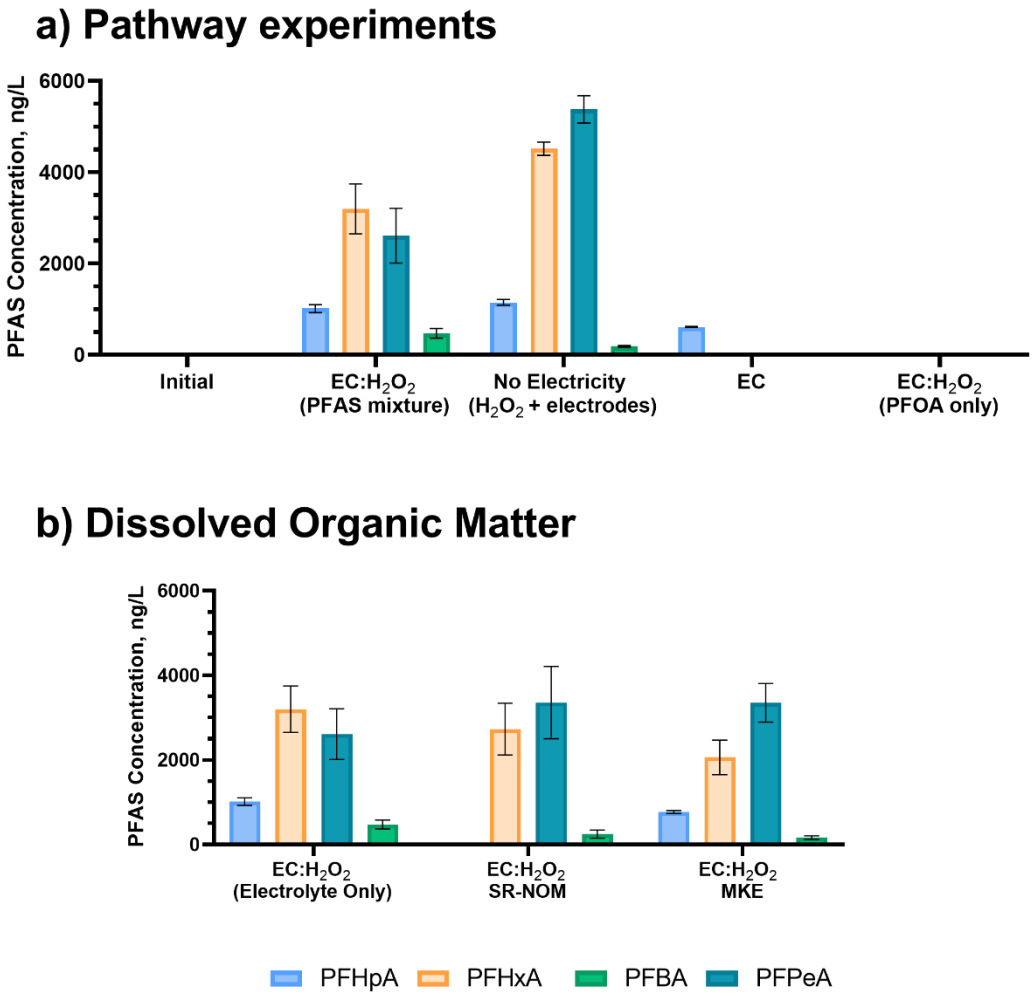

Figure 5.5. The occurrence of short-chain PFAS transformation products in A) pathway experiments in 4 mM HCO_3^- and B) EC:H_2O_2 DOM experiments. Concentration reflects the PFAS measured via LC-MS 8060. All experiments were conducted at pH 3 adjusted with 3 N HCl (Final Cl^- = 170 mg/L). All four PFAS (PFOA, 5:3 FTCA, PFOS, and 6:2 FtS) were spiked at 0.5 µM each. The EC:H_2O_2 and EC-only experiments were run at 7.4 mA/cm^2 for 20 minutes. During EC:H_2O_2, 60 mg/L of H_2O_2 was spiked every 5 minutes. In "No Electricity (H_2O_2 + electrodes)", 60 mg/L H_2O_2 was spiked every 5 minutes in the presence of the iron electrodes. Error bars indicate ±1 standard deviation of triplicate experiments.

In studies of the oxidation of 6:2 FtS using UV advanced oxidation processes, cobalt-activated peroxymonosulfate oxidation, and boron-doped diamond electrooxidation, PFHxA was the major initial transformation product, followed by

PFHpA (Carrillo-Abad et al., 2018; Yang et al., 2014; Zhang et al., 2020). For 5:3 FTCA, oxidation via zinc oxide photocatalysis formed PFHxA, PFPeA, and PFBA (Abada et al., 2018). These findings coincide with this study, wherein higher concentrations of PFHxA, PFPeA, and PFHpA were observed following treatment. Oxidation of 5:3 FTCA and 6:2 FtS likely proceeds through the hydrogen abstraction of their hydrogenated alkyl groups via HO• (Abada et al., 2018; Carrillo-Abad et al., 2018; Yang et al., 2014; Zhang et al., 2020).

Unlike the fluorotelomers, PFOA and PFOS do not contain extractable C-H hydrogens that are susceptible to oxidation via HO•; therefore, additional PFOA-only experiments were conducted to gauge byproduct generation for fully fluorinated PFAS during EC:H_2O_2. The PFOA-only tests did not produce quantifiable PFCA products. This absence of products implies that PFOA may undergo a separate degradation reaction mechanism that does not yield the shorter-chain PFAS assessed in this work, such as direct defluorination, or formation of other transformation products. In this work, PFOA removal was ascribed to destructive pathways (based on EC:H_2O_2 and "No Electricity (H_2O_2 + electrodes)" controls), and minimal removal was observed for the non-destructive pathways (EC only, Fe^{3+} coagulation, electrodes only) (Figure 5.4). Accordingly, future research is needed to assess the potential PFOA degradation pathway in EC:H_2O_2, and the potential for direct defluorination and destructive treatment (Le et al., 2019).

However, during EC:H_2O_2 experiments in the 4 mM HCO_3^- electrolyte only matrix, some non-destructive PFOA removal was observed based on the flotation enrichment

factor greater than 1 (i.e., EF = 2.6 ± 0.7 in PFAS mixture and 3.8 ± 0.9 in PFOA only system), indicating that PFOA partitioned to the flotation layer in the absence of PFOS (Appendix 5.3). The addition of H_2O_2 may improve PFAS removal via foam fractionation as H_2O_2 decays into dissolved oxygen that incorporates into the flotation layer over the course of treatment. However, during EC-only, the PFOA enrichment factor did not increase beyond approximately 1, indicating that the PFOA concentration in the flotation layer was similar to the concentration in the bulk solution (Appendix 5.3). The observed PFOA removal (Appendix 5.4) may indicate that PFOA oxidation proceeds through a separate reaction mechanism that does not produce the four short chains typically produced during the PFAS un-zipping cycle that is typically instigated via direct electron transfers at the anode surface, as described in boron-doped diamond electrooxidation studies (Kim et al., 2020; Radjenovic et al., 2020). However, if direct electron transfers at the anode surface contributed to oxidative removal in this system, more 5:3 FTCA and PFOA removal would be observed in the EC-only controls, which have the same electrical loading conditions as EC:H_2O_2. Thus, direct electron transfer is unlikely during EC at the current and water quality conditions tested in this work. All of these pathways may co-occur during EC:H_2O_2, adding to the complexity of understanding PFAS removal, therefore future work is needed to separate the different oxidants that may occur in EC:H_2O_2 that may correspond to PFOA removal, in addition to a controlled mass-balance analysis of the fate of PFOA between the destructive and non-destructive mechanisms occurring.

A range of reactive oxygen species can be active in iron-based systems, including hydroperoxide anions (HO_2^-), superoxide ($O_2^-\bullet$), perhydroxyl radical ($HO_2\bullet$), hydroperoxide anions (HO_2^-), and other oxidative species that can oxidize PFOA (Li et al., 2022; Mitchell et al., 2013). Previous studies focused on isolating the role of HO•, which is the most commonly referenced oxidant during advanced oxidation processes, showed that HO• alone does not initiate defluorination processes (Javed et al., 2020; Radjenovic et al., 2020). However, other species such as HO_2^- and $O_2^-\bullet$ may play an important role in PFAS degradation. For example, Mitchell et al. (2013) studied the role of iron-catalyzed H_2O_2 reactions for PFOA degradation and showed that HO_2^- was responsible for PFOA degradation whereas HO• alone had minimal contribution to overall PFOA degradation. This phenomenon could help to explain results in this study due to the low pH and the combination of iron and H_2O_2 leading to catalyzed H_2O_2 propagation reactions (Watts et al. 2013). Production of HO_2^- proceeds by the initial oxidation of Fe^{2+} by H_2O_2 (Eqn 5.1), that yields HO•, which can react with H_2O_2 to form $HO_2\bullet$ (Eqn 5.2). At the pH 3 conditions tested for EC:H_2O_2, $HO_2\bullet$ will remain in the acid form rather than converting to $O_2^-\bullet$ (Eqn. 5.3). Accordingly, the $HO_2\bullet$ can then react with Fe^{2+} to form HO_2^- (Eqn. 5.4). This HO_2^- can proceed with PFOA mineralization reactions based on Mitchell et al. (2013). This route of PFAS oxidation can proceed in the EC:H_2O_2 and "No Electricity (H_2O_2 + electrodes)" pathways due to the presence of high H_2O_2 concentrations and iron at low pH conditions. Future work is needed to quantify defluorination following EC:H_2O_2 treatment to help resolve uncertainties surrounding PFAS removal pathways.

$$Fe^{2+} + H_2O_2 \rightarrow Fe^{3+} + HO^{\bullet} + OH^{-} \quad \text{Eqn. 5.1}$$

$$HO^{\bullet} + H_2O_2 \rightarrow HO_2^{\bullet} + H_2O \quad \text{Eqn. 5.2}$$

$$HO_2^{\bullet} \leftrightarrow O_2^{-\bullet} + H^{+}, \text{ pKa = 4.8} \quad \text{Eqn. 5.3}$$

$$HO_2^{\bullet} + Fe^{2+} \rightarrow HO_2^{-} + Fe^{3+} \quad \text{Eqn. 5.4}$$

5.3.4. Flotation Layer Accumulation

When DOM was present in the system, the mean concentration of all PFAS in the flotation layer increased following EC:H_2O_2 (Figure 5.6, Appendix 5.5). With the exception of humic acid, the PFAS concentrations in the DOM-impacted flotation layer ranged from roughly 400 µg/L to as high 1200 µg/L for PFOA, PFOS, and 6:2 FtS. In general, PFOS had the highest mean concentration in the flotation layer, but it was not statistically different from PFOA and 6:2 FtS for the DOM sources that resulted in the highest levels of PFAS within the flotation layer (*p<0.05,* two way ANOVA). The concentration of 5:3 FTCA in the flotation layer was the lowest relative to other PFAS, primarily due to the lower concentration initially spiked, as 5:3 FTCA has the lowest molecular weight and all PFAS were spiked at equimolar concentrations (0.5 µM). The flotation layer enrichment factor indicated that the PFAS present in the flotation layer could be up to 200 times higher than the treated bulk solution when DOM was present in the system, indicating that the four PFAS tested accumulated at the air-water interface. Overall, these data indicate that the presence of DOM enhanced partitioning of PFAS into the flotation layer and increased non-destructive removal pathways compared to DOM-free water matrices.

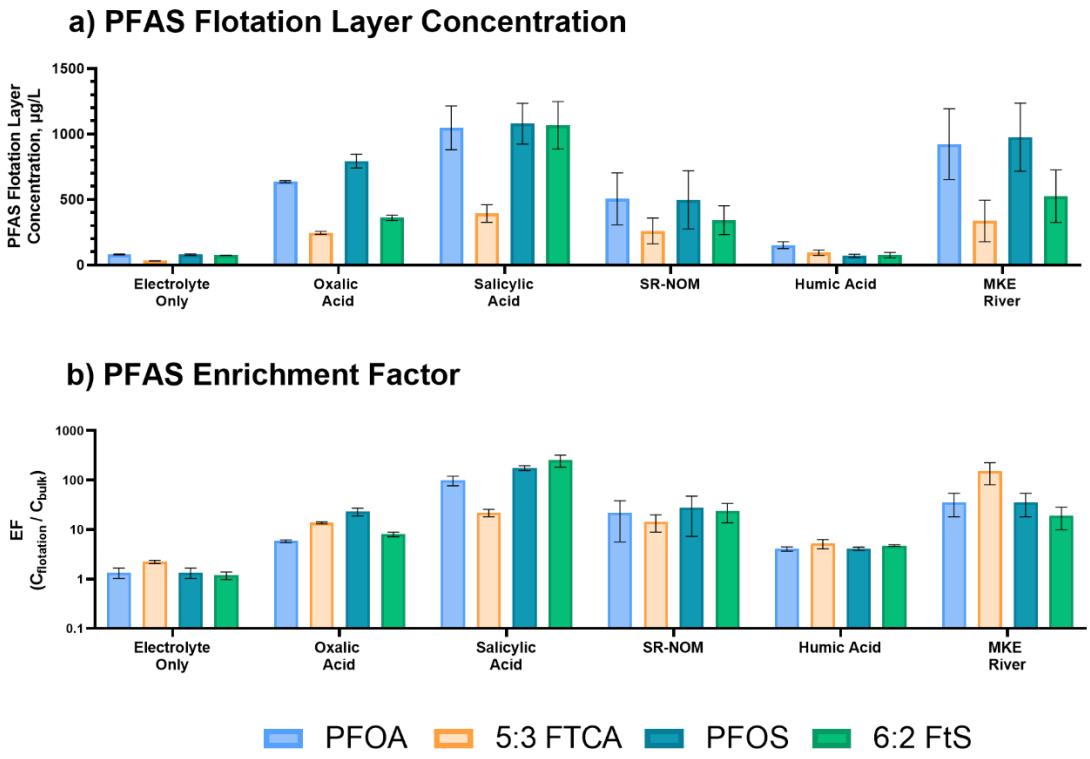

Figure 5.6. The impact of DOM on PFAS occurrence in the flotation layer after EC:H_2O_2 treatment in 4 mM HCO_3^- as the electrolyte source (with the exception of MKE River), where pH was adjusted to pH 3 using 3 N HCl (final Cl^- = 170 mg Cl^-/L). **A)** The PFAS concentration in the flotation layer and **B)** The enrichment factor EF, or $C_{flotation\ layer}/C_{bulk}$, comparing the concentration in the flotation layer to the treated bulk solution. Electrolysis was run at 7.4 mA/cm^2 for 20 minutes. During EC:H_2O_2 electrolysis, 60 mg/L of H_2O_2 was spiked every 5 minutes. The four PFAS species were spiked at 0.5 µM each. All DOM sources were added at 10 mg-C/L except for Electrolyte Only (no DOM added). The DOC concentration was 7.0 mg-C/L in the MKE River. Error bars indicate ±1 standard deviation of triplicate experiments.

5.3.5. The Influence of Dissolved Organic Matter on PFAS Accumulation in the EC:H_2O_2 Flotation Layer

PFAS concentration in the flotation layer varied amongst the different DOM sources (Figure 5.6.). Generally, the DOM sources containing larger fractions of low molecular weight DOM (<1 kDa) had the highest amounts of PFAS in the flotation layer. Of the DOMs tested, salicylic acid and MKE River contained the highest PFAS concentrations, followed by oxalic acid, SR-NOM, and humic acid. This increased

accumulation in the flotation layer may be due to the formation of ternary complexes of DOM, PFAS, and iron. Iron can be present as divalent (Fe^{2+}) and trivalent (Fe^{3+}) cations that can bind with the carboxylic and phenolic anions in DOM and the PFAS anions. This aggregation can form larger complexes that are more buoyant and amenable to accumulation in the flotation layer during foam formation, similar to previous studies wherein the addition of coagulants in dissolved air flotation improved DOM flotation (Shi et al., 2017; Shutova et al., 2016). This synergy between DOM, cations (Fe^{3+}, Fe^{2+}, Ca^{2+}, and Mg^{2+}), and PFAS has been shown to increase PFAS concentrations in foam, promote greater removal via sorptive processes, and lead to PFAS accumulation in soil systems (Buckley et al., 2022; Campos Pereira et al., 2018; Wang et al., 2015). For electrochemical treatment specifically, DOM improved the removal of the cationic surfactant benzalkonium chloride in both EC and electrooxidation processes, likely due to organic complexation leading to improved mass transfer during electrooxidation and improved sorption to flocs (Ryan et al., 2021).

Pearson correlations were conducted to assess the multicollinearity between DOM characteristics and flotation layer accumulation of PFAS. SUVA was well correlated with the molecular weight fractions, where there was a positive correlation for all fractions greater than 1 kDa (i.e., $R^2_{1\text{-}3\ kDa:SUVA}$=0.23, $R^2_{3\text{-}10\ kDa:SUVA}$ = 0.46, $R^2_{>10kDa:SUVA}$ = 0.92; Pearson correlation, Appendix 5.6), indicating that higher molecular weight constituents had higher amounts of aromatic chromophoric DOM. The lower molecular weight DOM, <1 kDa, had a negative correlation with SUVA ($R^2_{<1\ kDa:SUVA}$ = -0.43, Pearson correlation) due to the higher occurrence of non-chromophoric DOM. These analyses

align with previous optical geochemistry works reports that higher SUVA corresponds to high molecular weight, electron dense DOM, while lower SUVA values are related to low molecular weight, potentially hydrophilic DOM moieties (Her et al., 2003; Matilainen et al., 2011; Mcknight et al., 2001; Phungsai et al., 2016; Remucal et al., 2012; Weishaar et al., 2003). These correlations also indicate that SUVA is multicollinear with the other DOC analytes; therefore, multivariable regressions were not performed.

To consider the impact of DOM on flotation layer accumulation for PFAS, Pearson analyses were conducted comparing PFAS concentrations in the flotation layer and DOM characteristics (SUVA, molecular weight distribution, fluorescence indices). SUVA and high fractions of >10 kDa DOM were negatively correlated with all four PFAS concentrations in the flotation layer ($R^2_{SUVA:Cfloat}$ = -0.3, -0.12, -0.39, and -0.36; $R^2_{>10\ kDa:Cfloat}$ = -0.46, -0.32, -0.53, and -0.44 for PFOA, 5:3 FTCA, PFOS, and 6:2 FtS, respectively; Appendix A5.6). Alternately, the presence of low molecular weight DOM (<1 kDa) had a positive, significant correlation for all PFAS ($R^2_{<1\ kDa:Cfloat}$ = 0.83, 0.76,0.88, and 0.76 for PFOA, 5:3 FTCA, PFOS, and 6:2 FtS, respectively; $p<0.05$ for all, Appendix A5.6).

In addition to UV spectroscopy and size distribution, fluorescence indices were used to garner more information on the chemical characteristics of DOM in relation to PFAS occurrence in the flotation layer. The fluorescence indices generally had higher, statistically significant, strengths of correlation to PFAS occurrence as compared to SUVA correlations (e.g., R^2 = 0.13 to 0.39 for SUVA compared to 0.63 to 0.89 for FIX, HIX, and BIX; Appendix A5.6). For example, HIX had a significant negative correlation for all

four PFAS in the floatation layer ($R^2_{HIX:Cfloat}$ =-0.82, -0.70, -0.85, and -0.84 for PFOA, 5:3 FTCA, PFOS, and 6:2 FtS; $p<0.05$ for all, Appendix A5.6). This HIX correlation further corroborates the finding that humic moieties may inhibit PFAS occurrence in the flotation layer relative to other DOM constituents, as HIX may be a more specific index for humic DOM constituents based on the fluorophores present. The BIX had a positive correlation to PFAS occurrence in the flotation layer ($R^2_{BIX:Cfloat}$ = 0.87, 0.62, 0.89, and 0.80 for PFOA, 5:3 FTCA, PFOS, and 6:2 FtS; $p<0.05$ for all, except 5:3 FTCA Appendix A5.6). This correlation aligns with previous research where the BIX was well correlated to long-chain alkanes that are associated with surfactants that can subsequently enhance transport during foam floatation (Ateia et al., 2017). In terms of FIX, previous studies have demonstrated that FIX is well associated with the capacity of DOM to complex with metals, such as iron to improve transport of metals in water (Ateia et al., 2017; Mcknight et al., 2001). Accordingly, FIX had a strong positive correlation with PFAS in the floatation layer ($R^2_{FIX:Cfloat}$ = 0.88, 0.63, 0.89, and 0.81 for PFOA, 5:3 FTCA, PFOS, and 6:2 FtS; $p<0.05$ for all, except 5:3 FTCA Appendix A5.6), which helps substantiate that complexation between iron, DOM, and PFAS can increase the occurrence of PFAS within the floatation layer following treatment.

Overall, these correlations indicate that the low molecular weight, low SUVA DOM constituents likely interact with iron and PFAS. For example, ionic bonding and hydrogen bonding via carboxylic acids may lead to accumulation in the flotation layer through the flotation of buoyant DOM-Iron-PFAS complexes. Alternately, high molecular weight DOM constituents were less effective for transferring PFAS into the flotation

layer, potentially due to weaker interactions between DOM and PFAS at the pH conditions tested. This difference makes sense as the hydrophobic attractions (such as van der Waals, and π-π interactions) that occur between high molecular weight constituents and iron and PFAS are weaker than ionic bonding and hydrogen bonding in terms of the stability of PFAS-Iron-DOM complexes (Goss and Schwarzenbach, 2001).

In terms of molecular interactions, DOM can proceed with different interactions that can impact the fate of PFAS including ionic interactions, hydrogen bonding, and hydrophobic attractions (such as van der Waals, π-π interactions) (Goss and Schwarzenbach, 2001; Kubicki and Apitz, 1999). Of these, ionic interactions can result from the anionic carboxylic acid functional groups and cations, such as iron. Hydrophobic interactions are weaker than ionic interactions, where van der Waals attraction increases with molecular weight, and π-π interactions are attributed to aromatic systems (Goss and Schwarzenbach, 2001). However, it is worth mentioning that the four PFAS studied in this work contain linear alkyl chains and do not contain aromatic systems containing conjugated π electrons capable of π-π interactions; therefore, π-π interactions will only occur between DOM constituents (Lin et al., 2015).

These DOM characteristics (e.g., ligand groups, degree of aromaticity) align with tests of different representative DOM sources including oxalic acid, salicylic acid, and humic acid in this study (Figure 5.6). These organic acids have carboxyl anions at the conditions tested (oxalic acid pKa = 1.28, 4.28; salicylic acid pKa = 2.97; Appendix A5.2), whereas the humic acid source is a bulk representative source containing a mixture of pKa values. Oxalic acid is a low molecular weight bidentate ligand containing two

carboxylic groups that are capable of ionic interactions with iron, but does not contain any aromatic groups capable of hydrophobic interactions with other organics (Hancock and Martell, 1989). Salicylic acid is also a bidentate ligand, but contains aromatic moieties that increase the overall molecular weight and promote hydrophobic interactions with other organics. Specifically, the anionic headgroup can pair with iron connected to PFAS, and the aromatic system can participate in hydrophobic interactions with other hydrophobic DOM moieties to form even larger complexes (Goss and Schwarzenbach, 2001). In contrast to ionic interactions, the humic acid system had the lowest flotation layer accumulation, potentially due to the weaker hydrophobic attractive forces (e.g., van der Waals and π-π interactions) that are associated with high SUVA, high molecular weight DOM (Goss and Schwarzenbach, 2001; Lan et al., 2021). Additionally, the high electronegativity of the aromatic systems in high-SUVA DOM may yield electrostatic repulsion with PFAS anions. This aligns with prior modeling studies that showed that humic DOM is fully protonated in acidic conditions and has minimal interactions with the bulk water phase and can instead self-aggregate into "droplet-like" humic systems (Lan et al., 2021). This trend was reflected in this work, as the humic acid system formed foam with visible humic precipitates and had less contribution to PFAS accumulation in the flotation layer.

The presence of DOM has major implications for the fate of PFAS during EC:H_2O_2 treatment as DOM is ubiquitous in water and wastewater. The majority of PFAS studies test simple matrices without DOM and may not accurately reflect real systems where PFAS can interact with organics and treatment media such as iron or other potential

adsorbents. This gap in literature hinders translation of bench-scale studies to scaled applications treating real waters containing background organics that can shift treatment trends. For example, this study showed that the presence of DOM led to PFAS accumulation in the flotation layer as opposed to the oxidative treatment that may dominate in DOM-free systems. To minimize this treatment bias, future studies should incorporate DOM characterization, such as SUVA and fluorescence indices as general parameters, to better understand the role of DOM on PFAS treatment process performance as these treatment technologies are increasingly applied.

5.3.6. Engineering Implications

Considering potential treatment applications, it is important to account for factors that can impact water quality with respect to treatment goals, including effluent water quality, residuals generated, and treatment byproducts, and residual PFAS following treatment. These parameters were assessed to better inform the potential implementation of EC:H_2O_2 for different water matrices such as drinking water, wastewater, and industrial treatment.

The acidic pH conditions (pH 3) used for effective PFAS treatment are potentially a major limitation for implementing EC:H_2O_2 for drinking water treatment due to the corrosive conditions and enhanced solubility of metals. Following EC:H_2O_2, pH ranged from 3.3 to 3.9 (Appendix A5.2), which would necessitate pH neutralization for drinking water treatment or wastewater and industrial treatment applications that require circumneutral pH conditions prior to discharge.

Beyond concerns over acidic effluents, regulated metals (iron and manganese) are also relevant considerations for EC and EC:H_2O_2. During electrolysis of iron electrodes, the metals that comprise the steel alloy (such as iron and manganese) are dissolved into solution following electrolysis. Under the conditions tested, both manganese and iron levels exceeded the secondary drinking water standards set by US EPA. Manganese was present at roughly 120 – 160 µg/L (which exceeds the secondary standard under the Safe Drinking Water Act is 50 µg/L, Appendix A5.7). Residual iron was also present at high concentrations (9 – 80 mg/L) due to the acidic conditions that promote iron solubility (the secondary iron standard is 0.3 mg Fe/L). Therefore, additional metals removal processes such as base-amended precipitation or membrane filtration are needed following EC and EC:H_2O_2 depending on the final treatment goals (e.g., drinking water for consumers, treated wastewater for discharge etc.).

To assess potential PFAS and contaminations due to frequent iron electrode use between experiments, a PFAS-free control experiment was conducted to assess if PFAS were added following EC and EC:H_2O_2 as a result of accumulation (and subsequent dissolution) in the pores of the iron electrodes or the reactor materials (stir bars and beakers) (Appendix A5.7). The PFAS-blank experiment indicated that the four target PFAS were present in the initial and treated water at concentrations less than 50 ng/L relative to Milli-Q blanks. The initial and treated concentrations were not statistically different from one another ($p>0.45$, *two-way ANOVA*), indicating that PFAS were not added as a result of EC:H_2O_2 treatment. This lack of "carry-over" is promising as the reactor itself may not serve as a potential route of PFAS addition to treated streams.

Overall, EC:H_2O_2 operation at acidic conditions may not be feasible as a standalone treatment technology due to the acidic effluent and elevated metals concentrations following treatment. However, this technology may serve as a unit process prior to some form of a precipitative flocculation process to neutralize the pH and settle the iron flocs. For other applications, EC:H_2O_2 may serve as a fractionation technology at an early stage of a process train that oxidizes contaminants and accumulates PFAS in the flotation layer (containing foam, iron, and PFAS). Following EC:H_2O_2, the PFAS-laden foam can be collected and processed by other side-stream destructive defluorination technologies such as electrooxidation.

5.4. CONCLUSIONS

The goal of this research was to evaluate EC:H_2O_2 for PFAS mitigation under varying water quality conditions and DOM sources and to assess the oxidative and non-destructive pathways for PFAS mitigation. Operation of EC:H_2O_2 at acidic pH 3 conditions improved PFAS mitigation relative to pH 6.3. Improved removal was likely due to a multitude of factors associated with acidic conditions such as higher oxidant yield via Fenton's reactions, higher zeta potentials of iron that lead to enhanced sorption of PFAS anions, and higher ionic strength (relative to neutral pH conditions) enhancing foam formation and corresponding flotation layer PFAS accumulation.

Pathway control experiments indicated that 5:3 FTCA and PFOA were likely removed via oxidative processes as both of the oxidative pathway experiments (EC:H_2O_2 and "No Electricity (H_2O_2 + Electrodes)") yielded removal, whereas the non-destructive

experiments (EC only and Fe^{3+} coagulation) had minimal removal. However, 6:2 FtS and PFOS had removal for both oxidative experiments and non-destructive removal experiments. Oxidation of 5:3 FTCA and 6:2 FtS was further substantiated based on formation of their oxidative transformation products PFPeA, PFHxA, and PFHpA.

When DOM was present, the non-destructive pathway via flotation layer accumulation was a prominent route of removal based on PFAS quantified in the flotation layer following EC:H_2O_2. Of the DOM characteristics evaluated, low molecular weight (<1 kDa), low SUVA DOM corresponded to higher PFAS levels in the flotation layer. This enhanced separation into the flotation layer was potentially due to the formation of DOM-Iron-PFAS complexes that are transferred to the air-water interface via bubbles formed at the cathode. Overall, EC:H_2O_2 provided both destructive and non-destructive removal of target PFAS, although when simulating real systems containing DOM, flotation layer accumulation was the more prominent removal pathway.

This work showed that the foam in the flotation layer following EC:H_2O_2 treatment contains elevated PFAS levels relative to the treated water stream. Accordingly, more research is needed to evaluate foam collection technologies to sequester PFAS for foam treatment and management practices to mitigate the risks associated with PFAS foams following EC:H_2O_2.

Future work assessing destructive PFAS removal in EC:H_2O_2 in terms of defluorination is needed. This study yielded promising removals, but did not evaluate the degree of defluorination occurring due to the low levels of PFAS spiked, the low resulting fluoride levels, and the overall matrix complexity following treatment that

complicates fluoride quantification. Accordingly, future work in analytical chemistry is needed for sample preconcentration for fluoride quantification in order to remove matrix complexities and improve the limit of detection for established fluoride quantification methods.

Finally, more applied research is needed for treatment of real PFAS-containing waters such as contaminated environmental sources, concentrated waste streams, and wastewater streams to evaluate the treatment of native PFAS mixtures (containing neutral, cationic, anionic, and zwitterionic PFAS s) and the influence of DOM on PFAS mitigation in such scenarios.

CHAPTER 6: KEY FINDINGS AND FUTURE WORK

Portions of this chapter were published as:

Ryan, D.R., McNamara, P.J., Mayer, B.K., 2020. Iron-electrocoagulation as a disinfection byproduct control strategy for drinking water treatment. Environ Sci (Camb) 6, 1116–1124. https://doi.org/10.1039/D0EW00106F

Ryan, D.R., Mayer, B.K., Baldus, C.K., McBeath, S.T., Wang, Y., McNamara, P.J., 2021. Electrochemical technologies for per- and polyfluoroalkyl substances mitigation in drinking water and water treatment residuals. AWWA Water Sci 3. https://doi.org/10.1002/aws2.1249

They are included here with modification to satisfy dissertation requirements.

6.1. Key Findings

The overarching goal of this dissertation research was to assess electrocoagulation (EC) as a treatment technology for a range of contaminants and to increase understanding of the impact of water matrix components, organic matter in particular, on process performance. This goal was achieved by confirming that EC is effective for mitigation of regulated disinfection byproducts in *Chapter 3*. In *Chapter 4*, the addition of hydrogen peroxide (i.e., EC:H_2O_2) was shown to stimulate advanced oxidation based on pCBA removal for a range of water matrices. In *Chapter 5*, EC:H_2O_2 was used to treat PFAS via a range of destructive and non-destructive treatment pathways. The influence of dissolved organic matter (DOM) on PFAS removal using EC:H_2O_2 was evaluated. The key findings of each research chapter and recommendations for future work are provided here.

6.1.1. Chapter 3: Iron-Electrocoagulation as a Disinfection Byproduct Control Strategy for Drinking Water Treatment

EC may serve as a disinfection byproduct (DBP) control strategy for small systems based on the technology's capacity to generate coagulant onsite, which can mitigate costs associated with material transport and storage. This chapter compared EC to conventional coagulation in terms of total trihalomethane (TTHM) formation potential and found that both processes performed similarly when conducted at the same initial pH condition. The TTHM formation potential data were compared to the U.S. EPA Stage 2 Disinfectants/Disinfection Byproducts Rule, demonstrating that EC was effective for decreasing TTHMs to safe drinking water levels when treating matrices containing 5 mg-DOC/L. These data are beneficial for the water engineering field as they inform the use of EC in the context of DBP-related surface water treatment and the influence of the water matrix relevant to DBP goals. Additionally, the comparative analysis between EC and conventional coagulation provides a benchmark for EC in comparison to conventional processes, where EC has an added benefit of *in-situ* coagulant generation that can be advantageous for remote water treatment processes and decentralized treatment.

6.1.2. Chapter 4: Peroxi-Electrocoagulation for Simultaneous Oxidation of Trace Organic Compounds and Removal of Natural Organic Matter at Neutral pH

This chapter focused on utilizing iron-EC paired with *ex-situ* H_2O_2 addition (peroxi-electrocoagulation [EC:H_2O_2]) to promote oxidative reactions at neutral pH conditions. The hydroxyl radical probe para-chlorobenzoic acid (pCBA) was used to

gauge oxidant activity and serve as a representative trace organic compound (TOrC). The impacts of water pH, current density, iron dose, H_2O_2 dose (i.e., $[H_2O_2]_{initial}/[Fe^{2+}]_{generated}$ ratio), and the presence of natural organic matter (NOM) were evaluated. Multivariable regressions determined that high levels of H_2O_2 relative to iron (i.e., $[H_2O_2]_{initial}/ [Fe^{2+}]_{generated}$ ratio > 0.7) inhibited the rate of pCBA oxidation, likely due to radical quenching from excess H_2O_2. Overall, oxidation of pCBA was confirmed at neutral pH conditions, indicating that EC:H_2O_2 may serve as a multi-mechanistic treatment technology capable of oxidation. Experiments were also conducted in real-world water samples to gauge EC:H_2O_2 applications for groundwater, river water, and primary treated wastewater. With the exception of the primary effluent sample, which had the highest degree of oxidant scavenging of all matrices tested, H_2O_2 addition enhanced the oxidative degradation of pCBA while still removing NOM. The electrical energy per order (E_{EO}) metric also demonstrated that EC:H_2O_2 is competitive with other TOrC oxidation technologies such as ozonation.

6.1.3. Chapter 5: Peroxi-Electrocoagulation for PFAS Mitigation: The Role of Water Quality and Dissolved Organic Matter on Removal Pathways

EC:H_2O_2 was shown to be effective as a PFAS mitigation technology for bicarbonate electrolyte matrices and DOM-containing waters (laboratory organics, bulk surrogates, and environmental DOM sources). Generally, PFAS removal was highest at pH 3 conditions, likely due to the combinations of enhanced oxidant yield, ionic interactions between iron and PFAS, and foam formation. Pathway experiments showed that oxidation was a key route of removal for the perfluoroalkyl carboxylic acids (PFCAs,

including 5:3 FTCA and PFOA in this study), and a combination of oxidative and non-destructive processes contributed to removal of perfluorosulfonic acids (PFSAs, including 6:2 FtS and PFOS in this study). However, when DOM was present in the system to better reflect the treatment of real water and wastewater systems, PFAS were more readily removed via flotation layer accumulation, potentially due to the formation of DOM-Iron-PFAS complexes. Of the DOM constituents assessed, low molecular weight, low SUVA DOM characteristics correlated most to PFAS occurrence in the flotation layer. In terms of implementation, EC:H_2O_2 may have limited feasibility for PFAS mitigation in drinking water due to the highly acidic pH conditions needed for treatment and the high concentrations of regulated metals remaining in the system following treatment. Accordingly, EC:H_2O_2 may better serve as a pre-treatment and fractionation technology for higher strength wastewaters (such as membrane concentrates and industrial wastewaters) prior to effective destructive technologies.

6.2. Future Work

This work demonstrated that electrochemical water treatment may be effective for DBP, TOrC, and PFAS mitigation at the lab scale. However, future research is needed to guide implementation of electrochemical treatment in the water and wastewater sector, as illustrated in Figure 6.1.

Figure 6.1: Summary of research needs for implementation of electrochemical treatment for water treatment. Each tier represents a different foundation of research that needs to be examined in order to progress to the goal of engineering application. Tier One research focuses on proof–of-concept research to verify that a technology can work for a specific contaminant. Tier Two research focuses on assessing different applications of research and the influence of matrix factors, transformation products, and the costs associated with treatment. Tier Three focuses on research explicitly focused on implementation for drinking water treatment and includes studying the impact of environmentally relevant conditions and is validated based on regulatory targets. Of note, PFAS are explicitly mentioned in Tier Three as they are the imminent regulatory target TOrC. The peak of the pyramid is “engineering application” which requires a stable foundation supported by the underlying tiers of research.

6.2.1. Research Recommendations for DBP Mitigation

6.2.1.1. NOM Characterization to Optimize DBP Precursor Control

In *Chapter 3*, a range of natural organic matter (NOM) sources was treated via EC. The specific TTHM formation potential (amount of DBPs formed per unit carbon) was similar following treatment for each of the NOM sources tested. This finding may indicate that the residual NOM following treatment contains similar NOM constituents that can yield DBPs. Accordingly, future research is needed to characterize the residual NOM following DBP precursor control technologies in order to understand the selective pressures that occur during treatment. These characterization data can be advantageous for understanding the general reactivity of residual NOM and assess if it can serve as a source of DBPs or present other challenges in the full treatment train or the distribution system prior to consumer use. By understanding the specific NOM composition, additional treatment technologies may be incorporated that can selectively treat the NOM constituents that are resistant to EC treatment. Additionally, this NOM characterization data can also be paired with DBP formation potential data for a range of regulated and non-regulated DBPs (i.e., haloacetic acids, haloacetonitriles etc.) to better understand the range of DBPs that may be generated following electrocoagulation to inform potential health risks beyond TTHM occurrence in waters.

6.2.1.2. Sustainability of EC for Rural and Decentralized Systems

In *Chapter 3,* EC was shown to prevent TTHM formation as compared to conventional coagulation. A key motivation for this study was to assess EC for potential

implementation in rural and decentralized systems that have been associated with elevated levels of DBPs (Allaire et al., 2018; Charrois et al., 2004). Accordingly, future work is needed to evaluate the potential sustainability (economic, environmental, and social impacts) of implementing EC for DBP prevention and precursor removal in rural and decentralized systems as compared to other precursor removal technologies such as granular activated carbon (GAC). For example, Jones et al., (2018) conducted a life cycle assessment of disinfection technologies for rural and decentralized systems. For EC and DBP prevention, factors that may inform sustainability considerations include materials requirements (i.e., iron electrodes vs. GAC), size of the population served, water demands, proximity to metropolitan areas, energy requirements, and residuals management. These findings will be important for future applications by informing the comprehensive impact of using DBP control technologies in rural and decentralized systems.

6.2.2. Research Recommendations for TOrCs and PFAS

6.2.2.1. Environmentally Relevant Contaminant Concentrations

TOrCs such as PFAS generally occur at ng/L to µg/L concentrations in drinking water sources, which are orders of magnitude lower than concentrations used in most electrochemical research. The concentrations used in this work were at µg/L levels for pCBA in *Chapter 4* and PFAS in *Chapter 5*, which reflect heavily contaminated systems and industrial waters, but may not directly translate to drinking water sources. For example, ng/L of target PFAS may not be high enough to act as surfactants. These high

contaminant concentrations can impact removal efficacy and the misrepresentation of initial concentrations can limit translation of the data to real world treatment goals. Accordingly, future electrochemical research should focus on environmentally relevant concentrations and demonstrate that the proposed processes can truly meet proposed regulations (Garcia-Segura et al., 2020; Radjenovic et al., 2020).

6.2.2.2. Research on Mitigation PFAS Transformation Products Following Electrochemical Treatment for Comprehensive Mitigation

The majority of existing treatment studies focus on PFOA and PFOS, which have been phased out and replaced by PFAS-related substitutes in manufacturing processes (Xiao, 2017). If treatment processes are designed for PFOA and PFOS removal, they will be under-designed with respect to short-chain compounds, which are more recalcitrant to destructive treatment due to their hydrophilic structure (relative to PFOA and PFOS) (Ateia et al., 2019). Accordingly, these residual PFAS may lead to health risks that are not fully accounted for in targeted analysis.

Extractable organofluorine can serve as an effective monitoring parameter/research metric for non-target PFAS analysis to assess the extent of total PFAS removal (Cousins et al., 2020). Non-target PFAS analyses are important given that a 2016 sampling campaign showed that 60% of the PFAS (based on extractable organofluorine) in tap water were not included in the targeted PFAS analysis, demonstrating the occurrence of unknown PFAS (Hu et al., 2019). To better assess destruction, it is also recommended to measure fluoride levels following treatment. Fluoride quantification following treatment of low levels of PFAS may be complex and

require sample processing and pre-concentration (similar to solid phase extraction for TOrCs) to improve fluoride quantification. Accordingly, future work is recommended to include extractable organofluorine to better capture the comprehensive PFAS treatment occurring in systems beyond mitigation of specific PFAS compounds.

6.2.3. Research Recommendations for Electrocoagulation and Peroxi-Electrocoagulation

6.2.3.1. Electrocoagulation Residuals Management and Treatment

Iron flocs were generated as a byproduct of EC and EC:H_2O_2. Although iron alone is not an acutely harmful contaminant, the contaminants associated with the flocs, namely PFAS, may require additional processing. Future work is needed to study and characterize the flocs following these processes to gauge their affinity for PFAS sorption, and potential mitigation via subsequent destructive treatment technologies such as incineration and pyrolysis. For example, pyrolysis has been well studied in the context of municipal solid waste and organic substrates and can generate materials such as biochar and catalytic materials for water and wastewater treatment (Liu et al., 2018). Similar to pyrolysis of waste material after wastewater treatment, it may be promising to assess pyrolysis of iron flocs leftover from EC-based processes to destroy the incorporated PFAS and potentially synthesize and reuse PFAS-free iron-derived catalytic material for other treatment technologies as a method to reuse the spent iron.

In addition to iron flocs, foam was generated when PFAS were present in the EC:H_2O_2 system. Accordingly, future work is needed to better understand the foam generated in electrochemical-based processes in terms of the PFAS levels in foam and

the rate of foam formation resulting from cathodic bubble generation. This may be achieved in a point-of-concept study with a modified electrochemical cell that allows measurement of the foam height, and a simple, effective method of foam collection and processing. This can aid in designing EC-based processes to control the amount of foam generated during EC in case foam generation is favored for non-destructive treatment, or inhibit foam generation to facilitate oxidative processes that can more readily proceed without the mass transfer complexities resulting from foam generation causing a multi-phase system.

6.2.3.2. Understanding Oxidative Processes during Electrocoagulation and Peroxi-Electrocoagulation

In this study, the oxidant activity of EC-only was unclear relative to other research works that have demonstrated oxidative activity in EC-only systems (Govindan et al., 2020a; Kim et al., 2020; Maher et al., 2019; Qian et al., 2019b). At the current density and water matrix conditions tested here for EC-only, oxidation was not apparent for the hydroxyl radical probe pCBA (*Chapter 4*) or the fluorotelomers (*Chapter 5*) (which are susceptible to hydroxyl radical oxidation). Additionally, other EC-only studies have demonstrated PFAS defluorination, potentially due to direct electron transfers at the anode surface to induce the PFAS un-zipping cycle (Kim et al., 2020). Accordingly, research is needed to determine the current density and water matrix conditions that are most favorable for oxidant production to determine if these matrix constituents can translate to water treatment applications, in terms of feasible energy conditions, and low levels of supporting electrolyte salts. These findings can be informative for

understanding the minimum current density and voltage conditions required for treatment applications to yield oxidants during EC.

Fundamental electrochemical research using cyclic voltammetry and potentiostatic analyses is needed to confirm the thermodynamic cell potentials in EC in order to validate that the occurrence of high potentials (3.6 V vs. standard hydrogen potential) required for PFAS to participate in direct electron transfers (Niu et al., 2016; Vecitis et al., 2009). These findings can greatly inform EC-based PFAS research and aid in resolving potential mechanisms at work for overall water and wastewater treatment.

For EC:H_2O_2, oxidation of TOrCs and PFAS was demonstrated with the *ex-situ* addition of H_2O_2 in *Chapters 4* and *5*. However, the H_2O_2 addition may be an impediment for some applications such as rural and decentralized systems as well as mobile water treatment systems due to the need of oxidant handling and storage. Accordingly, future work should consider air diffusion carbon felt cathodes in order to provide *in-situ* H_2O_2 generation similar to other electrochemical works (Cotillas et al., 2015; Mavrikis et al., 2021; Serra-Clusellas et al., 2021). The optimization of *in-situ* H_2O_2 generating systems can be advantageous for EC-based applications by minimizing the reliance on auxiliary chemicals for decentralized systems.

6.2.3.3. Systems-level Analysis for Cost Effective Treatment Goals

Systems-level analyses are needed to delineate the impact of system parameters such as energy costs, electrode costs, treatment times, materials cost, and treatment goals and better assess the components relative to the overall system with respect to

economic and environmental impacts. Economic analyses are useful to inform the status quo and future projections related to electrode development, process scale-up, and environmental impacts (Soriano et al., 2020). These analyses can also be applied to evaluate the costs of different electrode materials as a function of electrode longevity, lifespan, stability, and materials cost, similar to the approach used by Soriano et al. (2020). Overall, systems-level analyses are an important step for scaling up emerging technology. These analyses can help substantiate the inclusion of EC and EC:H_2O_2 as potential technologies in the context of rural and decentralized water treatment to better convey their benefits for those communities.

Future research is also needed to parameterize the comprehensive water quality benefits that cascade from targeting PFAS. PFAS treatment is complicated by other water quality parameters that can inhibit targeted treatment (i.e., DOM, which can also lead to DBP formation). By focusing on PFAS, co-contaminants may also be treated (e.g., removing DOM as a PFAS oxidant scavenger contributes to mitigating DBP formation). Thus, although PFAS treatment technologies are expected to be expensive and costly, their regulations can also be indirectly effective for a range of water quality contaminants and lead to overall improved water quality and consumer safety due to the comprehensive nature of PFAS mitigation needs.

7. BIBLIOGRAPHY

Abada, B., Alivio, T.E.G., Shao, Y., O'Loughlin, T.E., Klemashevich, C., Banerjee, S., Jayaraman, A., Chu, K.H., 2018. Photodegradation of fluorotelomer carboxylic 5:3 acid and perfluorooctanoic acid using zinc oxide. Environmental Pollution 243, 637–644. https://doi.org/10.1016/j.envpol.2018.09.023

Ahn, Y., Lee, D., Kwon, M., Choi, I. hwan, Nam, S.N., Kang, J.W., 2017. Characteristics and fate of natural organic matter during UV oxidation processes. Chemosphere 184, 960–968. https://doi.org/10.1016/j.chemosphere.2017.06.079

Allaire, M., Wu, H., Lall, U., 2018. National trends in drinking water quality violations. Proc Natl Acad Sci U S A 115, 2078–2083. https://doi.org/10.1073/pnas.1719805115

Andrews, D.Q., Naidenko, O. V, 2020. Population-Wide Exposure to Per- And Polyfluoroalkyl Substances from Drinking Water in the United States. Environ Sci Technol Lett 7, 931–936. https://doi.org/10.1021/acs.estlett.0c00713

Ateia, M., Maroli, A., Tharayil, N., Karanfil, T., 2019. The overlooked short- and ultrashort-chain poly- and perfluorinated substances: A review. Chemosphere. https://doi.org/10.1016/j.chemosphere.2018.12.186

Ateia, M., Ran, J., Fujii, M., Yoshimura, C., 2017. The relationship between molecular composition and fluorescence properties of humic substances. International Journal of Environmental Science and Technology 14, 867–880. https://doi.org/10.1007/s13762-016-1214-x

Ates, N., Kitis, M., Yetis, U., 2007. Formation of chlorination by-products in waters with low SUVA—correlations with SUVA and differential UV spectroscopy. Water Res 41, 4139–4148. https://doi.org/10.1016/j.watres.2007.05.042

Bagotsky, V.S., 2005. Fundamentals of Electrochemistry: Second Ed., Fundamentals of Electrochemistry: Second Ed. https://doi.org/10.1002/047174199X

Barazesh, J.M., Hennebel, T., Jasper, J.T., Sedlak, D.L., 2015. Modular Advanced Oxidation Process Enabled by Cathodic Hydrogen Peroxide Production. Environ Sci Technol 49, 7391–7399. https://doi.org/10.1021/acs.est.5b01254

Barazesh, J.M., Prasse, C., Sedlak, D.L., 2016. Electrochemical Transformation of Trace Organic Contaminants in the Presence of Halide and Carbonate Ions. Environ Sci Technol 50, 10143–10152. https://doi.org/10.1021/acs.est.6b02232

Behin, J., Farhadian, N., Ahmadi, M., Parvizi, M., 2015. Ozone assisted electrocoagulation in a rectangular internal-loop airlift reactor: Application to decolorization of acid dye. Journal of Water Process Engineering 8, 171–178. https://doi.org/10.1016/j.jwpe.2015.10.003

Belkouteb, N., Franke, V., McCleaf, P., Köhler, S., Ahrens, L., 2020. Removal of per- and polyfluoroalkyl substances (PFASs) in a full-scale drinking water treatment plant: Long-term performance of granular activated carbon (GAC) and influence of flow-rate. Water Res 182. https://doi.org/10.1016/j.watres.2020.115913

Ben-Sasson, M., Zidon, Y., Calvo, R., Adin, A., 2013. Enhanced removal of natural organic matter by hybrid process of electrocoagulation and dead-end microfiltration. Chemical Engineering Journal 232, 338–345. https://doi.org/10.1016/j.cej.2013.07.101

Bocos, E., Brillas, E., Sanromán, M.Á., Sirés, I., 2016. Electrocoagulation: Simply a Phase Separation Technology? the Case of Bronopol Compared to Its Treatment by EAOPs. Environ Sci Technol 50, 7679–7686. https://doi.org/10.1021/acs.est.6b02057

Bolton, J.R., Bircher, K.G., Tumas, W., Tolman, C.A., 2001. Figures-of-merit for the technical development and application of advanced oxidation technologies for both electric- and solar-driven systems (IUPAC Technical Report). Pure and Applied Chemistry. https://doi.org/10.1351/pac200173040627

Boone, J.S., Vigo, C., Boone, T., Byrne, C., Ferrario, J., Benson, R., Donohue, J., Simmons, J.E., Kolpin, D.W., Furlong, E.T., Glassmeyer, S.T., 2019. Per- and polyfluoroalkyl substances in source and treated drinking waters of the United States. Science of the Total Environment 653, 359–369. https://doi.org/10.1016/j.scitotenv.2018.10.245

Boorman, G.A., Dellarco, V., Dunnick, J.K., Chapin, R.E., Hunter, S., Hauchman, F., Gardner, H., Cox, M., Sills ', R.C., 1999. Drinking Water Disinfection Byproducs: Review and Approach to Toxicity Evaluation. -Environ Health Perspect 107, 207–217.

Borkin, D., Némethová, A., Michaľčonok, G., Maiorov, K., 2019. Impact of Data Normalization on Classification Model Accuracy. Research Papers Faculty of Materials Science and Technology Slovak University of Technology 27, 79–84. https://doi.org/10.2478/rput-2019-0029

Buckley, T., Karanam, K., Xu, X., Shukla, P., Firouzi, M., Rudolph, V., 2022. Effect of mono-and di-valent cations on PFAS removal from water using foam fractionation-A modelling and experimental study. Sep Purif Technol 286, 120508. https://doi.org/10.1016/j.seppur.2022.120508

Burns, D.J., Stevenson, P., Murphy, P.J.C., 2021. PFAS removal from groundwaters using Surface-Active Foam Fractionation. Remediation 31, 19–33. https://doi.org/10.1002/REM.21694

Buxton, G. V, Greenstock, C.L., Phillips Helman, W., Ross, A.B., Helman, W.P., 1988. Critical Review of Aqueous Solution Reaction Rate Constants for. Aqueous Solution Journal of Physical and Chemical Reference Data 17, 23103. https://doi.org/10.1063/1.555805

Campos Pereira, H., Ullberg, M., Kleja, D.B., Gustafsson, J.P., Ahrens, L., 2018. Sorption of perfluoroalkyl substances (PFASs) to an organic soil horizon – Effect of cation composition and pH. Chemosphere 207, 183–191. https://doi.org/10.1016/J.CHEMOSPHERE.2018.05.012

Carrillo-Abad, J., Pérez-Herranz, V., Urtiaga, A., 2018. Electrochemical oxidation of 6:2 fluorotelomer sulfonic acid (6:2 FTSA) on BDD: electrode characterization and mechanistic investigation. J Appl Electrochem 48, 589–596. https://doi.org/10.1007/s10800-018-1180-8

Chaplin, B.P., 2019. The Prospect of Electrochemical Technologies Advancing Worldwide Water Treatment. Acc Chem Res 52, 596–604. https://doi.org/10.1021/acs.accounts.8b00611

Chaplin, B.P., 2014. Critical review of electrochemical advanced oxidation processes for water treatment applications. Environ Sci Process Impacts 16, 1182–1203. https://doi.org/https://doi.org/10.1039/C3EM00679D

Charrois, J.W.A., Graham, D., Hrudey, S.E., Froese, K.L., 2004. Disinfection by-products in small Alberta community drinking-water supplies. J Toxicol Environ Health A 67, 1797–1803. https://doi.org/10.1080/15287390490492494

Chen, G., 2004. Electrochemical technologies in wastewater treatment. Sep Purif Technol 38, 11–41. https://doi.org/10.1016/j.seppur.2003.10.006

Collins, M.R., Eighmy, T.T., Fenstermacher, J.M., Spanos, S.K., 1992. Removing natural organic matter by conventional slow sand filtration. J Am Water Works Assoc 84, 80–90. https://doi.org/10.1002/j.1551-8833.1992.tb07357.x

Cotillas, S., Llanos, J., Rodrigo, M.A., Cañizares, P., 2015. Use of carbon felt cathodes for the electrochemical reclamation of urban treated wastewaters. Appl Catal B 162, 252–259. https://doi.org/10.1016/j.apcatb.2014.07.004

Cousins, I.T., Dewitt, J.C., Glüge, J., Goldenman, G., Herzke, D., Lohmann, R., Miller, M., Ng, C.A., Scheringer, M., Vierke, L., Wang, Z., 2020. Strategies for grouping per-and polyfluoroalkyl substances (PFAS) to protect human and environmental health. Environ Sci Process Impacts 22, 1444–1460. https://doi.org/10.1039/d0em00147c

Crittenden, J.C., Trussell, R.R., Hand, D.W., Howe, K.J., Tchobanoglous, G., 2012. MWH's Water Treatment: Principles and Design: Third Edition, MWH's Water Treatment: Principles and Design: Third Edition. https://doi.org/10.1002/9781118131473

Cui, J., Gao, P., Deng, Y., 2020. Destruction of Per- A nd Polyfluoroalkyl Substances (PFAS) with Advanced Reduction Processes (ARPs): A Critical Review. Environ Sci Technol 54, 3752–3766. https://doi.org/10.1021/acs.est.9b05565

Daugherty, E.E., Gilbert, B., Nico, P.S., Borch, T., 2017. Complexation and Redox Buffering of Iron(II) by Dissolved Organic Matter. Environ Sci Technol 51, 11096–11104. https://doi.org/10.1021/acs.est.7b03152

Dixit, F., Barbeau, B., Mostafavi, S.G., Mohseni, M., 2020. Removal of legacy PFAS and other fluorotelomers: Optimized regeneration strategies in DOM-rich waters. Water Res 183. https://doi.org/10.1016/j.watres.2020.116098

Dixit, F., Dutta, R., Barbeau, B., Berube, P., Mohseni, M., 2021. PFAS removal by ion exchange resins: A review. Chemosphere 272. https://doi.org/10.1016/j.chemosphere.2021.129777

dos Santos, E.V., Sena, S.F.M., da Silva, D.R., Ferro, S., De Battisti, A., Martínez-Huitle, C.A., 2014. Scale-up of electrochemical oxidation system for treatment of produced water generated by Brazilian petrochemical industry. Environmental Science and Pollution Research 21, 8466–8475. https://doi.org/10.1007/s11356-014-2779-x

Dotson, A.D., Keen, V.S., Metz, D., Linden, K.G., 2010. UV/H2O2 treatment of drinking water increases post-chlorination DBP formation. Water Res 44, 3703–3713. https://doi.org/10.1016/j.watres.2010.04.006

Drever, J.I., 1982. The geochemistry of natural waters., in: The Geochemistry of Natural Waters. Prentice Hall, Englewood Cliffs, New Jersey, pp. 38–39. https://doi.org/10.1029/97eo00305

Dubrawski, K.L., Mohseni, M., 2013a. Standardizing electrocoagulation reactor design: Iron electrodes for NOM removal. Chemosphere 91, 55–60. https://doi.org/10.1016/j.chemosphere.2012.11.075

Dubrawski, K.L., Mohseni, M., 2013b. In-situ identification of iron electrocoagulation speciation and application for natural organic matter (NOM) removal. Water Res 47, 5371–5380. https://doi.org/10.1016/j.watres.2013.06.021

Dubrawski, K.L., Mohseni, M., 2013c. In-situ identification of iron electrocoagulation speciation and application for natural organic matter (NOM)

removal. Water Res 47, 5371–5380. https://doi.org/10.1016/j.watres.2013.06.021

Dubrawski, K.L., Mohseni, M., 2013d. Standardizing electrocoagulation reactor design: Iron electrodes for NOM removal. Chemosphere 91, 55–60. https://doi.org/10.1016/j.chemosphere.2012.11.075

Dubrawski, K.L., Van Genuchten, C.M., Delaire, C., Amrose, S.E., Gadgil, A.J., Mohseni, M., 2015. Production and transformation of mixed-valent nanoparticles generated by Fe(0) electrocoagulation. Environ Sci Technol 49, 2171–2179. https://doi.org/10.1021/es505059d

Edzwald, J.K., 1993. Coagulation in drinking water treatment: Particles, organics and coagulants. Water Science and Technology 27, 21–35. https://doi.org/10.2166/wst.1993.0261

Edzwald, J.K., Becker, W.C., Wattier, K.L., 1985. Surrogate Parameters for Monitoring Organic Matter and THM Precursors. Source Journal (American Water Works Association) Removing THMs 77, 122–132.

Environmental Protection Agency (EPA), 2011. National Characteristics of Drinking Water Systems: Serving 10,000 or Fewer People, Office of Water.

Environmental Protection Agency (EPA), 1999. Enhanced Coagulation and Enhanced Precipitative Softening Guidance Manual.

Fabris, R., Chow, C.W.K., Drikas, M., Eikebrokk, B., 2008. Comparison of NOM character in selected Australian and Norwegian drinking waters. https://doi.org/10.1016/j.watres.2008.06.023

Fenton, H.J.H., 1894. Oxidation of tartaric acid in presence of iron. Journal of the Chemical Society, Transactions 65, 899–910. https://doi.org/10.1039/CT8946500899

Fischbacher, A., von Sonntag, C., Schmidt, T.C., 2017. Hydroxyl radical yields in the Fenton process under various pH, ligand concentrations and hydrogen peroxide/Fe(II) ratios. Chemosphere 182, 738–744. https://doi.org/10.1016/j.chemosphere.2017.05.039

Franke, V., Mccleaf, P., Lindegren, K., Ahrens, L., 2019. Environmental Science Environmental Science Water Research & Technology COMMUNICATION Efficient removal of per-and polyfluoroalkyl substances (PFASs) in drinking water treatment: nanofiltration combined with active carbon or anion exchange †. Environ. Sci.: Water Res. Technol 5, 1836. https://doi.org/10.1039/c9ew00286c

Gagliano, E., Sgroi, M., Falciglia, P.P., Vagliasindi, F.G.A., Roccaro, P., 2020. Removal of poly- and perfluoroalkyl substances (PFAS) from water by

adsorption: Role of PFAS chain length, effect of organic matter and challenges in adsorbent regeneration. Water Res 171. https://doi.org/10.1016/j.watres.2019.115381

Garcia-Segura, S., Eiband, M.M.S.G., de Melo, J.V., Martínez-Huitle, C.A., 2017. Electrocoagulation and advanced electrocoagulation processes: A general review about the fundamentals, emerging applications and its association with other technologies. Journal of Electroanalytical Chemistry 801, 267–299. https://doi.org/10.1016/j.jelechem.2017.07.047

Garcia-Segura, S., Nienhauser, A.B., Fajardo, A.S., Bansal, R., Coonrod, C.L., Fortner, J.D., Marcos-Hernández, M., Rogers, T., Villagran, D., Wong, M.S., Westerhoff, P., 2020. Disparities between experimental and environmental conditions: Research steps toward making electrochemical water treatment a reality. Curr Opin Electrochem 22, 9–16. https://doi.org/10.1016/j.coelec.2020.03.001

Gerrity, D., Gamage, S., Jones, D., Korshin, G. V., Lee, Y., Pisarenko, A., Trenholm, R.A., von Gunten, U., Wert, E.C., Snyder, S.A., 2012. Development of surrogate correlation models to predict trace organic contaminant oxidation and microbial inactivation during ozonation. Water Res 46, 6257–6272. https://doi.org/10.1016/j.watres.2012.08.037

Gerrity, D., Mayer, B., Ryu, H., Crittenden, J., Abbaszadegan, M., 2009. A comparison of pilot-scale photocatalysis and enhanced coagulation for disinfection byproduct mitigation. Water Res 43, 1597–1610. https://doi.org/10.1016/j.watres.2009.01.010

Ghanbari, F., Moradi, M., 2015a. A comparative study of electrocoagulation, electrochemical Fenton, electro-Fenton and peroxi-coagulation for decolorization of real textile wastewater: Electrical energy consumption and biodegradability improvement. Biochem Pharmacol 3, 499–506. https://doi.org/10.1016/j.jece.2014.12.018

Ghanbari, F., Moradi, M., 2015b. A comparative study of electrocoagulation, electrochemical Fenton, electro-Fenton and peroxi-coagulation for decolorization of real textile wastewater: Electrical energy consumption and biodegradability improvement. J Environ Chem Eng 3, 499–506. https://doi.org/10.1016/j.jece.2014.12.018

Giesy, J.P., Kannan, K., 2001. Global distribution of perfluorooctane sulfonate in wildlife. Environ Sci Technol 35, 1339–1342. https://doi.org/10.1021/es001834k

Glover, C.M., Quiñones, O., Dickenson, E.R.V., 2018. Removal of perfluoroalkyl and polyfluoroalkyl substances in potable reuse systems. Water Res 144, 454–461. https://doi.org/10.1016/j.watres.2018.07.018

Golea, D.M., Upton, A., Jarvis, P., Moore, G., Sutherland, S., Parsons, S.A., Judd, S.J., 2017. THM and HAA formation from NOM in raw and treated surface waters. Water Res 112, 226–235. https://doi.org/10.1016/j.watres.2017.01.051

Goodrich, J.A., Adams, J.Q., Lykins, B.W., Clark, R.M., 1992. Safe drinking water from small systems. Treatment options. J Am Water Works Assoc 84, 49–55. https://doi.org/10.1002/j.1551-8833.1992.tb07353.x

Goss, K.U., Schwarzenbach, R.P., 2001. Linear free energy relationships used to evaluate equilibrium partitioning of organic compounds. Environ Sci Technol. https://doi.org/10.1021/es000996d

Govindan, K., Angelin, A., Kalpana, M., Rangarajan, M., Shankar, P., Jang, A., 2020a. Electrocoagulants Characteristics and Application of Electrocoagulation for Micropollutant Removal and Transformation Mechanism. ACS Appl Mater Interfaces 12, 1775–1788. https://doi.org/10.1021/acsami.9b16559

Govindan, K., Angelin, A., Kalpana, M., Rangarajan, M., Shankar, P., Jang, A., 2020b. Electrocoagulants Characteristics and Application of Electrocoagulation for Micropollutant Removal and Transformation Mechanism. ACS Appl Mater Interfaces 12, 1775–1788. https://doi.org/10.1021/acsami.9b16559

Gu, B., Schmitt, J., Chen, Z., Liang, L., McCarthy, J.F., 1995. Adsorption and desorption of different organic matter fractions on iron oxide. Geochim Cosmochim Acta 59, 219–229. https://doi.org/10.1016/0016-7037(94)00282-Q

Guilherme, S., Rodriguez, M.J., 2017. Models for estimation of the presence of non-regulated disinfection by-products in small drinking water systems. Environ Monit Assess 189, 1–14. https://doi.org/10.1007/s10661-017-6296-5

Guilherme, S., Rodriguez, M.J., 2014. Occurrence of regulated and non-regulated disinfection by-products in small drinking water systems. Chemosphere 117, 425–432. https://doi.org/10.1016/j.chemosphere.2014.08.002

Haber, F., Weiss, J., 1934. The catalytic decomposition of hydrogen peroxide Iron Salts*. Proceedings of the Royal Society of London 147, 1070–1091. https://doi.org/10.1021/j150472a009

Hancock, R.D., Martell, A.E., 1989. Ligand Design for Selective Complexation of Metal Ions in Aqueous Solution Specific Complexation of Larger Metal 1908 Ions Such As Ca(II) and Pb(II) 2. Ligands for Complexing More Highly. Chem. Rev 89, 1875–1914.

Hand, D.W., Perram, D.L., Crittenden, J.C., 1995. Destruction of DBP precursors with catalytic oxidation. J Am Water Works Assoc 87, 84–96.

Heffron, J., Marhefke, M., Mayer, B.K., 2016. Removal of trace metal contaminants from potable water by electrocoagulation. Sci Rep 6, 1–9. https://doi.org/10.1038/srep28478

Heffron, J., McDermid, B., Maher, E., McNamara, P.J., Mayer, B.K., 2019a. Mechanisms of virus mitigation and suitability of bacteriophages as surrogates in drinking water treatment by iron electrocoagulation. Water Res 163, 114877. https://doi.org/10.1016/j.watres.2019.114877

Heffron, J., McDermid, B., Mayer, B.K., 2019b. Bacteriophage inactivation as a function of ferrous iron oxidation. Environ Sci (Camb) 5, 1309–1317. https://doi.org/10.1039/c9ew00190e

Heffron, J., Ryan, D.R., Mayer, B.K., 2019c. Sequential electrocoagulation-electrooxidation for virus mitigation in drinking water. Water Res 160, 435–444. https://doi.org/10.1016/j.watres.2019.05.078

Helmer, R.W., Reeves, D.M., Cassidy, D.P., 2022. Per- and Polyfluorinated Alkyl Substances (PFAS) cycling within Michigan: Contaminated sites, landfills and wastewater treatment plants. Water Res 210. https://doi.org/10.1016/j.watres.2021.117983

Her, N., Amy, G., McKnight, D., Sohn, J., Yoon, Y., 2003. Characterization of DOM as a function of MW by fluorescence EEM and HPLC-SEC using UVA, DOC, and fluorescence detection. Water Res 37, 4295–4303. https://doi.org/10.1016/S0043-1354(03)00317-8

Howe, K.J., Hand, D.W., Crittenden, J.C., Trussell, R. Rhodes, Tchobanoglous, G., 2012. Principles of Water Treatment [WWW Document]. John Wiley & Sons. URL https://app.knovel.com/web/toc.v/cid:kpPWT00004/principles-of-water?_ga=2.11339764.1920316558.1550169603-1208604398.1548273099 (accessed 2.13.19).

Hu, X.C., Andrews, D.Q., Lindstrom, A.B., Bruton, T.A., Schaider, L.A., Grandjean, P., Lohmann, R., Carignan, C.C., Blum, A., Balan, S.A., Higgins, C.P., Sunderland, E.M., 2016. Detection of Poly- and Perfluoroalkyl Substances (PFASs) in U.S. Drinking Water Linked to Industrial Sites, Military Fire Training Areas, and Wastewater Treatment Plants. Environ Sci Technol Lett 3, 344–350. https://doi.org/10.1021/acs.estlett.6b00260

Hu, X.C., Tokranov, A.K., Liddie, J., Zhang, X., Grandjean, P., Hart, J.E., Laden, F., Sun, Q., Yeung, L.W.Y., Sunderland, E.M., 2019. Tap water contributions to plasma concentrations of poly- and perfluoroalkyl substances (PFAS) in a nationwide prospective cohort of U.S. women. Environ Health Perspect 127. https://doi.org/10.1289/EHP4093

Hua, G., Reckhow, D.A., 2007. Characterization of disinfection byproduct precursors based on hydrophobicity and molecular size. Environ Sci Technol 41, 3309–15.

Hug, S.J., Leupin, O., 2003. Iron-catalyzed oxidation of Arsenic(III) by oxygen and by hydrogen peroxide: pH-dependent formation of oxidants in the Fenton reaction. Environ Sci Technol 37, 2734–2742. https://doi.org/10.1021/es026208x

Ingelsson, M., Yasri, N., Roberts, E.P.L., 2020. Electrode passivation, faradaic efficiency, and performance enhancement strategies in electrocoagulation—a review. Water Res 187. https://doi.org/10.1016/j.watres.2020.116433

Ishii, S.K.L., Boyer, T.H., 2012. Behavior of reoccurring parafac components in fluorescent dissolved organic matter in natural and engineered systems: A critical review. Environ Sci Technol. https://doi.org/10.1021/es2043504

Jasper, J.T., Yang, Y., Hoffmann, M.R., 2017. Toxic Byproduct Formation during Electrochemical Treatment of Latrine Wastewater. Environ Sci Technol 51, 7111–7119. https://doi.org/10.1021/acs.est.7b01002

Javed, H., Lyu, C., Sun, R., Zhang, D., Alvarez, P.J.J., 2020. Discerning the inefficacy of hydroxyl radicals during perfluorooctanoic acid degradation. Chemosphere 247. https://doi.org/10.1016/J.CHEMOSPHERE.2020.125883

Johnson, R.L., Anschutz, A.J., Smolen, J.M., Simcik, M.F., Lee Penn, R., 2007. The adsorption of perfluorooctane sulfonate onto sand, clay, and iron oxide surfaces. J Chem Eng Data 52, 1165–1170. https://doi.org/10.1021/je060285g

Jones, C.H., Shilling, E.G., Linden, K.G., Cook, S.M., 2018. Life Cycle Environmental Impacts of Disinfection Technologies Used in Small Drinking Water Systems. Environ Sci Technol 52, 2998–3007. https://doi.org/10.1021/acs.est.7b04448

Kastl, G., Sathasivan, A., Fisher, I., Van Leeuwen, J., 2004. Modeling DOC Removal by Enhanced Coagulation. J Am Water Works Assoc 96, 79–89. https://doi.org/10.1002/j.1551-8833.2004.tb10557.x

Kim, H.-C., Yu, M.-J., 2007. Characterization of aquatic humic substances to DBPs formation in advanced treatment processes for conventionally treated water. J Hazard Mater 143, 486–493. https://doi.org/10.1016/j.jhazmat.2006.09.063

Kim, M.-K., Kim, T., Kim, T.-K., Joo, S.-W., Zoh, K.-D., 2020. Degradation mechanism of perfluorooctanoic acid (PFOA) during electrocoagulation using Fe electrode. Sep Purif Technol 247, 116911. https://doi.org/10.1016/j.seppur.2020.116911

Kleiser, G, Frimmel, F.H., 2000. Removal of precursors for disinfection by-products (DBPs) - Differences between ozone- and OH-radical-induced oxidation. Science of the Total Environment 256, 1–9. https://doi.org/10.1016/S0048-9697(00)00377-6

Kleiser, G., Frimmel, F.H., 2000. Removal of precursors for disinfection by-products (DBPs) — differences between ozone- and OH-radical-induced oxidation. Science of The Total Environment 256, 1–9. https://doi.org/10.1016/S0048-9697(00)00377-6

Kothawala, D.N., Köhler, S.J., Östlund, A., Wiberg, K., Ahrens, L., 2017. Influence of dissolved organic matter concentration and composition on the removal efficiency of perfluoroalkyl substances (PFASs) during drinking water treatment. Water Res 121, 320–328. https://doi.org/10.1016/j.watres.2017.05.047

Kubicki, J.D., Apitz, S.E., 1999. Models of natural organic matter and interactions with organic contaminants. Org Geochem 30, 911–927.

Kumar, A., Nidheesh, P. V., Suresh Kumar, M., 2018. Composite wastewater treatment by aerated electrocoagulation and modified peroxi-coagulation processes. Chemosphere 205, 587–593. https://doi.org/10.1016/j.chemosphere.2018.04.141

Kwiatkowski, C.F., Andrews, D.Q., Birnbaum, L.S., Bruton, T.A., Dewitt, J.C., Knappe, D.R.U., Maffini, M. V., Miller, M.F., Pelch, K.E., Reade, A., Soehl, A., Trier, X., Venier, M., Wagner, C.C., Wang, Z., Blum, A., 2020. Scientific Basis for Managing PFAS as a Chemical Class. Environ Sci Technol Lett 7, 532–543. https://doi.org/10.1021/acs.estlett.0c00255

Lakshmanan, D., Clifford, D.A., Samanta, G., 2009. Ferrous and ferric ion generation during iron electrocoagulation. Environ Sci Technol 43, 3853–3859. https://doi.org/10.1021/es8036669

Lan, T., Wu, P., Liu, Z., Stroet, M., Liao, J., Chai, Z., Mark, A.E., Liu, N., Wang, D., 2021. Understanding the Effect of pH on the Solubility and Aggregation Extent of Humic Acid in Solution by Combining Simulation and the Experiment. Environ Sci Technol. https://doi.org/10.1021/acs.est.1c05938

Lavonen, E.E., Kothawala, D.N., Tranvik, L.J., Gonsior, M., Schmitt-Kopplin, P., Köhler, S.J., 2015. Tracking changes in the optical properties and molecular composition of dissolved organic matter during drinking water production. Water Res 85, 286–294. https://doi.org/10.1016/j.watres.2015.08.024

Le, T.X.H., Haflich, H., Shah, A.D., Chaplin, B.P., 2019. Energy-Efficient Electrochemical Oxidation of Perfluoroalkyl Substances Using a Ti4O7 Reactive Electrochemical Membrane Anode. Environ Sci Technol Lett 6, 504–510. https://doi.org/10.1021/acs.estlett.9b00397

Lee, S.Y., Gagnon, G.A., 2016. Comparing the growth and structure of flocs from electrocoagulation and chemical coagulation. Journal of Water Process Engineering 10, 20–29. https://doi.org/10.1016/j.jwpe.2016.01.012

Lee, Y.-C., Wang, P.-Y., Lo, S.-L., Huang, C.P., 2017. Recovery of perfluorooctane sulfonate (PFOS) and perfluorooctanoate (PFOA) from dilute water solution by foam flotation. Sep Purif Technol 173, 280–285.

Lenka, S.P., Kah, M., Padhye, L.P., 2021. A review of the occurrence, transformation, and removal of poly- and perfluoroalkyl substances (PFAS) in wastewater treatment plants. Water Res 199. https://doi.org/10.1016/J.WATRES.2021.117187

Li, L., Wang, Y., Zhang, W., Yu, S., Wang, X., Gao, N., 2020. New advances in fluorescence excitation-emission matrix spectroscopy for the characterization of dissolved organic matter in drinking water treatment: A review. Chemical Engineering Journal. https://doi.org/10.1016/j.cej.2019.122676

Li, L., Yin, Z., Cheng, M., Qin, L., Liu, S., Yi, H., Zhang, M., Fu, Y., Yang, X., Zhou, X., Zeng, G., Lai, C., 2022. Insights into reactive species generation and organics selective degradation in Fe-based heterogeneous Fenton-like systems: A critical review. Chemical Engineering Journal 140126. https://doi.org/10.1016/j.cej.2022.140126

Li, M., Mo, C.-H., Luo, X., He, K.-Y., Yan, J.-F., Wu, Q., Yu, P.-F., Han, W., Feng, N.-X., YEUNG, K.L., Zhou, S.-Q., 2021. Exploring key reaction sites and deep degradation mechanism of perfluorooctane sulfonate via peroxymonosulfate activation under electrocoagulation process. Water Res 207, 117849. https://doi.org/10.1016/j.watres.2021.117849

Lin, H., Wang, Y., Niu, J., Yue, Z., Huang, Q., 2015. Efficient Sorption and Removal of Perfluoroalkyl Acids (PFAAs) from Aqueous Solution by Metal Hydroxides Generated in Situ by Electrocoagulation. Environ Sci Technol 49, 10562–10569. https://doi.org/10.1021/acs.est.5b02092

Linares-Hernández, I., Barrera-Díaz, C., Roa-Morales, G., Bilyeu, B., Ureña-Núñez, F., 2009. Influence of the anodic material on electrocoagulation performance. Chemical Engineering Journal 148, 97–105. https://doi.org/10.1016/j.cej.2008.08.007

Liu, S., Lim, M., Fabris, R., Chow, C., Drikas, M., Amal, R., 2008. TiO2 photocatalysis of natural organic matter in surface water: Impact on trihalomethane and haloacetic acid formation potential. Environ Sci Technol 42, 6218–6223. https://doi.org/10.1021/es800887s

Liu, Z., Singer, S., Tong, Y., Kimbell, L., Anderson, E., Hughes, M., Zitomer, D., McNamara, P., 2018. Characteristics and applications of biochars derived from

wastewater solids. Renewable and Sustainable Energy Reviews 90, 650–664. https://doi.org/10.1016/j.rser.2018.02.040

Lu, D., Sha, S., Luo, J., Huang, Z., Zhang Jackie, X., 2020. Treatment train approaches for the remediation of per- and polyfluoroalkyl substances (PFAS): A critical review. J Hazard Mater 386. https://doi.org/10.1016/j.jhazmat.2019.121963

Lv, L., Jiang, T., Zhang, S., Yu, X., 2014. Exposure to mutagenic disinfection byproducts leads to increase of antibiotic resistance in pseudomonas aeruginosa. Environ Sci Technol 48, 8188–8195. https://doi.org/10.1021/es501646n

Maher, E.K., O'Malley, K.N., Heffron, J., Huo, J., Mayer, B.K., Wang, Y., McNamara, P.J., 2018. Analysis of Operational Parameters, Reactor Kinetics, and Floc Characterization for the Removal of Estrogens via Electrocoagulation. Chemosphere 220, 1141–1149. https://doi.org/https://doi.org/10.1016/j.chemosphere.2018.12.161

Maher, E.K., O'Malley, K.N., Heffron, J., Huo, J., Wang, Y., Mayer, B.K., McNamara, P.J., 2019. Removal of estrogenic compounds: Via iron electrocoagulation: Impact of water quality and assessment of removal mechanisms. Environ Sci (Camb) 5, 956–966. https://doi.org/10.1039/c9ew00087a

Maldonado, V.Y., Schwichtenberg, T., Schmokel, C., Witt, S.E., Field, J.A., 2022. Electrochemical Transformations of Perfluoroalkyl Acid (PFAA) Precursors and PFAAs in Landfill Leachates. https://doi.org/10.1021/acsestwater.1c00479

Matilainen, A., Gjessing, E.T., Lahtinen, T., Hed, L., Bhatnagar, A., Sillanpää, M., 2011. An overview of the methods used in the characterisation of natural organic matter (NOM) in relation to drinking water treatment. Chemosphere 83, 1431–1442. https://doi.org/10.1016/j.chemosphere.2011.01.018

Matilainen, A., Sillanpää, M., 2010. Removal of natural organic matter from drinking water by advanced oxidation processes. Chemosphere. https://doi.org/10.1016/j.chemosphere.2010.04.067

Mavrikis, S., Perry, S.C., Leung, P.K., Wang, L., Ponce De León, C., 2021. Recent Advances in Electrochemical Water Oxidation to Produce Hydrogen Peroxide: A Mechanistic Perspective. ACS Sustain Chem Eng. https://doi.org/10.1021/acssuschemeng.0c07263

Mayer, B.K., Daugherty, E., Abbaszadegan, M., 2014. Disinfection byproduct formation resulting from settled, filtered, and finished water treated by titanium dioxide photocatalysis. Chemosphere 117, 72–78. https://doi.org/10.1016/j.chemosphere.2014.05.073

Mayer, B.K., Ryan, D.R., 2017. Impact on Disinfection Byproducts Using Advanced Oxidation Processes for Drinking Water Treatment, in: Applications of Advanced Oxidation Processes (AOPs) in Drinking Water Treatment. Springer, pp. 345–386. https://doi.org/10.1007/698_2017_82

McBeath, S.T., Mohseni, M., Wilkinson, D.P., 2020a. Pilot-scale iron electrocoagulation treatment for natural organic matter removal. Environ Technol 41, 577–585. https://doi.org/10.1080/09593330.2018.1505965

McBeath, S.T., Wilkinson, D.P., Graham, N.J.D., 2020b. Exploiting water contaminants: In-situ electrochemical generation of ferrates using ambient raw water iron (Fe2+). J Environ Chem Eng 8. https://doi.org/10.1016/j.jece.2020.103834

McBeath, S.T., Wilkinson, D.P., Graham, N.J.D., 2020c. Advanced electrochemical oxidation for the simultaneous removal of manganese and generation of permanganate oxidant. Environ Sci (Camb) 6, 2405–2415. https://doi.org/10.1039/d0ew00261e

McCleaf, P., Kjellgren, Y., Ahrens, L., 2021. Foam fractionation removal of multiple per- and polyfluoroalkyl substances from landfill leachate. AWWA Water Sci 3. https://doi.org/10.1002/aws2.1238

Mcknight, D.M., Boyer, E.W., Westerhoff, P.K., Doran, P.T., Kulbe, T., Andersen, D.T., 2001. Spectrofluorometric characterization of dissolved organic matter for indication of precursor organic material and aromaticity, Limnol. Oceanogr.

Meng, P., Deng, S., Maimaiti, A., Wang, B., Huang, J., Wang, Y., Cousins, I.T., Yu, G., 2018. Efficient removal of perfluorooctane sulfonate from aqueous film-forming foam solution by aeration-foam collection. https://doi.org/10.1016/j.chemosphere.2018.03.183

Mercier Shanks, C., Sérodes, J.B., Rodriguez, M.J., 2013. Spatio-temporal variability of non-regulated disinfection by-products within a drinking water distribution network. Water Res 47, 3231–3243. https://doi.org/10.1016/j.watres.2013.03.033

Miklos, D.B., Remy, C., Jekel, M., Linden, K.G., Drewes, J.E., Hübner, U., 2018. Evaluation of advanced oxidation processes for water and wastewater treatment – A critical review. Water Res 139, 118–131. https://doi.org/10.1016/j.watres.2018.03.042

Min, X., Wang, Y., 2023. Enhanced adsorption of short-chain perfluorobutanoic acid by functionalized periodic mesoporous organosilica: Performance and mechanisms. J Hazard Mater 449, 131047. https://doi.org/10.1016/j.jhazmat.2023.131047

Mitchell, S.M., Ahmad, M., Teel, A.L., Watts, R.J., 2013. Degradation of Perfluorooctanoic Acid by Reactive Species Generated through Catalyzed H 2 O 2 Propagation Reactions. Environ Sci Technol Lett 1, 117–121. https://doi.org/10.1021/ez4000862

Mohora, E., Rončeví, S., Dalmacija, B., Agbaba, J., Watson, M., Karloví, E., Dalmacija, M., 2012. Removal of natural organic matter and arsenic from water by electrocoagulation/flotation continuous flow reactor. J Hazard Mater 235–236, 257–264. https://doi.org/10.1016/j.jhazmat.2012.07.056

Niu, J., Li, Y., Shang, E., Xu, Z., Liu, J., 2016. Electrochemical oxidation of perfluorinated compounds in water. Chemosphere 146, 526–538. https://doi.org/10.1016/j.chemosphere.2015.11.115

Olusegun Akinwande, M., Garba Dikko, H., Samson, A., 2015. Variance Inflation Factor: As a Condition for the Inclusion of Suppressor Variable(s) in Regression Analysis. Open J Stat 5, 754–767. https://doi.org/10.4236/ojs.2015.57075

Park, M., Wu, S., Lopez, I.J., Chang, J.Y., Karanfil, T., Snyder, S.A., 2020. Adsorption of perfluoroalkyl substances (PFAS) in groundwater by granular activated carbons: Roles of hydrophobicity of PFAS and carbon characteristics. Water Res 170. https://doi.org/10.1016/j.watres.2019.115364

Phungsai, P., Kurisu, F., Kasuga, I., Furumai, H., 2016. Molecular characterization of low molecular weight dissolved organic matter in water reclamation processes using Orbitrap mass spectrometry. Water Res 100, 526–536. https://doi.org/10.1016/j.watres.2016.05.047

Pi, Y., Schumacher, J., Jekel, M., 2005. The use of para-chlorobenzoic acid (pCBA) as an ozone/hydroxyl radical probe compound. Ozone Sci Eng. https://doi.org/10.1080/01919510500349309

Pifer, A.D., Fairey, J.L., 2012. Improving on SUVA254 using fluorescence-PARAFAC analysis and asymmetric flow-field flow fractionation for assessing disinfection byproduct formation and control. Water Res 46, 2927–2936. https://doi.org/10.1016/j.watres.2012.03.002

Pignatello, J.J., Oliveros, E.;, Mackay, A., 2006. Advanced Oxidation Processes for Organic Contaminant Destruction Based on the Fenton Reaction and Related Chemistry. Crit Rev Environ Sci Technol 36.

Postigo, C., Richardson, S.D., 2014. Transformation of pharmaceuticals during oxidation/disinfection processes in drinking water treatment. J Hazard Mater. https://doi.org/10.1016/j.jhazmat.2014.07.029

Pratap, K., Lemley, A.T., 1998. Fenton Electrochemical Treatment of Aqueous Atrazine and Metolachlor. J Agric Food Chem 46, 3285–3291. https://doi.org/10.1021/jf9710342

Pratap, K., Lemley, A.T., 1994. Electrochemical Peroxide Treatment of Aqueous Herbicide Solutions. J Agric Food Chem 42, 209–215. https://doi.org/10.1021/jf00037a038

Qian, A., Yuan, S., Xie, S., Tong, M., Zhang, P., Zheng, Y., 2019a. Oxidizing Capacity of Iron Electrocoagulation Systems for Refractory Organic Contaminant Transformation. Environ Sci Technol 53, 12629–12638. https://doi.org/10.1021/acs.est.9b03754

Qian, A., Yuan, S., Xie, S., Tong, M., Zhang, P., Zheng, Y., 2019b. Oxidizing Capacity of Iron Electrocoagulation Systems for Refractory Organic Contaminant Transformation. Environ Sci Technol 53, 12629–12638. https://doi.org/10.1021/acs.est.9b03754

Radjenovic, J., Duinslaeger, N., Avval, S.S., Chaplin, B.P., 2020. Facing the Challenge of Poly- And Perfluoroalkyl Substances in Water: Is Electrochemical Oxidation the Answer? Environ Sci Technol 54, 14815–14829. https://doi.org/10.1021/acs.est.0c06212

Radjenovic, J., Petrovic, M., 2016. Sulfate-mediated electrooxidation of X-ray contrast media on boron-doped diamond anode. Water Res 94, 128–135. https://doi.org/10.1016/j.watres.2016.02.045

Rahman, M.F., Peldszus, S., Anderson, W.B., 2014. Behaviour and fate of perfluoroalkyl and polyfluoroalkyl substances (PFASs) in drinking water treatment: A review. Water Res 50, 318–340. https://doi.org/10.1016/j.watres.2013.10.045

Remucal, C.K., Cory, R.M., Sander, M., McNeill, K., 2012. Low molecular weight components in an aquatic humic substance as characterized by membrane dialysis and Orbitrap mass spectrometry. Environ Sci Technol 46, 9350–9359. https://doi.org/10.1021/es302468q

Richardson, S.D., Plewa, M.J., Wagner, E.D., Schoeny, R., DeMarini, D.M., 2007. Occurrence, genotoxicity, and carcinogenicity of regulated and emerging disinfection by-products in drinking water: A review and roadmap for research. Mutat Res Rev Mutat Res 636, 178–242. https://doi.org/10.1016/j.mrrev.2007.09.001

Richardson, S.D., Postigo, C., 2012. Drinking Water Disinfection By-products, in: Handbook of Environmental Chemistry. pp. 93–137. https://doi.org/10.1007/698_2011_125

Richardson, S.D., Ternes, T.A., 2018. Water Analysis: Emerging Contaminants and Current Issues. Anal Chem 90, 398–428. https://doi.org/10.1021/acs.analchem.7b04577

Robey, N.M., Da Silva, B.F., Annable, M.D., Townsend, T.G., Bowden, J.A., 2020. Concentrating Per- And Polyfluoroalkyl Substances (PFAS) in Municipal Solid Waste Landfill Leachate Using Foam Separation. Environ Sci Technol 54, 12550–12559. https://doi.org/10.1021/acs.est.0c01266

Rook, J.J., 1976. Haloforms in drinking water. J Am Water Works Assoc. https://doi.org/10.2307/41268395

Rosario-Ortiz, F.L., Canonica, S., 2016. Probe compounds to assess the photochemical activity of dissolved organic matter. Environ Sci Technol. https://doi.org/10.1021/acs.est.6b02776

Rosenfeldt, E.J., Linden, K.G., Canonica, S., Von Gunten, U., 2006. OH radical formation during ozonation and the advanced oxidation processes O 3 /H 2 O 2 and UV/H 2 O 2. https://doi.org/10.1016/j.watres.2006.09.008

Ryan, D.R., Maher, E.K., Heffron, J., Mayer, B.K., McNamara, P.J., 2021. Electrocoagulation-electrooxidation for mitigating trace organic compounds in model drinking water sources. Chemosphere 273. https://doi.org/10.1016/j.chemosphere.2020.129377

Ryan, Donald R., Maher, E.K., Heffron, J., Mayer, B.K., McNamara, P.J., 2021. Electrocoagulation-electrooxidation for mitigating trace organic compounds in model drinking water sources. Chemosphere 273. https://doi.org/10.1016/j.chemosphere.2020.129377

Ryan, D.R., McNamara, P.J., Mayer, B.K., 2020. Iron-electrocoagulation as a disinfection byproduct control strategy for drinking water treatment. Environ Sci (Camb) 6, 1116–1124. https://doi.org/10.1039/D0EW00106F

Sarathy, S., Mohseni, M., 2010. Effects of UV/H 2 O 2 advanced oxidation on chemical characteristics and chlorine reactivity of surface water natural organic matter. Water Res 44, 4087–4096. https://doi.org/10.1016/j.watres.2010.05.025

Sawyer, C.N., McCarty, P.L.,, Parkin, G.F., 2003. Chemistry for Environmental Engineering and Science, 5th Edition. ed. McGraw Hill Inc, New York.

Schaefer, C.E., Lemes, M.C.S., Schwichtenberg, T., Field, J.A., 2022. Enrichment of poly- and perfluoroalkyl substances (PFAS) in the surface microlayer and foam in synthetic and natural waters. J Hazard Mater 440, 129782. https://doi.org/10.1016/j.jhazmat.2022.129782

Schwichtenberg, T., Bogdan, D., Carignan, C.C., Reardon, P., Rewerts, J., Wanzek, T., Field, J.A., 2020. PFAS and Dissolved Organic Carbon Enrichment in

Surface Water Foams on a Northern U.S. Freshwater Lake. Environ. Sci. Technol 54, 56. https://doi.org/10.1021/acs.est.0c05697

Serra-Clusellas, A., Sbardella, L., Herrero, P., Delpino-Rius, A., Riu, M., Correa, M. de L., Casadellà, A., Canela, N., Martínez-Lladó, X., 2021. Erythromycin abatement from water by electro-fenton and peroxyelectrocoagulation treatments. Water (Switzerland) 13. https://doi.org/10.3390/w13081129

Sharp, E.L., Jarvis, P., Parsons, S.A., Jefferson, B., 2006. Impact of fractional character on the coagulation of NOM. Colloids Surf A Physicochem Eng Asp 286, 104–111. https://doi.org/10.1016/j.colsurfa.2006.03.009

Sharp, Emma L., Parsons, S.A., Jefferson, B., 2006. Seasonal variations in natural organic matter and its impact on coagulation in water treatment. Science of the Total Environment 363, 183–194. https://doi.org/10.1016/j.scitotenv.2005.05.032

Shi, H., Chiang, S.Y. (Dora), Wang, Yaye, Wang, Yifei, Liang, S., Zhou, J., Fontanez, R., Gao, S., Huang, Q., 2021. An electrocoagulation and electrooxidation treatment train to remove and degrade per- and polyfluoroalkyl substances in aqueous solution. Science of the Total Environment 788. https://doi.org/10.1016/j.scitotenv.2021.147723

Shi, Y., Yang, J., Ma, J., Luo, C., 2017. Feasibility of bubble surface modification for natural organic matter removal from river water using dissolved air flotation. Front Environ Sci Eng 11. https://doi.org/10.1007/s11783-017-0954-2

Shutova, Y., Karna, B.L., Hambly, A.C., Lau, B., Henderson, R.K., Le-Clech, P., 2016. Enhancing organic matter removal in desalination pretreatment systems by application of dissolved air flotation. Desalination 383, 12–21. https://doi.org/10.1016/j.desal.2015.12.018

Singh, S., Lo, S.L., Srivastava, V.C., Qiao, Q., Sharma, P., 2021. Mineralization of perfluorooctanoic acid by combined aerated electrocoagulation and Modified peroxi-coagulation methods. J Taiwan Inst Chem Eng 118, 169–178. https://doi.org/10.1016/j.jtice.2021.01.006

Soriano, A., Schaefer, C., Urtiaga, A., 2020. Enhanced treatment of perfluoroalkyl acids in groundwater by membrane separation and electrochemical oxidation. Chemical Engineering Journal Advances 4, 100042. https://doi.org/10.1016/j.ceja.2020.100042

Stirling, R., Walker, W.S., Westerhoff, P., Garcia-Segura, S., 2020. Techno-economic analysis to identify key innovations required for electrochemical oxidation as point-of-use treatment systems. Electrochim Acta 338. https://doi.org/10.1016/j.electacta.2020.135874

Stoiber, T., Evans, S., Naidenko, O. V., 2020. Disposal of products and materials containing per- and polyfluoroalkyl substances (PFAS): A cyclical problem. Chemosphere 260. https://doi.org/10.1016/j.chemosphere.2020.127659

Stumm, W., Lee, G.F., 1961. Oxygenation of Ferrous Iron. Ind Eng Chem 53, 143–146. https://doi.org/10.1021/ie50614a030

Takagi, S., Adachi, F., Miyano, K., Koizumi, Y., Tanaka, H., Watanabe, I., Tanabe, S., Kannan, K., 2011. Fate of Perfluorooctanesulfonate and perfluorooctanoate in drinking water treatment processes. Water Res 45, 3925–3932. https://doi.org/10.1016/j.watres.2011.04.052

Thurman, E.M., 1985. Organic Geochemistry of Natural Waters, Organic Geochemistry of Natural Waters. Springer Netherlands. https://doi.org/10.1007/978-94-009-5095-5

Tubi, A., Agbaba, J., Zo Dalmacija, B., Molnar, J., Zana Maleti, S., Watson, M., Ugar, S., Perovi, C., 2013. Insight into changes during coagulation in NOM reactivity for trihalomethanes and haloacetic acids formation. J Environ Manage 118, 153–160. https://doi.org/10.1016/j.jenvman.2012.11.046

Ulu, F., Barişçi, S., Kobya, M., Särkkä, H., Sillanpää, M., 2014. Removal of humic substances by electrocoagulation (EC) process and characterization of floc size growth mechanism under optimum conditions. Sep Purif Technol 133, 246–253. https://doi.org/10.1016/j.seppur.2014.07.003

USEPA, 2006. National Primary Drinking Water Regulations: Stage 2 Disinfectants and Disinfection Byproducts Rule.

Uwayezu, J.N., Yeung, L.W.Y., Bäckström, M., 2019. Sorption of PFOS isomers on goethite as a function of pH, dissolved organic matter (humic and fulvic acid) and sulfate. Chemosphere 233, 896–904. https://doi.org/10.1016/j.chemosphere.2019.05.252

van Leeuwen, J., Daly, R., Holmes, M., 2005. Modeling the treatment of drinking water to maximize dissolved organic matter removal and minimize disinfection by-product formation. Desalination 176, 81–89. https://doi.org/10.1016/j.desal.2004.10.024

Vanderford, B.J., Rosario-Ortiz, F.L., Snyder, S.A., 2007. Analysis of p-chlorobenzoic acid in water by liquid chromatography-tandem mass spectrometry. J Chromatogr A 1164, 219–223. https://doi.org/10.1016/j.chroma.2007.07.035

Vasudevan, S., 2014. An efficient removal of phenol from water by peroxi-electrocoagulation processes. Journal of Water Process Engineering 2, 53–57. https://doi.org/10.1016/j.jwpe.2014.05.002

Vecitis, C.D., Park, H., Cheng, J., Mader, B.T., Hoffmann, M.R., 2009. Treatment technologies for aqueous perfluorooctanesulfonate (PFOS) and perfluorooctanoate (PFOA). Frontiers of Environmental Science and Engineering in China 3, 129–151. https://doi.org/10.1007/s11783-009-0022-7

Vik, E.A., Carlson, D.A., Eikum, A.S., Gjessing, E.T., 1984. Electrocoagulation of potable water. Water Res 18, 1355–1360. https://doi.org/10.1016/0043-1354(84)90003-4

Volk, C., Bell, K., Ibrahim, E., Verges, D., Amy, G., Lechevallier, M., 2000. Impact of enhanced and optimized coagulation on removal of organic matter and its biodegradable fraction in drinking water. Water Res 34, 3247–3257. https://doi.org/10.1016/S0043-1354(00)00033-6

Von Gunten, U., 2018. Oxidation Processes in Water Treatment: Are We on Track? Environ Sci Technol. https://doi.org/10.1021/acs.est.8b00586

Waite, T.D., 2006. Process Optimization of Fenton Oxidation Using Kinetic Modeling 40, 4189–4195. https://doi.org/10.1021/es060311v

Wang, F., Shih, K., Leckie, J.O., 2015. Effect of humic acid on the sorption of perfluorooctane sulfonate (PFOS) and perfluorobutane sulfonate (PFBS) on boehmite. Chemosphere 118, 213–218. https://doi.org/10.1016/j.chemosphere.2014.08.080

Wang, L., Nickelsen, M., Chiang, S.-Y. (Dora), Woodard, S., Wang, Y., Liang, S., Mora, R., Fontanez, R., Anderson, H., Huang, Q., 2021. Treatment of perfluoroalkyl acids in concentrated wastes from regeneration of spent ion exchange resin by electrochemical oxidation using Magnéli phase Ti4O7 anode. Chemical Engineering Journal Advances 5, 100078. https://doi.org/10.1016/j.ceja.2020.100078

Wang, X., Zhang, H., Zhang, Y., Shi, Q., Wang, J., Yu, J., Yang, M., 2017. New Insights into Trihalomethane and Haloacetic Acid Formation Potentials: Correlation with the Molecular Composition of Natural Organic Matter in Source Water. Environ Sci Technol 51, 2015–2021. https://doi.org/10.1021/acs.est.6b04817

Weinberg, H.S., Krasner, S.W., Richardson, S.D., Thruston, a D., 2002. The Occurrence of Disinfection By-Products (DBPs) of Health Concern in Drinking Water: Results of a Nationwide DBP Occurrence Study. National Exposure Research Laboratory, Athens, Ga. 462p. https://doi.org/EPA/600/R-02/068

Weishaar, J.L., Aiken, G.R., Bergamaschi, B.A., Fram, M.S., Fujii, R., Mopper, K., 2003. Evaluation of specific ultraviolet absorbance as an indicator of the chemical composition and reactivity of dissolved organic carbon. Environ Sci Technol 37, 4702–4708. https://doi.org/10.1021/es030360x

Weng, L.P., Koopal, L.K., Hiemstra, T., Meeussen, J.C.L., Van Riemsdijk, W.H., 2005. Interactions of calcium and fulvic acid at the goethite-water interface. Geochim Cosmochim Acta 69, 325–339. https://doi.org/10.1016/j.gca.2004.07.002

Westerhoff, P., Aiken, G., Amy, G., Debroux, J., 1999. Relationships between the structure of natural organic matter and its reactivity towards molecular ozone and hydroxyl radicals. Water Res 33, 2265–2276. https://doi.org/http://dx.doi.org/10.1016/S0043-1354(98)00447-3

Westerhoff, P., Yoon, Y., Snyder, S., Wert, E., 2005. Fate of endocrine-disruptor, pharmaceutical, and personal care product chemicals during simulated drinking water treatment processes. Environ Sci Technol 39, 6649–6663. https://doi.org/10.1021/es0484799

Wright, J.M., Evans, A., Kaufman, J.A., Rivera-Núñez, Z., Narotsky, M.G., 2017. Disinfection by-product exposures and the risk of specific cardiac birth defects. Environ Health Perspect 125, 269–277. https://doi.org/10.1289/EHP103

Xiao, F., 2017. Emerging poly- and perfluoroalkyl substances in the aquatic environment: A review of current literature. Water Res 124, 482–495. https://doi.org/10.1016/j.watres.2017.07.024

Xiao, F., Simcik, M.F., Gulliver, J.S., 2013. Mechanisms for removal of perfluorooctane sulfonate (PFOS) and perfluorooctanoate (PFOA) from drinking water by conventional and enhanced coagulation. Water Res 47, 49–56. https://doi.org/10.1016/j.watres.2012.09.024

Xu, B., Iskander, S.M., He, Z., 2020. Dominant formation of unregulated disinfection by-products during electrocoagulation treatment of landfill leachate. Environ Res 182. https://doi.org/10.1016/j.envres.2019.109006

Xu, H., Guo, L., 2017. Molecular size-dependent abundance and composition of dissolved organic matter in river, lake and sea waters. Water Res 117, 115–126. https://doi.org/10.1016/j.watres.2017.04.006

Yang, B., Han, Y., Deng, Y., Li, Y., Zhuo, Q., Wu, J., 2016a. Highly efficient removal of perfluorooctanoic acid from aqueous solution by H2O2-enhanced electrocoagulation-electroflotation technique. Emerg Contam 2, 49–55. https://doi.org/10.1016/j.emcon.2016.04.001

Yang, B., Han, Y., Yu, G., Zhuo, Q., Deng, S., Wu, J., Zhang, P., 2016b. Efficient removal of perfluoroalkyl acids (PFAAs) from aqueous solution by electrocoagulation using iron electrode. Chemical Engineering Journal 303, 384–390. https://doi.org/10.1016/j.cej.2016.06.011

Yang, L., Hur, J., Zhuang, W., 2015. Occurrence and behaviors of fluorescence EEM-PARAFAC components in drinking water and wastewater treatment

systems and their applications: A review. Environmental Science and Pollution Research. https://doi.org/10.1007/s11356-015-4214-3

Yang, X., Huang, J., Zhang, K., Yu, G., Deng, S., Wang, B., 2014. Stability of 6:2 fluorotelomer sulfonate in advanced oxidation processes: Degradation kinetics and pathway. Environmental Science and Pollution Research 21, 4634–4642. https://doi.org/10.1007/s11356-013-2389-z

Yazdanbakhsh, A.R., Kermani, M., Komasi, S., Aghayani, E., Sheikhmohammadi, A., 2015a. Humic acid removal from aqueous solutions by peroxi-electrocoagulation process.

Yazdanbakhsh, A.R., Massoudinegad, M.R., Eliasi, S., Mohammadi, A.S., 2015b. The influence of operational parameters on reduce of azithromyin COD from wastewater using the peroxi -electrocoagulation process. Journal of Water Process Engineering 6, 51–57. https://doi.org/10.1016/j.jwpe.2015.03.005

Yu, J., Lv, L., Lan, P., Zhang, S., Pan, B., Zhang, W., 2012. Effect of effluent organic matter on the adsorption of perfluorinated compounds onto activated carbon. J Hazard Mater 225–226, 99–106. https://doi.org/10.1016/j.jhazmat.2012.04.073

Yüksel, E., Şengil, I.A., Özacar, M., 2009. The removal of sodium dodecyl sulfate in synthetic wastewater by peroxi-electrocoagulation method. Chemical Engineering Journal 152, 347–353. https://doi.org/10.1016/j.cej.2009.04.058

Zhang, H., Zheng, Y., Wang, X.C., Wang, Y., Dzakpasu, M., 2021. Characterization and biogeochemical implications of dissolved organic matter in aquatic environments. J Environ Manage. https://doi.org/10.1016/j.jenvman.2021.113041

Zhang, W., Cheng, C.Y., 2007. Manganese metallurgy review. Part I: Leaching of ores/secondary materials and recovery of electrolytic/chemical manganese dioxide. Hydrometallurgy 89, 137–159. https://doi.org/10.1016/j.hydromet.2007.08.010

Zhang, Y., Liu, J., Moores, A., Ghoshal, S., 2020. Transformation of 6:2 Fluorotelomer Sulfonate by Cobalt(II)-Activated Peroxymonosulfate. Cite This: Environ. Sci. Technol 54, 4640. https://doi.org/10.1021/acs.est.9b07113

Zhao, Y., Xiao, F., Wang, D., Yan, M., Bi, Z., 2013. Disinfection byproduct precursor removal by enhanced coagulation and their distribution in chemical fractions. Journal of Environmental Sciences 25, 2207–2213. https://doi.org/10.1016/S1001-0742(12)60286-1

Zhou, S., Bu, L., Shi, Z., Bi, C., Yi, Q., 2016. A novel advanced oxidation process using iron electrodes and ozone in atrazine degradation: Performance and mechanism. https://doi.org/10.1016/j.cej.2016.08.001

Zhou, Z., Guo, L., Minor, E.C., 2016. Characterization of bulk and chromophoric dissolved organic matter in the Laurentian Great Lakes during summer 2013. J Great Lakes Res 42, 789–801. https://doi.org/10.1016/j.jglr.2016.04.006

8. APPENDICES AND SUPPLEMENTARY INFORMATION

A3: CHAPTER 3 APPENDIX

Appendix A3.1. Faradaic efficiency of electrocoagulation experimental conditions

The faradaic efficiency was assessed for electrocoagulation, results of which are shown in Table A1. The electro-generated iron doses were not statistically different among the pH conditions tested (p=0.3).

Table A3.1. Iron dose following electrocoagulation and the corresponding faradaic efficiency. Values are the averages of triplicate tests ± 1 standard deviation.

Sample	pH 6 Model River Water	pH 8 River Water
Electrocoagulation Iron dose, mg-Fe/L	29 ± 1.7	30 ± 0.14
Faradaic Efficiency, %	83 ± 4.8	86 ± 0.41

Appendix A3.2. The impact of electrocoagulation on effluent water pH

Electrocoagulation generally did not increase pH relative to the control samples for initial pH levels of 6 and pH 7 (Figure A3.1). However, EC at initial pH 8 raised the resulting pH relative to the no EC control tests. During the control experiments, the water matrix pH was adjusted to the target initial conditions, and the tests were conducted following the same procedure as EC experiments without undergoing electrolysis. The pH was measured after the 20-minute settling period.

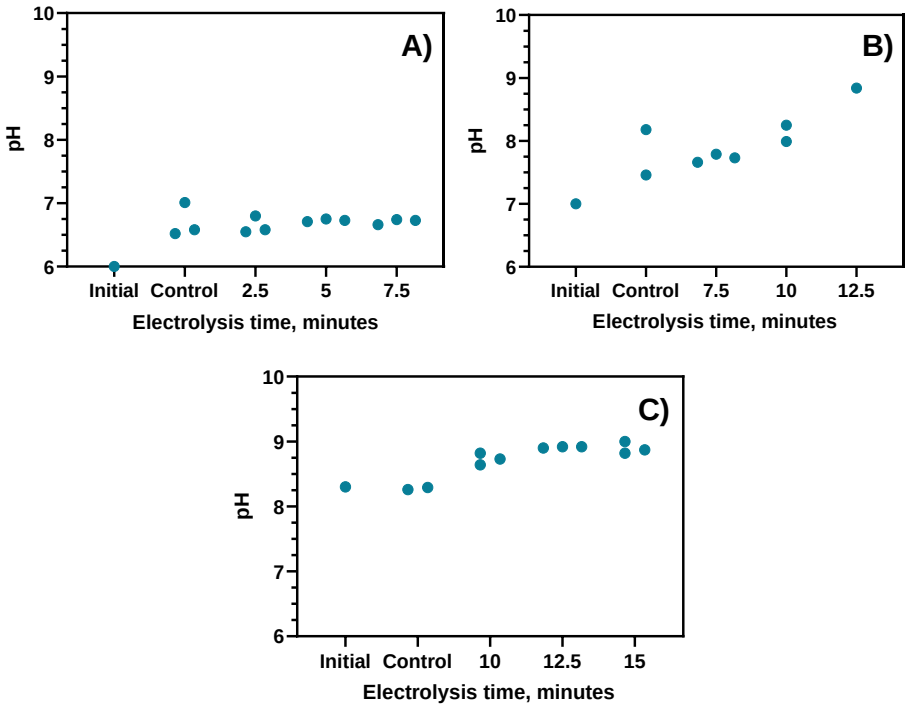

Figure A3.1: Final pH after electrocoagulation treatment at a range of electrolysis times at different initial pH conditions. A) initial pH = 6, B) initial pH = 7, and C) initial pH = 8.3. Control experiments were conducted by adjusting pH and mixing the sample without electrolysis. Each point is a single replicate.

ESI 3: Residual iron and free chlorine following electrocoagulation treatment

Residual iron and free chlorine levels following electrocoagulation treatment of the model river water are shown in Table A1.

Table A2. Total iron, soluble iron, and free chlorine generation following electrocoagulation. Values shown are the averages of triplicate tests ± 1 standard deviation.

Sample	Theoretical Coagulant Dose mg-Fe/L	Total Iron mg-Fe/L	Soluble Iron mg-Fe/L	Free Chlorine mg-Cl_2/L
EC, pH 6, 5 minutes	35	5.8 ± 1.1	0.005 ± 0.004	0.07 ± 0.04
EC, pH 8, 17.5 minutes	140	4.62 ± 0.5	0.035 ± 0.011	0.05 ± 0.05

A4: CHAPTER 4 APPENDIX

Appendix A4.1. Liquid Chromatography Mass Spectrometry Operating Conditions

TOrCs were quantified using a liquid chromatography-mass spectrometer (LC-MS, Shimadzu LC-MS 2020). The HPLC and chromatography conditions for pCBA analysis were adapted from (Vanderford et al., (2007), as summarized in Table A4.1.1. The m/z ratios used for pCBA was 155. Gradient flow was used for pCBA separation (Table A4.1.1). The mobile phase was ultrapure water with 0.1% formic acid and the organic phase was HPLC grade methanol.

Eluent conditions are provided in Table A4.1.1 and other instrument parameters and column information are in Table A4.1.2. Ten-point standard curves were used with concentrations ranging from 4 µg/L to 400 µg/L. Each standard curve was prepared in the respective water matrix to normalize the LC-MS response to ionic interference in each matrix. The limit of quantification used for analyses was 4 µg/L for all TOrCs because it was the lowest concentration that met the 10:1 signal-to-noise requirement for quantification.

Table A4.1.1. LC-MS 2020 gradient flow time progression utilized to quantify pCBA.

Time (min)	Organic Phase (% of flow)[a]
0 - 5	10
5.0-5.5	60
5.5 – 10	100
10-12	100
12-15	10
15-18	10
18	End of run

[a] = organic phase is HPLC-grade methanol

Table A4.1.2. LC-MS 2020 instrument information for pCBA quantification.

Parameter	Value
Eluent Type	Gradient
Mobile Phase A	Milli-Q water + 0.1% formic acid
Mobile Phase B	Methanol
Flow Rate	0.2 mL min^{-1}
Column Temperature	35°C
Detection	Electrospray Mass Spec (ESMS) at 40°C
Injection Volume	50 µL
Acquisition Mode	Single ion mode
Interface Temperature	350°C
DL Temperature	250°C
Nebulizer Gas Flow	1.5 L min^{-1}
Heat Block	400°C
Drying Gas Flow	15 L min^{-1}

Appendix A4.2. Hydroxyl radical quantification using pCBA degradation

The hydroxyl radical concentrations during EC:H_2O_2 were estimated by the pseudo-first order degradation of pCBA (Eqn. S4.1).

$$-\ln\frac{\mathrm{pCBA_t}}{\mathrm{pCBA_0}} = \mathrm{k_{HO:pCBA}[HO\bullet]} \times \mathrm{t} \qquad \text{Eqn. S4.1}$$

Where $k_{HO:pCBA}$ is the second order rate constant in units of $M^{-1}*s^{-1}$, HO• is the hydroxyl radical concentration over the course of treatment, and t is the treatment time in seconds. This method was adapted from (Rosario-Ortiz and Canonica, (2016).

Appendix A4.3. Hydroxyl radical availability for pCBA oxidation

Hydroxyl radical scavenging was estimated for EC:H_2O_2 using Eqn. S4.2 as a function of H_2O_2 concentration to assess whether higher H_2O_2 could inhibit oxidation. It was assumed that pCBA, H_2O_2, and HCO_3^- were the primary constituents competing for the radicals. Results are shown in Figure A4.3.1.

$$\frac{d[\mathrm{HO\bullet}]}{dt} = k_{\mathrm{HO\bullet:pCBA}}C_{pCBA}[\mathrm{HO\bullet}] + k_{\mathrm{HO\bullet:H2O2}}C_{H2O2}[\mathrm{HO\bullet}] + k_{\mathrm{HO\bullet:HCO3}}C_{HCO3}[\mathrm{HO\bullet}]$$

Eqn. S4.2

$$\frac{d[\mathrm{HO\bullet}]}{dt} = [\mathrm{HO\bullet}]\left(k_{\mathrm{HO\bullet:pCBA}}C_{pCBA} + k_{\mathrm{HO\bullet:H2O2}}C_{H2O2} + k_{\mathrm{HO\bullet:HCO3}}C_{HCO3}\right)$$

Eqn. S4.3

$$Fraction\ of\ [\mathrm{HO\bullet}]\ for\ pCBA\ removal = \frac{k_{\mathrm{HO\bullet:pCBA}}C_{pCBA}}{k_{\mathrm{HO\bullet:pCBA}}C_{pCBA}+k_{\mathrm{HO\bullet:H2O2}}C_{H2O2}+k_{\mathrm{HO\bullet:HCO3}}C_{HCO3}}$$

Eqn. S4.4

Table A4.3.1 Second order rate constant for hydroxyl radicals and target compounds (Buxton et al., 1988).

Target compound	Hydroxyl radical rate constant, $k_{HO\bullet:i}$, 1/ M-s
pCBA	5×10^9
H_2O_2	2.7×10^7
HCO_3^-	8.5×10^6

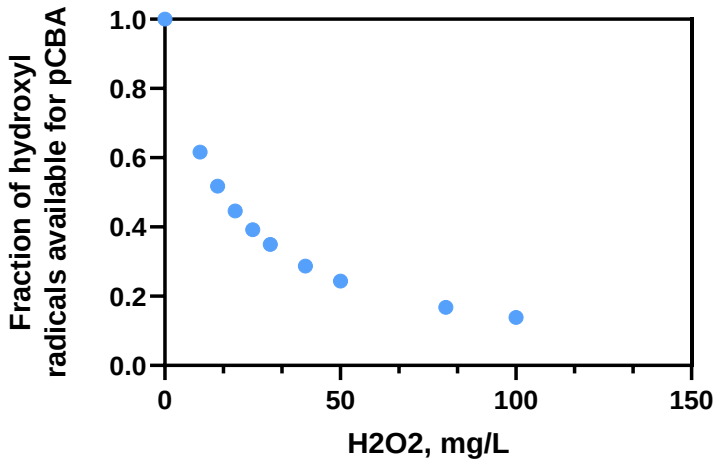

Figure A4.3.1. The estimated fraction of hydroxyl radicals available for pCBA oxidation as a function of increasing H_2O_2 concentrations based on calculated values for Eqn. S3. Values were estimated using the second-order rate constants for H_2O_2 (0 - 100 mg/L), pCBA (2.5 µM), and HCO_3^- (4 mM) to quantify matrix interference.

Appendix A4.5 Oxidant competition for ferrous iron

Oxidant competition for Fe^{2+} was estimated using the rate constants for H_2O_2 and O_2 oxidizing Fe^{2+}. These theoretical calculations relied on the assumption that dissolved oxygen was present at the saturation concentration (9.1 mg O_2/L) (Sawyer et al., 2003). Competition was assessed for pH 6.3 to 14 to evaluate the influence of $[OH^-]$ on Fe^{2+} depletion. The kinetic rate constant for Fe^{2+} and O_2 was 1.1 x 10^{10} L^3/mol^3-min (Stumm and Lee, 1961). The Fe^{2+} and H_2O_2 rate constant used for analyses was 3780 L/mol-min (S. Zhou et al., 2016). The rate constants and associated oxidant concentrations were input into the rate equations (Eqn S4.6 and Eqn S4.7) and compared as a ratio with Eqn S4.8.

$$\frac{d[Fe^{2+}]}{dt} = k_{Fe^{2+}:H_2O_2}\left[Fe^{2+}\right][H_2O_2] \quad \text{Eqn. S4.6}$$

$$\frac{d[Fe^{2+}]}{dt} = k_{Fe^{2+}:O_2}\left[Fe^{2+}\right][O_2][OH^-]^2 \qquad \text{Eqn. S4.7}$$

$$ratio = \frac{k_{Fe^{2+}:H_2O_2}[H_2O_2]}{k_{Fe^{2+}:O_2}[O_2][OH^-]^2} \quad \text{Eqn. S4.8}$$

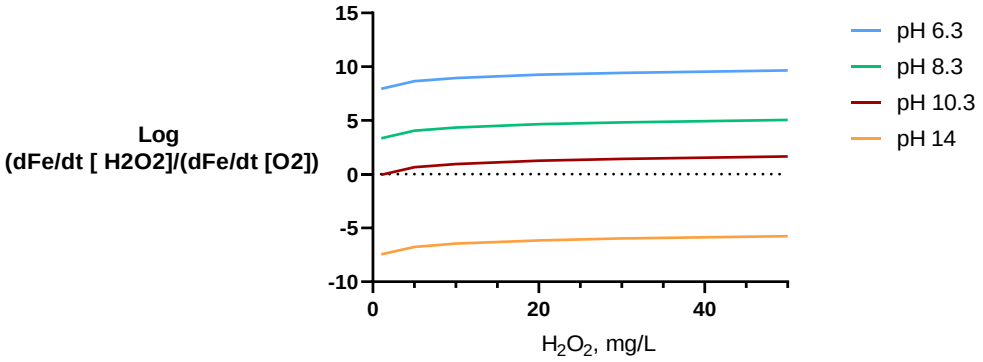

Figure A4.5.1. Relative ratio of Fe^{2+} oxidation due to H_2O_2 and dissolved oxygen. In all scenarios, dissolved oxygen was assumed to be saturated (9.1 mg O_2/L) as a conservative assumption to maximize the influence of dissolved oxygen on the model.

Appendix A4.6. Pseudo-first order rate constants for EC:H_2O_2

Experiments were conducted at a range of current densities and $H_2O_2]_{initial}$ /$[Fe^{2+}]_{generated}$ ratios. Throughout experiments, samples were taken at t=0, 2.5, 5, 7.5, 10, and 15 minutes to quantify pseudo-first order rate constants, as shown in Table A4.6.1.

Table A4.6.1 Pseudo-first order rate constants resulting from reactor inputs (s^{-1}) for EC:H_2O_2 experiments discussed in 4.3.2.

$[H_2O_2]_{initial}$ / $[Fe^{2+}]_{generated}$	Current Density, mA/cm^2				
	3	5.5	7.4	11.1	15
0	1.4×10^{-4}	2.7×10^{-4}	2.9×10^{-4}	2.5×10^{-4}	2.7×10^{-4}
0.35	-	1.1×10^{-3}	1.5×10^{-3}	1.6×10^{-3}	1.5×10^{-3}
0.5	8.4×10^{-4}	1.3×10^{-3}	1.5×10^{-3}	1.6×10^{-3}	-
0.7	-	1.1×10^{-3}	-	1.3×10^{-3}	-
1.6	5.8×10^{-4}	6.5×10^{-4}	-	-	7.7×10^{-4}

"-" indicates test was not conducted.

Appendix A4.8. Statistical Analyses

Appendix A4.8.1 Pearson Correlations

Pearson correlations were conducted on reactor inputs prior to multivariable linear regressions to select parameters correlated to removal and rate and assess multicollinearity between other parameters. The data included in these analyses are results from EC:H_2O_2 experiments at neutral pH and H_2O_2 and EC controls.

Table A4.8.1. Pearson correlations (R^2) for EC:H_2O_2 experiments at neutral pH. Data inputs also include H_2O_2 and EC-only controls. ** indicates $p<0.05$.

Regression: H_2O_2 0 - 40 mg/L; (H_2O_2 and EC Controls included)							
	Removal	Current	H_2O_2	H_2O_2 / Fe	Fe applied	H_2O_2/pCBA	Fe/pCBA
Removal	1.00						
Current	**0.47****	1.00					
H_2O_2	0.003	-0.04	1.00				
H_2O_2 / Fe	0.28	-0.06	**0.64****	1.00			
Fe applied	**0.46****	**0.90****	0.23	0.16	1.00		
H_2O_2/pCBA	0.00	-0.04	**1.00****	**0.64****	0.23	1.00	
Fe/pCBA	**0.46****	**0.90****	0.23	0.16	**1.00****	0.23	1.00

Table A4.8.2. Pearson correlation (R^2) for EC:H_2O_2 experiments for H_2O_2 doses up to 40 mg/L. ** indicates $p<0.05$.

Regression: H_2O_2 0 - 40 mg/L							
	Removal	Current	H_2O_2	H_2O_2 / Fe	Fe applied	H_2O_2/pCBA	Fe/pCBA
Removal	1.00						
Current	0.18	1.00					
H_2O_2	**0.84****	0.23	1.00				
H_2O_2 / Fe	**0.84****	-0.24	**0.77****	1.00			
Fe applied	0.18	**0.92****	0.40	-0.15	1.00		
H_2O_2/pCBA	**0.84****	0.23	**1.00****	**0.77****	**0.40****	1.00	
Fe/pCBA	0.18	**0.92****	0.39	-0.15	**1.00****	**0.39****	1.00

Table A4.8.3. Pearson correlation (R^2) for EC:H2O2 experiments for H_2O_2 doses of 40 – 200 mg/L H_2O_2. ** indicates p<0.05.

Regression: H_2O_2 40 - 200 mg/L							
	Removal	Current	H_2O_2	H_2O_2 / Fe	Fe applied	H_2O_2/pCBA	Fe/pCBA
Removal	1.00						
Current	**0.84****	1.00					
H_2O_2	-0.38	0.01	1.00				
H_2O_2/ Fe	0.10	0.08	0.40	1.00			
Fe applied	**0.77****	**0.97****	0.09	0.13	1.00		
H_2O_2/pCBA	-0.38	0.01	**1.00****	0.40	0.09	1.00	
Fe/pCBA	**0.77****	**0.97****	0.10	0.13	**1.00****	0.10	1

Table A4.8.4. Pearson correlation (R^2) for EC:H_2O_2 experiments for current densities up to 7.4 mA/cm^2. Regression only contains data for EC:H_2O_2 experiments. EC only experiments are excluded from regression due to poor removal. ** indicates p<0.05.

Regression: Current density < 7.4 mA/cm^2							
	Removal	Current	H_2O_2	H_2O_2 / Fe	Fe applied	H_2O_2/pCBA	Fe/pCBA
Removal	1.00						
Current	**0.63****	1.00					
H_2O_2	-0.42	-0.06	1.00				
H_2O_2 / Fe	**-0.59****	-0.38	**0.90****	1.00			
Fe applied	0.29	0.57	**0.64****	0.31	1.00		
H_2O_2/pCBA	-0.42	-0.06	**1.00****	**0.90****	**0.64****	1.00	
Fe/pCBA	0.30	0.57	**0.64****	0.31	**1.00****	**0.64****	1.00

Table A4.8.5. Pearson correlation (R^2) for EC:H_2O_2 experiments for current densities ranging from 7.4 mA/cm^2 to 15 mA/cm^2. Regression only contains data for EC:H_2O_2 experiments. EC only experiments are excluded from regression due to poor removal. ** indicates p<0.05.

Regression: Current density = 7.4 mA/cm2 to 15 mA/cm2							
	Removal	Current	H_2O_2	H_2O_2 / Fe	Fe applied	H_2O_2/pCBA	Fe/pCBA
Removal	1.00						
Current	0.14	1.00					
H_2O_2	**-0.67****	0.09	1.00				
H_2O_2/ Fe	**-0.69****	-0.16	**0.96****	1.00			
Fe applied	-0.05	**0.80****	0.47	0.23	1.00		
H_2O_2/pCBA	**-0.67****	0.09	**1.00****	**0.96****	0.47	1.00	
Fe/pCBA	-0.05	**0.80****	0.47	0.23	**1.00****	0.47	1.00

Appendix A4.8.2. Multivariable Analysis Tables

Table A4.8.6. Normalized multivariable linear regressions for EC:H_2O_2 experiments.

Title	Scenario	Current Density (β_1)	H_2O_2 / Fe^{2+} (β_2)	pH (β_3)	Model R^2	Akaike information Criterion (AIC)	Number of points
			Removal vs. reactor inputs				
%R, neutral	Reactor Inputs All $[H_2O_2]_{initial}$ / $[Fe^{2+}]_{generated}$ (Neutral pH only)	0.5±0.15 *(p=0.0012)*	0.31±0.14 (*p=0.032)*	-	0.31	265	39
%R, low	Reactor Inputs vs. Removal ($[H_2O_2]_{initial}$ / $[Fe^{2+}]_{generated}$ =0-0.77), neutral pH	0.43±0.07 *(p=0.0010)*	0.77±0.06 *(p<0.0001)*	-	0.86	177.4	33
%R, high	Reactor Inputs vs. Removal ($[H_2O_2]_{initial}$ / $[Fe^{2+}]_{generated}$ =0.33 – 1.6	0.41±0.12 *(p=0.002)*	-0.42±0.11 *(p=0.0008)*	-	0.60	173	28
%R, all	Reactor inputs vs. pCBA removal (all $[H_2O_2]_{initial}$ / $[Fe^{2+}]_{generated)}$, all pH	0.36±0.09 *(p=0.008)*	0.22±0.09 *(p=0.0219)*	-0.91±0.15 *(p<0.0001)*	0.58	270	45
			Pseudo first order rate vs. reactor inputs				
k, all	All $[H_2O_2]_{initial}$ / $[Fe^{2+}]_{generated}$, all pH	0.063±0.075 (*p=0.40)*	0.033±0.08 (*p=0.68)*	-0.977±0.12 (*p<0.0001)*	0.63	235	42
k, low, neutral pH	$[H_2O_2]_{initial}$ / $[Fe^{2+}]_{generated}$ 0-0.77, rate, neutral pH	0.33±0.16 (*p=0.0045)*	0.76±0.11 (*p<0.0001)*	-	0.68	186	30
k, EC: H_2O_2 only, neutral pH	$[H_2O_2]_{initial}$ / $[Fe^{2+}]_{generated}$ = 0.33 – 1.6, neutral pH	0.32±0.11 *(p = 0.009)*	-0.59±0.11 (*p<0.0001)*	-	0.68	170	28

Appendix A4.9 H_2O_2 depletion during EC:H_2O_2

The hydrogen peroxide levels during EC:H_2O_2 at pH 3 and pH 6.3 conditions were measured at the reaction stagnation points after 5 minutes, as shown in Table A4.9.1. Additionally, the residual iron following no electricity controls was measured to better assess the

Table A4.9.1. H_2O_2 remaining after 5 minutes of EC:H_2O_2 at pH =3 and pH =6.3.Tests were conducted in triplicate.

Treatment	Residual H_2O_2 Concentration, mg/L		H_2O_2 Removal	
	Average	Standard Deviation	Average	Standard Deviation
EC: H_2O_2 pH 3	1.5	0.2	95.1	0.8
No electricity (H_2O_2 + electrodes) pH 3[a]	0.73	0.12	97.5	0.4
EC: H_2O_2 pH 6.3	9.7	1.5	67.8	5.1

[a]= the treatment time for this no electricity control was 15 minutes to match usual experiments

Table A4.9.2. Residual iron following no electricity control experiments of 30 mg/L H2O2 and iron electrodes. pH =3 and pH =6.3.Tests were conducted in triplicate.

No electricity (H_2O_2 + electrodes)	Residual Iron, mg/L		$[H_2O_2]_{initial}$ / $[Fe^{2+}]_{generated}$	
	Average	Standard Deviation	Average	Standard Deviation
pH 3	32.2	0.4	1.53	0.02
pH 6.3	1.01	0.4	50.6	10.7

Appendix A4.10 Pearson Correlation and Multivariable Analysis: the impact of water quality on pCBA removal

Pearson correlations and multivariable analyses were conducted to assess the role of water quality on pCBA removal following EC:H_2O_2. Results are shown in Table A4.10.1 – A4.10.4.

Table A4.10.1 Pearson correlation of the impact of water quality on E_{EO} and pseudo-first order rate for all matrices ** indicates p<0.05.

	DOC initial	Alkalinity	pH	H_2O_2 demand	pCBA Removal	DOC removal
DOC initial	1.00					
Alkalinity	**-0.57****	1.00				
pH	-0.26	-0.01	1.00			
H_2O_2 demand	**0.89****	**-0.58****	-0.25	1.00		
pCBA Removal	**-0.53****	0.35	**-0.60****	**-0.47****	1.00	
DOC removal	**0.54****	**-0.78****	-0.30	**0.62****	**-0.47****	1.00

Table A4.10.2 Pearson correlation of the impact of water quality on E_{EO} and pseudo-first order rate for all matrices with the exception of the primary influent ** indicates p<0.05.

	DOC initial	Alkalinity	pH	H_2O_2 demand	pCBA Removal	DOC removal
DOC initial	1.00					
Alkalinity	**-0.39****	1.00				
pH	-0.20	-0.16	1.00			
H_2O_2 demand	0.13	-0.31	-0.11	1.00		
pCBA Removal	0.12	0.09	**-0.91****	0.07	1.00	
DOC removal	-0.10	**-0.72****	-0.18	0.36	0.08	1.00

Table A4.10.3 Pearson correlation of the impact of water quality on E_{EO} and pseudo-first order rate. This regression includes all waters tested ** indicates p<0.05.

Matrices	$DOC_{initial}$ (β_1)	Alkalinity (β_2)	pH (β_3)	H_2O_2 demand (β_4)	Model R^2	AIC	Number of points
All Matrices	-0.72±0.18 (*p<0.0001)*	-0.11±0.08 (*p=0.0013)*	-0.81±0.08 (*p<0.0001)*	-0.11±0.17 (*p<0.0001)*	0.88	127	20

Table A4.10.4 Multivariable linear regression of the impact of water quality on E_{EO} and pseudo first order rate. This regression includes all waters tested with the exception of the "Primary effluent test" ** indicates p<0.05.

Matrices	**$DOC_{initial}$ (β_1)**	**Alkalinity (β_2)**	**pH (β_3)**	**Model R^2**	**AIC**	**Number of points**
All Source water Matrices	-0.07±0.07 (*p<0.34)*	-0.08±0.09 (*p=0.393)*	-0.80±0.09 (*p<0.0001)*	0.88	112	17

Appendix A4.11. Lack of flocculation following EC:H2O2 for SR-NOM at pH = 8.3

Following EC:H_2O_2 of SR-NOM at pH 8.3, the treated solution was orange (Figure A4.11.1), indicating the presence of iron, and no visible floc formation, indicating unsuccessful coagulation and flocculation. Accordingly, DOC was not measured for this experiment.

Figure A4.11.1. Unsuccessful floc precipitation following EC:H_2O_2 of SR-NOM at pH 8.3 in 4 mM HCO_3^-.

Appendix A4.12 Multivariable analysis: Electrical Energy per order

The multivariable regressions for electrical energy per order are shown in Table A4.12.1 and for water quality impacts, they are shown in Table A4.12.3. Additionally, the Pearson correlations are provided for water quality impacts in Table A4.12.2.

Table A4.12.1. Multiple regression of process inputs on E_{EO}.

Matrices	H_2O_2/Fe (β_1)	Current Density (β_2)	Model R^2	AIC	Number of points
All ratios	-0.13±0.09 (*p=0.16)*	0.36±0.09 (*p<0.0001)*	0.40	214	36

Table A4.12.2. Pearson correlation of the impact of water quality on E_{EO} and pseudo-first order rate. ** indicates p<0.05.

	EEO	Rate Constant	DOC initial	Alkalinity	pH	Conductivity
EEO	1.00					
Rate Constant	**-0.73****	1.00				
DOC initial	**0.58****	**-0.55****	1.00			
Alkalinity	-0.18	**0.46****	**-0.55****	1.00		
pH	**0.46****	**-0.66****	-0.13	-0.27	1.00	
Conductivity	0.06	**-0.44****	**0.59****	**-0.39****	-0.12	1.00

Table A4.12.3. Multivariable linear regression of water quality impact on E_{EO}.

Matrices	$DOC_{initial}$ (β_1)	Alkalinity (β_2)	pH (β_3)	Conductivity (β_4)	Model R^2	AIC	Number of points
All Matrices	1.2±0.15 (*p<0.0001)*	0.45±0.11 (*p=0.0013)*	0.63±0.09 (*p<0.0001)*	-0.29±0.1 (*p<0.0001)*	0.86	123	20

A5: CHAPTER 5 ELECTRONIC SUPPLEMENTARY INFORMATION

Appendix A5.1: PFAS Characteristics and Quantification

Four target PFAS containing a range of molecular weights and functional groups and were quantified via LC-MS 2020 for µg/L quantification and LC-MS 8060 for ng/L quantification. QA/QC experiments were conducted to verify that PFAS were not artificially removed via filtration during sampling.

Table A5.1.1. LC-MS 2020 gradient flow time progression for PFAS quantification.

Time (min)	Organic Phase (% of flow)[a]
0 – 1.0	50
1.0 – 4.0	95
4.0 – 6.5	95
6.5 – 6.6	50
6.60 – 9.0	50
9.0	End of run

[a] = organic phase is HPLC-grade acetonitrile + 0.1% formic acid

Table A5.1.2. LC-MS 2020 instrument information for PFAS quantification.

Parameter	Value
Eluent Type	Gradient
Mobile Phase A	Milli-Q water + 0.1% formic acid
Mobile Phase B	Acetonitrile + 0.1% formic acid
Flow Rate	0.4 mL/min
Column Temperature	40°C
Detection	Electrospray Mass Spec (ESMS) at 40°C
Injection Volume	10 µL
Acquisition Mode	Single ion mode
Interface Temperature	350°C
DL Temperature	250°C
Nebulizer Gas Flow	1.0 L/min
Heat Block	400°C
Drying Gas Flow	9 L/min

Table A5.1.3. LC-MS 8060 gradient flow time progression for PFAS quantification. Mobile phase is Milli-Q Water + 20 mM Ammonium Formate. Organic phase is acetonitrile.

Time (min)	Organic Phase (% of flow)[a]
0 – 0.01	10
0.01 – 2.00	30
2 – 9.00	55
9.00 – 11.00	80
11.00 – 13.00	80
13.00 – 14.00	10
14.00 – 15.00	10
15.00	End of Run

Table A5.1.4. LC-MS/MS 8060 instrument information for PFAS quantification. LC-MS 8060 conditions are adapted from previous works (Min and Wang, 2023)

Parameter	Value
Eluent Type	Gradient
Mobile Phase A	Milli-Q water + 20mM Ammonium Formate
Mobile Phase B	Acetonitrile
Flow Rate	0.4 mL min^{-1}
Column Temperature	40°C
Detection	Electrospray Mass Spec (ESMS) at 40°C
Injection Volume	50 µL
Acquisition Mode	Multiple Reaction Monitoring
Interface Temperature	300°C
DL Temperature	105°C
Nebulizer Gas Flow	2.7 L min^{-1}
Heat Block	200°C
Drying Gas Flow	5 L min^{-1}
Needle Position	1.5

Table A5.1.5. PFAS concentration with and without filtration with 0.22 µm polyethersulfone (PES) membrane filters.

	Filtered		Not filtered		
PFAS compound	Average	Standard Deviation	Average	Standard Deviation	% Difference
PFOA	228.19	1.33	221.87	2.71	2.85
FTCA	194.32	3.02	189.55	4.18	2.52
PFOS	211.26	3.69	207.59	0.94	1.77
6:2 FtS	206.75	3.78	196.68	3.21	5.12

Appendix A5.2: Residual H_2O_2 and final pH following EC:H_2O_2

Following EC:H_2O_2 treatment for 20 minutes, the residual H_2O_2 was quantified to assess the remaining H_2O_2 in the system and overall H_2O_2 reactivity and removal at the conditions tested. Additionally, the pH after treatment was measured.

Table A5.2.1. Residual H_2O_2 concentration and removal following treatment. Data reflect triplicate experiments.

H_2O_2 conditions during EC:H_2O_2				
	Residual Concentration		H_2O_2 Removal	
	Average	Standard Deviation	Average	Standard Deviation
EC:H_2O_2 test				
EC: H_2O_2 bicarb	3.1	0.1	98.7	0.0
EC: H_2O_2 t = 5 minutes	8.3	3.2	0.9	0.1
No electricity control	27.7	5.5	88.5	2.3
H_2O_2 only	233.3	11.5	2.8	4.8
PFAS Blank	3.1	0.1	98.7	0.0
EC: H_2O_2 neutral pH	56.7	14.4	76.4	6.0
DOM Tests				
Oxalic Acid	21.3	3.2	91.1	1.3
Salicylic Acid	5.0	1.0	97.9	0.4
SR-NOM	3.7	1.6	98.5	0.7
Humic Acid	3.3	1.5	98.6	0.6
MKE River	21.3	2.3	91.1	1.0

Table A5.2.2. Final pH following experiments for 20 minutes. Initial pH was pH 3, unless otherwise noted. Average and standard deviations result from triplicate experiments.

Experiment	Average	Standard Deviation
EC:H_2O_2 test		
EC: H_2O_2 bicarb	3.23	0.02
No electricity control	3.16	0.02
electrodes only	4.54	0.10
PFOA only	3.21	0.01
H_2O_2 only	3.14	0.04
PFAS Blank	3.21	0.03
EC: H_2O_2 (pH = 6.3)	6.96	0.14
DOM Tests		
Oxalic Acid	3.58	0.01
Salicylic Acid	3.29	0.01
SR-NOM	2.89	0.57
Humic Acid	3.28	0.01
MKE River	3.36	0.01
EC Controls		
EC control	6.67	0.03
EC - SRNOM	6.86	0.17
EC MKE	6.24	0.08

* value from single replicate.

Appendix A5.3: PFAS mitigation Pathway Experiments

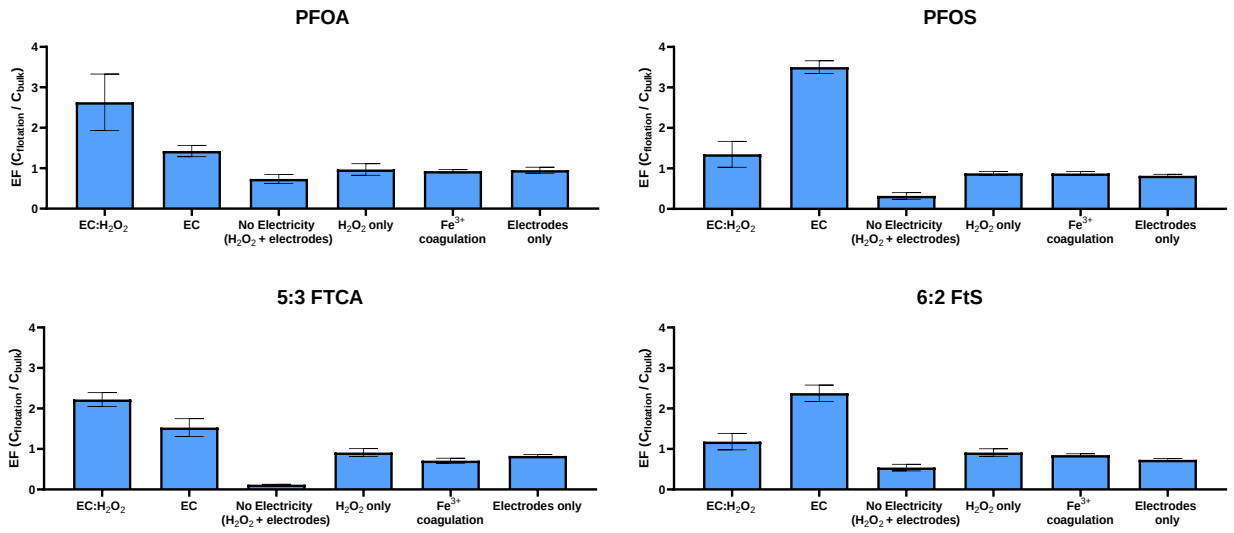

Figure A5.3.1. The flotation enrichment factor (EF) following pathway isolation experiments. All four PFAS (PFOA, 5:3 FTCA, PFOS, and 6:2 FtS) were spiked at 0.5 µM each in 4 mM HCO_3^- buffer at pH 3. The EC:H_2O_2 experiments were run at 7.4 mA/cm^2 for 20 minutes. During electrolysis, 60 mg/L of H_2O_2 was spiked every 5 minutes. During EC-only, electrolysis was run at 7.4 mA/cm^2 for 20 minutes. In No Electricity (H_2O_2 + electrodes), 60 mg/L H_2O_2 was spiked every 5 minutes in the presence of the iron electrodes. In H_2O_2 only, 60 mg/L of H_2O_2 was spiked every 5 minutes. For Fe^{3+} coagulation, 190 mg Fe^{3+}/L was spiked as $FeCl_3 \bullet 6H_2O$ to match the estimated iron concentration generated during EC and EC:H_2O_2. For Electrodes only, reactors were stirred for 20 minutes with the electrodes in the solution. Error bars indicate ±1 standard deviation of triplicate experiments.

Appendix A5.4: PFOA only Experiment Comparison

PFOA-only experiments were conducted and compared to PFAS mixture experiments to assess removal in mixtures vs. PFOA only to help understand the potential interactions between other PFAS during treatment.

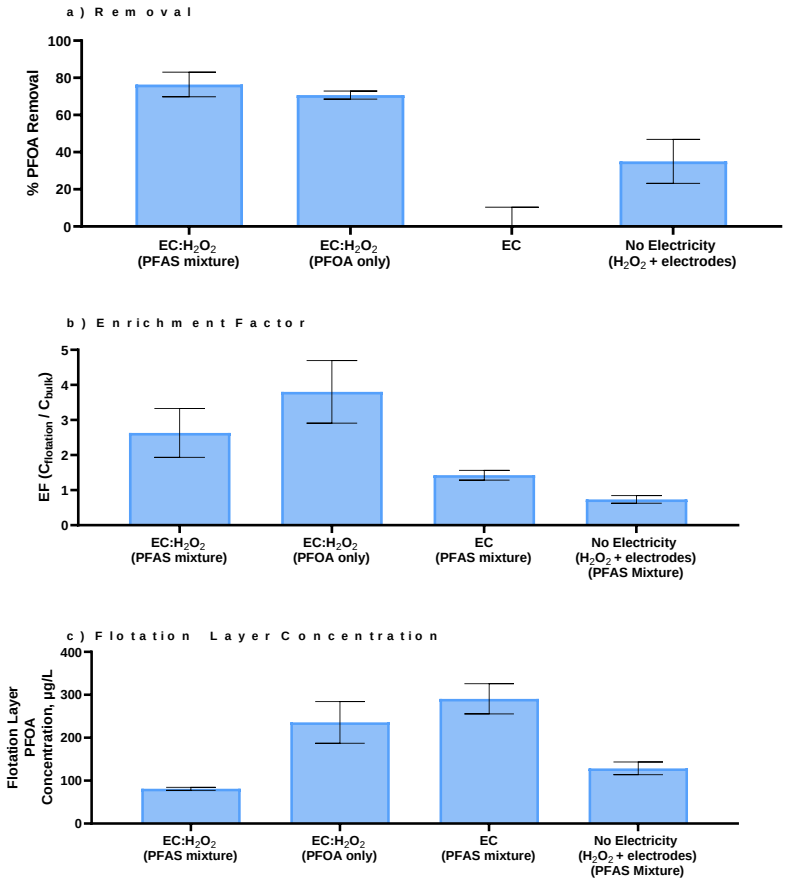

Figure A5.4.1. EC:H_2O_2 pathway experiments for PFOA removal, in addition to EC:H_2O_2 treating a PFAS mixture. For the PFAS mixture, all four PFAS (PFOA, 5:3 FTCA, PFOS, and 6:2 FtS) were spiked at 0.5 µM each. All experiments were conducted in 4 mM HCO_3^- at pH 3 adjusted with 3N HCl. The EC:H_2O_2 and EC experiments were run at 7.4 mA/cm^2 for 20 minutes. During electrolysis, 60 mg/L of H_2O_2 was spiked every 5 minutes. In "EC:H_2O_2 (PFAS mixture)" experiments were conducted to assess the potential interaction with PFOA and other PFAS that may promote surfactant activity. In "No Electricity (H_2O_2 + electrodes)", H_2O_2 only, 60 mg/L of H_2O_2 was spiked every 5 minutes in the presence of iron electrodes. For Fe^{3+} coagulation, a concentration of 190 mg Fe^{3+}/L was spiked as $FeCl_3 \bullet 6H_2O$ to match the estimated iron concentration generated during EC and EC:H_2O_2. Error bars indicate ±1 standard deviation of triplicate experiments.

Appendix A5.5: Foam formation following EC:H_2O_2

During EC:H_2O_2 experiments, foam formed (Figure A5.5.1). Twenty mL of flotation layer and foam was sampled and blended with an equal volume of 20 mL of methanol to dissolve the foam.

Foam formed after EC:H_2O_2

Foam separated from water following EC:H_2O_2 salicylic acid experiment

Humic acid precipitates in flotation layer

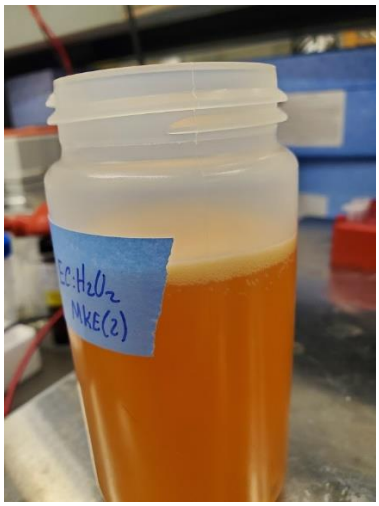

Foam prior to sampling for EC:H_2O_2 of MKE

Figure A5.5.1. Foam generated following EC:H_2O_2 treatment.

Appendix A5.6 Pearson correlations and DOM analyses

Pearson correlations were conducted using DOM characterization data to understand similarities between characterization parameters and provide correlation information for the impact of DOM characteristics on PFAS occurrence in the flotation layer (Tables A5.6.1 and S5.6.2). Additionally, the electron excitation emission matrices for the bulk DOM constituents are provided for the bulk DOM and <1 kDa fractions (Figure A5.6.1).

Table A5.6.1. Pearson correlation of DOM characterization parameters to assess multicollinearity. An asterisk (*) indicates statistically significant correlations ($p < 0.05$).

	DOM Characterization Parameters					
	SUVA	>10 kDa	3 - 10 kDa	1 - 3 kDa	<1 kDa	$DOC_{initial}$
	Correlation, R^2					
SUVA	1.00					
>10 kDa	**0.92***	1.00				
3 - 10 kDa	**0.46***	0.09	1.00			
1 - 3 kDa	0.23	0.02	**0.65***	1.00		
<1 kDa	**-0.43***	**-0.47***	-0.16	-0.17	1.00	
$DOC_{initial}$	**0.44***	0.44	0.12	-0.13	**0.47***	1.00

Table A5.6.2. Pearson correlation comparing DOM characteristics to PFAS concentration in the flotation layer following EC:H_2O_2 following treatment for all DOM containing experiments. An asterisk (*) indicates statistically significant correlations ($p < 0.05$).

	PFOA Flotation Concentration	5:3 FTCA Flotation Concentration	PFOS Flotation Concentration	6:2 FtS Flotation Concentration
	Correlation, R^2			
SUVA	-0.30	-0.12	-0.39	-0.36
>10 kDa	-0.46	-0.32	**-0.53***	-0.44
3 - 10 kDa	0.04	0.17	-0.02	-0.14
1 - 3 kDa	-0.38	-0.14	-0.45	-0.36
<1 kDa	**0.83***	**0.76***	**0.88***	**0.76***
$DOC_{initial}$	0.30	0.46	0.27	0.27
FIX	**0.88***	0.63	**0.89***	**0.81***
BIX	**0.87***	0.62	**0.89***	**0.80***
HIX	**-0.82***	**-0.70***	**-0.85***	**-0.84***
HIX/BIX	**-0.83***	**-0.70***	**-0.86***	**-0.84***

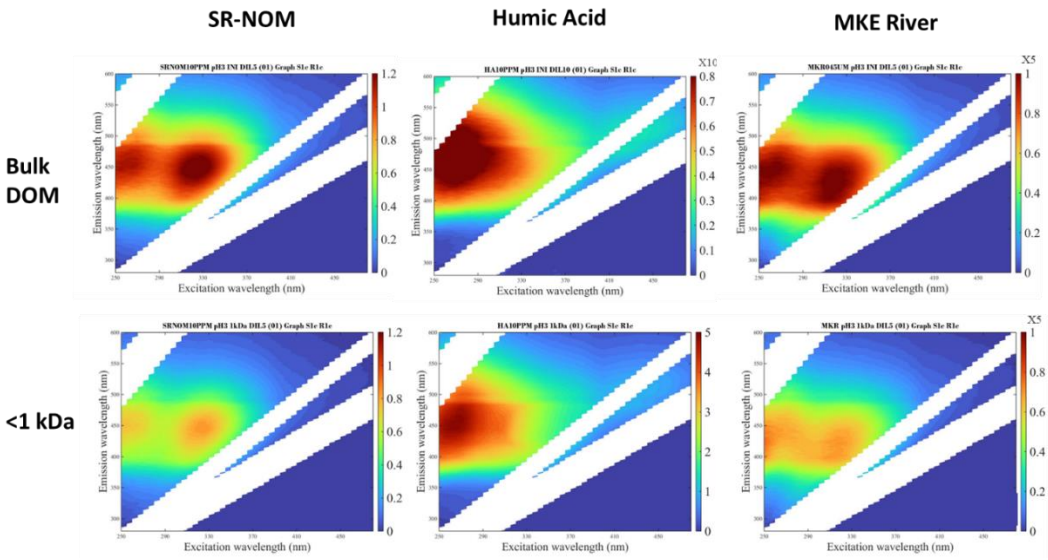

Figure A5.6.1. Fluorescence excitation emission matrices for bulk DOM and <1 kDa DOM for bulk organic mixture matrices at pH 3.

Appendix A5.7 Residuals produced following electrocoagulation and peroxi-electrocoagulation

Following EC:H_2O_2, samples were taken to assess the residual metals concentrations generated from electrolysis. Additionally, PFAS blanks were conducted to assess carryover of PFAS between tests.

Table A5.7.1. Metals (manganese and iron) produced following 20 minutes of EC and EC:H_2O_2 experiments in Electrolyte-only and MKE River tests.

Sample Matrix	Mn, µg/L	Fe, mg/L
EC:H_2O_2	137.2 ± 27.9	78.9 ± 1.9
EC	123.8 ± 11.7	9.9 ± 0.4
No Electricity	68.7 ± 23.4	19.3 ± 0.9
MKE initial	2.95 ± 0.10	0.02 ± 3.5 x 10^{-4}
EC:H2O2 MKE	154.1 ± 25.8	0.43 ± 0.26
EC MKE	122.8 ± 3.2	10.35 ± 0.11

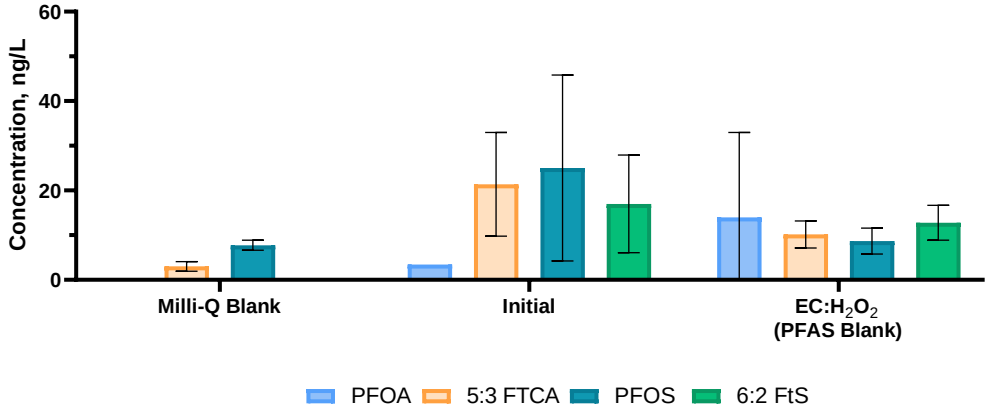

Figure A5.7.1. PFAS in samples following EC:H_2O_2 treatment. All experiments were conducted in 4 mM HCO_3^- buffer at pH 3 without PFAS additions. The EC:H_2O_2 experiments were run at 7.4 mA/cm^2 for 20 minutes. During electrolysis, 60 mg/L of H_2O_2 was spiked every 5 minutes. Error bars indicate ±1 standard deviation of triplicate experiments.